Thesis for the degree
Doctor of Philosophy

Submitted to the Scientific Council of the
Weizmann Institute of Science
Rehovot, Israel

עבודת גמר (תזה) לתואר
דוקטור לפילוסופיה

מוגשת למועצה המדעית של
מכון ויצמן למדע
רחובות, ישראל

By
Sébastien Trzebanski

מאת
סבסטיאן טשבנסקי

לימוד התמיינות והטרוגניות מונוציטים

Studying monocyte differentiation and heterogeneity

Advisor:
Prof. Steffen Jung

מנחה:
פרופסור סטפן יונג

Month and Year
October 2023

חודש ושנה עבריים
אוקטובר 2023

Acknowledgments

I would like to express my sincere gratitude to Prof. Steffen Jung for his guidance and support throughout the years. I have learned more than I could ever have imagined in the past few years. Scientifically, I have received invaluable training that will allow me to take on the next challenges in my scientific career. More importantly, I have learned from Steffen how to guide people, show compassion, and act without (too much) compulsion. I could not have wished for a better mentor and might very well not be writing this thesis without him.

Further, I am immensely grateful to all past and present Jung group lab members that have provided a great atmosphere and fruitful discussions in group meetings. Special thanks go to Jung-Seok Kim and Niss Larossi who were not only vital to many experiments, in planning, execution, and analysis, but also grew close to my heart as friends. Particularly, Jung-Seok's contribution to my PhD path, both professionally and personally, cannot be emphasized enough.

Moreover, I need to thank Prof. Gustavo Mostoslavsky and Shlomit Gilad for absolute expert help and patience in the CRISPR project. Without the help of Gustavo, no hematopoietic cell would ever have lit up in bright green/red. Shlomit was the vital driving force for the solution to the CROPseq amplification. To a degree, the CRISPR project was built and maintained on their shoulders.

I also thank all other collaborators which I had the pleasure to assist or be assisted by. Of note, Prof. Kiavash Movahedi, Prof. Simon Yona, Dotan Hoffman, Uli Koehler, and Montaser Haddad were tremendous fun to discuss science and/or work with.

Lastly, I thank my close friends who have made these 4.5 years unforgettable outside of the lab. Most importantly, I thank my partner Melina and my son Leon for giving me a tangible reason to stay out of the lab if not truly needed.

Declaration

Hereby, I declare that this thesis is a summary of my own independent research.

Table of Contents

List of abbreviations

bp	base pairs
BM	bone marrow
Cas9	CRISPR-associated protein 9
CM	classical monocyte
CMP	common myeloid progenitor
cMoP	common monocyte precursor
CRISPR	clustered regularly interspaced short palindromic repeats
DC	dendritic cell
DCMo	DC-like monocyte
DEG	differentially expressed gene
EMP	erythro-myeloid progenitor
FL	fetal liver
GMP	granulocyte and macrophage precursor
HSC	hematopoietic stem cell
KO	knock-out
LSK	lineage-negative, Sca-1- and c-Kit-positive HSC fraction
LTR	long terminal repeat
MDP	macrophage and dendritic cell precursor
moDC	monocyte-derived DC
NCM	non-classical monocyte
NeuMo	neutrophil-like monocyte
PCR	polymerase chain reaction
sgRNA	single-guide RNA
TF	transcription factor
TU	transducing units
TRM	tissue-resident macrophage
YS	yolk sac

Abstract

Monocytes are short-lived cells of the innate immune system that originate from adult hematopoiesis. After maturation in the bone marrow (BM), they are released into the bloodstream. In mammals, two primary monocyte subsets have been identified. In mice, these are known as classical or 'inflammatory' Ly6Chigh monocytes (referred to as CM) and non-classical or 'patrolling' Ly6Clow monocytes (referred to as NCM). CM primarily differentiate into tissue-resident macrophages (TRM) in peripheral tissues, particularly under inflammatory conditions, and, to a lesser extent, homeostasis. For instance, in healthy mice, circulating monocytes replenish gut TRM every 3-4 weeks. Interestingly, monocyte-derived TRM in the small and large intestines have distinct gene expression profiles, although the signals guiding this local differentiation process remain unclear.

In **Project 1**, we focused on the impact of transcription factors (TF) that are differentially expressed in ileal or colonic TRM on monocyte differentiation. We utilized a CRISPR/Cas9 screening system that targets immune cells and performed a pooled CRISPR screen for 10 ileum- or colon-specific TF. We subjected sgRNA-bearing gut TRM to single-cell transcriptomics to evaluate the effects of CRISPR-induced DNA modifications on the cell fates.

The advent of single-cell transcriptomics has revealed heterogeneity within what were previously thought to be homogenous CM populations. Specifically, based on intricate lineage tracing experiments and gene expression signatures, the existence of neutrophil-like (NeuMo) and dendritic cell-like (DCMo) monocytes has been proposed. However, until recently, this heterogeneity had only been confirmed at the transcriptional level.

In **Project 2**, we identified surface markers that allowed us to distinguish NeuMo and DCMo at the phenotypic, functional, and transcriptomic levels, consistent with earlier reports. Furthermore, we demonstrated that these CM subsets could serve as macrophage progenitors. When adoptively transferred into TRM-depleted recipients, both subsets contributed equally to homeostatic monocyte fates such as NCM and gut TRM. However, DCMo showed a preference for giving rise to lung TRM, while NeuMo exclusively populated the dura mater in the brain. Importantly, we linked these phenomena to distinct precursor populations in the BM. In conclusion, we provide comprehensive evidence supporting the existence of CM subsets and demonstrate that diverse monocyte populations give rise to varied TRM.

Introduction

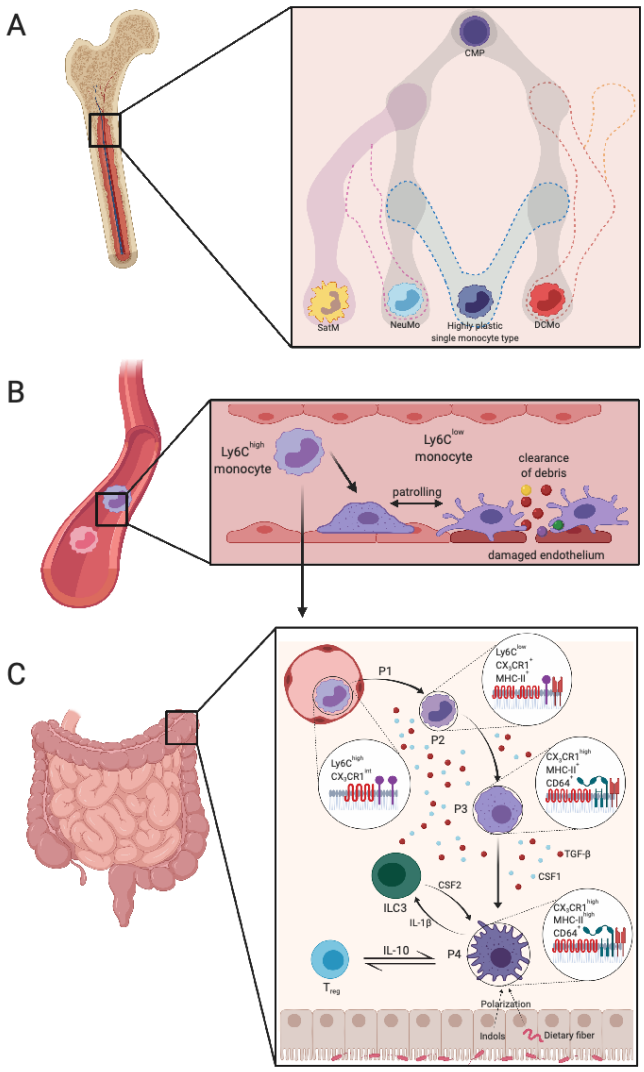

Figure 1: (A) Monocyte development in the BM. (B) Monocyte subsets in the blood circulation. (C) Monocyte differentiation in the intestine.

Monocytes and macrophages have long been grouped under the term 'Mononuclear Phagocyte System' (MPS), a term coined by van Furth and Cohn in 1968. However, despite this collective categorization, monocytes and macrophages exhibit significant differences with respect to their roles in tissue homeostasis and innate immunity. Adult hematopoiesis constantly generates substantial quantities of monocytes within the bone marrow (BM) (**Fig 1A**).

Monocytes, along with neutrophils, act as the initial responders at sites of inflammation and are also recruited to tissues in chronic conditions (Guilliams et al., 2018). While various functions of monocytes have been described, their primary role remains their transformation into myeloid effector cells with characteristics resembling both macrophages and dendritic cells (DC).

Macrophages, on the other hand, are non-migratory and represent tissue-resident cells that play a critical role as primary immune sentinels. Initially, it was believed that tissue-resident macrophages (TRM) were exclusively derived from monocytes (Furth and Cohn, 1968). However, over the last decade, fate mapping experiments conducted in mice have established that the majority of TRM are established during embryonic development and do not rely on monocyte involvement in the absence of inflammation (Ginhoux and Guilliams, 2016; Guilliams et al., 2018; Hoeffel and Ginhoux, 2018; Mass et al., 2016; Prinz et al., 2019; Werner et al., 2020; Yona et al., 2013).

Monocyte subsets and fates

Three decades ago, human monocytes were classified into two primary categories: CD14+ monocytes, which were subsequently subdivided into CD16+ and CD16- cells (Passlick et al., 1989), and CD14lowCD16+ monocytes (Geissmann et al., 2003; ZIEGLER-HEITBROCK et al., 1994). Since then, the existence of blood monocytes has been confirmed in various mammalian species, including non-human primates (Kim et al., 2010; Kwissa et al., 2012), pigs (Ziegler-Heitbrock et al., 1994), rodents (Ahuja et al., 1995; Geissmann et al., 2003; Palframan et al., 2001) (Ahuja et al., 1995; Geissmann et al., 2003a; Palframan et al., 2001), and cows (Hussen et al., 2013). In mice, the two primary monocyte subsets are now defined as $Ly6C^{hi}Cx3cr1^{int}CCR2^{+}$ classical or 'inflammatory' monocytes (CM) and $Ly6C^{lo}Cx3cr1^{hi}CCR2^{lo}$ non-classical or 'patrolling' monocytes (NCM) (**Fig 1B**) (Guilliams et al., 2018).

Recent advances in reporter systems and transcriptomic platforms have provided insights into the functions and destinies of murine blood monocyte subsets (Gross-Vered et al., 2020; Ingersoll et al., 2010; Mildner et al., 2017; Weinreb et al., 2020; Yáñez et al., 2017). Murine monocyte subsets do not only differ in their transcriptomes but, more importantly, significantly vary in their functions and locations. Their respective abilities to extravasate and differentiate vary greatly, with NCM being severely limited in this regard (Auffray et al., 2007; Guilliams et al., 2018; Varol et al., 2009). While there is substantial evidence supporting the migration of CM into inflamed tissues, only a few reports link NCM to tissue-resident derivatives in specific contexts (Hou et al., 2019; Misharin et al., 2014; Nahrendorf et al., 2007; Schyns et al., 2019).

In adult animals, monocytes originate from dedicated BM precursors , but they can also arise in extramedullary niches, like the spleen (Hettinger et al., 2013; Swirski et al., 2009). Once they have matured, monocytes enter the bloodstream in a CCR2-dependent manner (Serbina and Pamer, 2006).

More recently, a third, more heterogeneous monocyte subset with intermediate Ly6C levels has been identified. This intermediate cell type shares phenotypic and transcriptomic characteristics with both CM and NCM (Menezes et al., 2016; Mildner et al., 2017). Moreover, it expresses the classical DC marker CD209a, resembling previously described monocyte-derived DC (moDC) (Menezes et al., 2016). However, further investigation is needed to fully understand this proposed monocyte-derived cell type, particularly in terms of its *in vivo* context and function, such as its role in the priming of naïve T cells. The moDC concept has also been challenged, as it was shown that a mixture of inflammatory type 2 classical DC (cDC2) and

classical monocyte-derived TRM can be found in the moDC flow cytometric gate (Bosteels et al., 2020).

Confusion also persists with respect to the phenotypic definition of monocytes, mature DC, and DC precursors, as these cell types share numerous surface markers. Discrimination based solely on surface marker profiles is challenging, although not impossible (Anderson et al., 2020). Notably, the classic $Ly6C^{+}CD115^{+}$ monocyte gate in the BM and blood has for instance been shown to include a contamination of DC precursors (Menezes et al., 2016), which was recently attributed to a novel DC population, previously described in humans as DC3 (Liu et al., 2023). Importantly, DC3 and their pro-DC3 precursors share a multitude of surface markers and transcriptomic markers with monocytes, adding to the complexity (Liu et al., 2023). In light of the discovery of monocyte-like DC3 in both mice and humans, further research is needed to fully understand the in vivo potential of monocytes to give rise to moDC.

A bifurcation in monopoiesis

Monocytes originate in the BM from hematopoietic stem cells (HSC), which are the earliest precursors in this process. HSC undergo a series of asymmetric cell divisions, leading through intermediate multipotent stages to the formation of common myeloid progenitors (CMP). CMP can differentiate into two primary lineages: granulocyte-and-macrophage progenitors (GMP) and macrophage-and-dendritic cell progenitors (MDP). Initially, it was thought that MDP were the exclusive precursors of monocytes in the BM (Auffray et al., 2009; Fogg et al., 2006; Varol et al., 2007) and that they directly descended from GMP (**Fig 2A**). However, more recent data suggest that both GMP and MDP can independently give rise to monocytes, and distinct transcriptomic signatures in resulting monocytes indicate functional differences based on their origin (**Fig 2B**). (Weinreb et al., 2020; Yáñez et al., 2017).

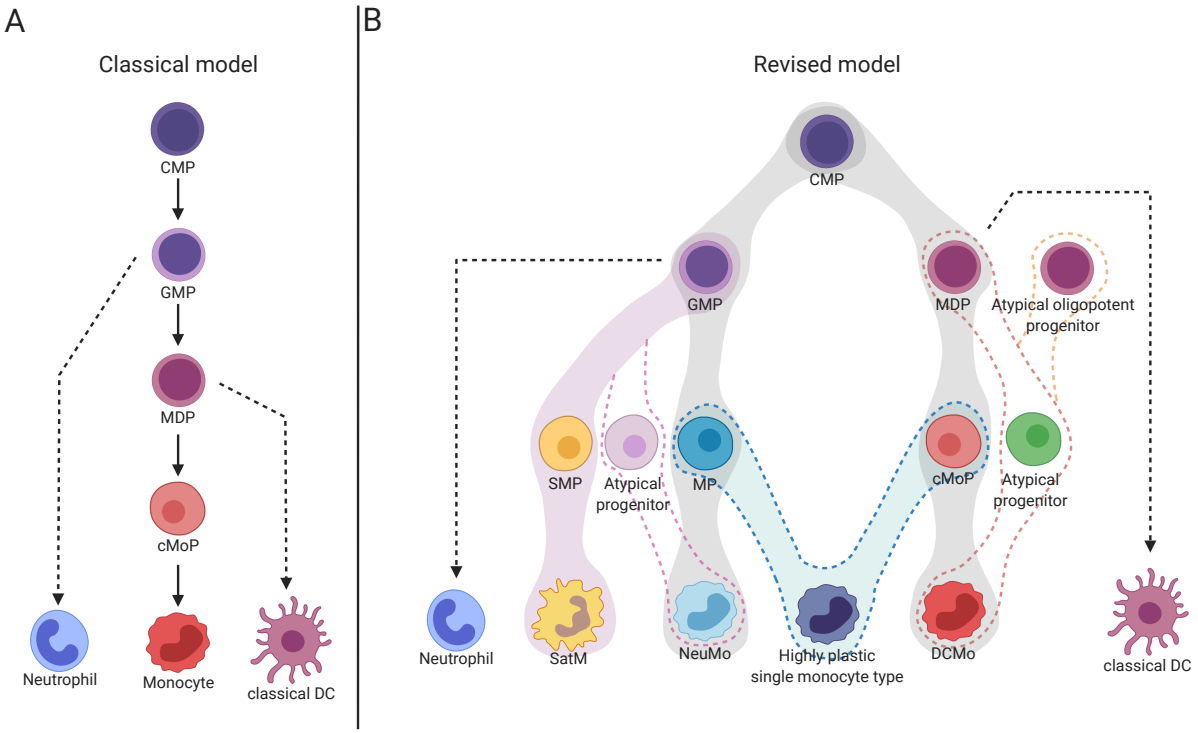

Figure 2: (A) Conventional model of myelopoiesis. (B) Revised model of myelopoiesis.

MDP give rise to committed monocyte progenitors (cMoP), which were originally believed to be the sole dedicated monocyte precursors (Hettinger et al., 2013). An alternative pathway proposed that GMP could also generate monocytes through an intermediate stage known as the monocyte precursor (MP) (Wolf et al., 2019; Yáñez et al., 2017, 2015). Importantly, it is currently not possible to distinguish between monocyte progenitors derived from MDP (cMoP) and those derived from GMP (MP) using surface markers alone. Rather, the existence of these precursors has been inferred from the presence of heterogeneous monocyte precursor populations in single-cell datasets (Weinreb et al., 2020; Yáñez et al., 2017). Adoptive transfer experiments have demonstrated that neutrophils and classical DC exclusively originate from GMP and MDP, respectively, while monocytes can arise from either precursor type (Yáñez et al., 2017). Therefore, reports on cMoP refer to a diverse population of heterogenous monocyte precursors. Additionally, beyond their transcriptomic differences, monocytes derived from GMP and MDP were shown to exhibit distinct responses to various microbial stimuli (Yáñez et al., 2017).

The concept of a bifurcation in monopoiesis, originally introduced by the Goodridge team (Yáñez et al., 2017), has been supported by Weinreb and colleagues, who combined advanced lineage tracing and single-cell RNA sequencing (scRNAseq) to confirm the existence of neutrophil-like monocytes (NeuMo) and dendritic cell-like monocytes (DCMo). NeuMo express high levels of neutrophil-related markers such as *S100a8*, *Chil3*, *Mpo*, and *Elane*,

consistent with previous reports. Conversely, DCMo are identified by the expression of DC-related genes, primarily associated with antigen presentation, including *Cd74* and MHC class 2 genes, as well as *Cd209a*. Importantly, differential expression of these markers was already observed at the GMP and MDP precursor stages (Weinreb et al., 2020).

In summary, ground-breaking studies have established a model of binary monocyte ontogeny, potentially established even at the oligopotent progenitor stage. However, it is worth noting that monocyte heterogeneity has so far been primarily based on transcriptomic signatures. Moreover, although monocytes displaying features of NeuMo and DCMo have been sporadically reported in disease contexts (Askenase et al., 2015; Ikeda et al., 2018; Satoh et al., 2017), functional implications of CM heterogeneity in health and disease are yet to be elucidated.

Atypical monocytes

Recent advancements in single-cell technologies, such as scRNAseq, have unveiled previously unnoticed heterogeneity within monocytes (Weinreb et al., 2020; Yáñez et al., 2017). However, a closer examination of literature reveals also earlier reports describing monocytes exhibiting prominent neutrophil and dendritic cell (DC) features in specific contexts.

One study focused on mature atypical monocytes and their precursors in a fibrosis model (Satoh et al., 2017) and reported segregated-nucleus-containing atypical monocytes (SatM) resembling neutrophil-like monocytes (NeuMo). SatM were shown to arise from granulocyte-and-macrophage progenitors (GMP)-derived precursors called segregated-nucleus-containing monocyte precursors (SMP). Importantly, SMP were distinct from cMoP, as they lacked CD117 and Ly6C expression. Mature SatM expressed CD115, indicating their affiliation with the monocytic lineage. SatM were further characterized by the expression of Ceacam1 and mannose receptor (CD204, Msr1), along with the presence of neutrophilic granule proteins such as lipocalin (encoded by *Lcn2*), neutrophil elastase (encoded by *Elane*), and S100a8. However, it should be noted that this report pertains to fibrosis and thus a highly disease-specific context, suggesting that SatM may represent a mere deviation of a more general NeuMo program.

Another NeuMo-associated feature is the expression of the lectin chitinase-3-like protein 3 (encoded by *Chil3*, *Ym1*). Using reporter animals, a Chil3^{+} CM subset was identified to proliferate during the late phase of gut inflammation, contributing to its resolution (Ikeda et

al., 2018). Chil3^{+} monocytes expressed additional NeuMo-related genes such as *S100a8, Lcn*2, and *Ngp* in response to lipopolysaccharide (LPS). Phenotypically, these cells expressed higher levels of CD204 compared to Chil3^{-} CM, akin to SatM (Satoh et al., 2017). Notably, GMP and cMoP, but not MDP, were found to give rise to Chil3^{+} monocytes upon adoptive transfer. Of note, a more recent study of the Asano team has suggested that a neutrophil precursor could give rise to Chil3^{+} monocytes upon LPS exposure (Ikeda et al., 2023).

While phenotypic definitions suggest the existence of distinct and categorizable cell populations, differentiation pathways are not fractal; rather, they represent a continuous and graded commitment (Naik et al., 2013). This notion is supported by less biased scRNAseq data (Giladi et al., 2018; Nestorowa et al., 2016; Olsson et al., 2016; Paul et al., 2015; Weinreb et al., 2020). Nevertheless, phenotypic definitions such as GMP, MDP, and cMoP, remain valuable for guiding our understanding of myelopoiesis. This is also the case for CXCR4^{hi} pre-monocytes, identified as immediate progeny of cMoP, maturing into CXCR4^{lo} CM (Chong et al., 2016). Interestingly, this study found differential expression of neutrophil granule proteins in cMoP compared to pre-monocytes, while *H2-Ab1* and *H2-Aa* expression was more characteristic of the mature CXCR4^{lo} CM. This finding raised the possibility that NeuMo and DCMo might represent distinct stages in monocyte maturation (Chong et al., 2016). Different prevalence of NeuMo and DCMo could reflect differential mobilization of immature and mature cells, or there could be a re-routing of monopoiesis or the omission of certain intermediates under pathological conditions. For example, in cases of high interferon exposure associated with certain parasite infections, a complete replacement of CM by a population of Cx3cr1^{lo} Sca1^{hi} CM was observed in *T. gondii*-infected mice (Askenase et al., 2015). These cells exhibited high levels of MHC-II, similar to DCMo, thus indicating developmental re-routing. Hence, the emergence of distinct precursors, akin to SMP, is conceivable in this disease context, as well (Satoh et al., 2017).

Also the role of monocytes in autoimmune disorders has garnered considerable interest, with reports of an interferon-induced CM subset in experimental autoimmune encephalomyelitis (EAE), a model of chronic multiple sclerosis (MS). Infiltrating monocyte subsets in this model displayed high expression of antigen-presenting molecules, resembling DCMo. Conversely, clear NeuMo signatures were absent from the profiled CM (Giladi et al., 2020). In line with the report that DCMo expand under this condition, (Yáñez et al., 2017), these findings suggest that DCMo may also be preferentially mobilized in response to interferon exposure.

Lineage commitment is driven by the interplay of specific transcription factors (TF), and these TFs likely shape the dichotomy of monopoiesis. A compelling case has been made for PU.1, encoded by *Spi1*, a lineage-determining TF for monocytes and macrophages (Menezes et al., 2016). High expression of PU.1 was shown to induce monocyte expression of DC-related transcripts, while low PU.1 expression led to differentiation into $iNOS^+$ $MHC\text{-}II^+$ macrophages. This suggests that PU.1 levels skew monocytes towards a monocyte-derived DC (moDC) or DCMo program or a macrophage differentiation program (Menezes et al., 2016).

In summary, we are facing a complex monopoiesis landscape, marked by a binary fate commitment of monocyte precursors in the BM. The precise contribution of GMP and MDP to the mature monocyte pool remains to be fully understood and may vary depending on specific environmental factors, including housing conditions. Much remains to be explored regarding the fate commitment of homeostatic monocytes and the functional implications for circulating monocytes and their tissue-resident progeny.

Tissue-resident macrophages

Macrophages are found in virtually every tissue throughout the body. Although it was initially believed that all macrophages originated from monocytes, recent research has revealed a more complex picture of macrophage development. Multiple waves of hematopoiesis contribute to the formation of various TRM populations. In mice, the first wave, known as primitive hematopoiesis, occurs in the yolk sac during early embryonic development and gives rise to tissue-resident macrophages in various embryonic tissues. Microglia in the brain parenchyma and CNS border-associated macrophages are among the few remnants of this initial wave in the adult mouse. Simultaneously, a second wave, referred to as transient definitive hematopoiesis, originates from early erythromyeloid progenitors (EMP) and later involves late or definitive EMP. This wave, occurring from E8.5 to E13.5 in murine embryonic development, leads to the formation of fetal liver monocytes (FLMo) around E12.5. FLMo were shown to replace the embryonic TRM in most tissues, except the brain. It is believed that the majority of adult TRM originate from this transient definitive wave. In later stages of development, HSC migrate from the fetal liver to the fetal spleen and eventually settle in BM, where they remain throughout adulthood. This last definitive wave of hematopoiesis gives rise to monocytes that persist into adulthood.

Of paramount importance, and widely accepted, is the notion of transcriptomic and epigenetic macrophage identity to be profoundly influenced by the local microenvironment

(Amit et al., 2016; Guilliams and Scott, 2017). Recent years have seen the identification of specific TF responsible for conferring tissue-specific macrophage identities. For instance, Gata6 plays a pivotal role in establishing macrophage identity within the peritoneal cavity (Okabe and Medzhitov, 2014), Nr1h3 is indispensable for Kupffer cells in the liver (Mass et al., 2016), and Sall1 and IRF8 are critical for microglia identity (Buttgereit et al., 2016; Hagemeyer et al., 2016). In addition, the C/EBPb TF are essential for driving the transition of CM into NCM, and Nr4a1 is required for NCM survival (Hanna et al., 2011; Mildner et al., 2017; Thomas et al., 2016).

TRM exhibit significant diversity both across different organs and within specific anatomical niches within those organs (Ginhoux and Guilliams, 2016; Lavin et al., 2014). Beyond their traditional role in the immune defence, TRM are increasingly recognized for their vital contributions to maintaining overall bodily equilibrium. Their involvement extends to various critical physiological processes, including the regulation of iron and energy metabolism (Nairz et al., 2017; Wolf et al., 2017), the facilitation of electrical conduction within the heart (Hulsmans et al., 2017), and the support of spermatogenesis (DeFalco et al., 2015; Lintukorpi et al., 2020). Notably, gut macrophages have been shown to be indispensable for the shaping the mucosal immune system, the preservation of the integrity of enteric neurons and vasculature, and even peristalsis (Gabanyi et al., 2016; Mortha et al., 2014; Muller et al., 2014; Schepper et al., 2018). While it was long believed that these TRM were all relatively short-lived (Varol et al. 2009, Bain et al. 2014), recent findings have uncovered self-sustaining, long-lived TRM populations in the gut as well (Schepper et al., 2018; Shaw et al., 2018).

We have recently demonstrated that macrophage populations exhibit distinct transcriptomic and chromatin characteristics across various segments of the gut (Gross-Vered et al., 2020; Lavin et al., 2014). Specifically, utilizing a model involving the conditional TRM removal and subsequent adoptive CM transfer, we established that macrophages in the ileum and colon acquire unique gene expression profiles (Gross-Vered et al., 2020). The ensuing CM transition to tissue residency, which phenotypically resembles a waterfall (Tamoutounour et al., 2012) results in the up- and downregulation of around two thousand differentially expressed genes (DEG) (Gross-Vered et al., 2020). Interestingly, this shift in transcriptional activity was shown to be gradual and exhibit significant variation between the two distinct gut segments. However, cell-intrinsic or -extrinsic factors driving monocyte differentiation in the gut remain to be determined.

Research Goals

During the course of my PhD studies, I focused on two outstanding questions in the monocyte field.

Firstly, we wanted to understand the molecular mechanisms underlying monocyte differentiation into transcriptionally distinct ileal and colonic macrophages (Gross-Vered et al., 2020). Monocyte differentiation in steady-state is notoriously hard to study given their limited contribution to most peripheral organs. However, the gut provides an attractive model tissue, as gut TRM are constantly replenished by circulating CM in steady-state (Bain et al., 2014; Varol et al., 2009). The lack of markers for differentiating monocytes within tissues has impeded in-depth studies of this process. To circumvent this problem, we resorted to a chimeric system of CRISPR-Cas9 mediated mutagenesis. This allowed us to target multiple genes in parallel within the same animal. Given the established importance of TF in conferring TRM identity (Amit et al., 2016; Guilliams and Scott, 2017), we targeted 10 TF that we had recently found to be differentially expressed in ileal and colonic TRM (Gross-Vered et al., 2020).

Secondly, I decided to investigate the physiological significance of monocyte heterogeneity. Here, our first aim was to identify surface markers that would allow to discriminate CM subsets that have so far been reported merely on the transcriptional level (Weinreb et al., 2020; Yáñez et al., 2017). We the markers at hand we then intended to perform an in-depth functional study of these putative subsets. Indeed, we found surface markers clearly delineating neutrophil- and DC-like CM subsets. To study the functional impact of these cells, we made use of adoptive cell transfers into macrophage-depleted recipients as previously described (Gross-Vered et al., 2020; Varol et al., 2009, 2007). Importantly, we found that the distinct GMP- and MDP-derived CM subsets dynamically give rise to distinct TRM populations in different tissues.

Part I - Studying monocyte differentiation

Introduction

Most macrophages in the adult mouse are seeded into the various tissues during embryonic development (Ginhoux and Jung, 2014; Prinz et al., 2019). Selected tissues experience during adult hood constant replenishment of their TRM by circulating monocytes in steady-state. Sites that display a particular high turn-over of their TRM populations by monocytes include tissues in contact with the outside environment, namely the skin and the intestine (Bain et al., 2014; Tamoutounour et al., 2013). Specifically, the majority of murine gut macrophages has been estimated to be replaced every 3-4 weeks by monocytic precursors (Ginhoux and Jung, 2014; Shaw et al., 2018).

Using adoptive monocyte transfer into conditionally macrophage-ablated animals, we have previously shown that TRM in the small and large intestine differ on the transcriptional level (Gross-Vered et al., 2020). Graft-derived TRM were in this study sorted to purity from both ileum and colon on different days after transfer. Transcriptomic sequencing revealed profound differences in the adoption of tissue-residency in each gut segment with a combined 1173 genes being differentially expressed between monocyte-derived TRM from both gut segments. Interestingly, the early ileum graft clustered with the colon graft in principal component analysis (Gross-Vered et al., 2020). This suggested that the colonic gene signature might be a ‘default’ for gut-infiltrating monocytes prior to ‘specialization’ to ileal environmental cues.

TRM display considerable heterogeneity among and within tissues (Lavin et al., 2014). The current dogma holds that local cues imprint TRM nature in tissue-specific niches (Ginhoux and Guilliams, 2016; Guilliams and Scott, 2017). Specifically, interactions with immune and non-immune cells, such as neurons, have been shown to drive the adoption of a tissue- and sub-niche-specific gene signature in tissues such as the adipose tissue, the gut, or the liver (Bonnardel et al., 2019; Mortha et al., 2014; Wolf et al., 2017). In the gut, microbiome-derived stimuli define the physiological ground state of the gut immune system. For instance, microbiota-driven IL-1β production by TRM stimulates ILC-derived CSF2 promoting the survival of TRM. Further, CSF2 was shown to promote secretion of anti-inflammatory IL-10 by TRM and regulatory T cells (Mortha et al., 2014; Zigmond et al., 2014, 2012).

Commensals in the gut may also directly affect monocyte-to-TRM transition (Rooks and Garrett, 2016). In fact, bacterial butyrate, a short-chain fatty acid, was shown to promote an anti-inflammatory gene signature in TRM (Chang et al., 2014; Schulthess et al., 2019). Further, bacterial indole and tryptophan metabolites may skew TRM towards an anti-inflammatory gene expression signature through binding of the aryl hydrocarbon receptor, a transcriptional sensor (Zelante et al., 2013; Zhu et al., 2018). Lastly, Western high-fat diet is suspected to induce a pro-inflammatory response in monocyte progenitors in the BM (Christ et al., 2018).

While we have some insights on environmental factors that shape local gut TRM identities, less is known about how the differentiation process initiated by infiltrating monocytes is influenced by intrinsic or extrinsic factors. Given the central role of TF in imprinting TRM identity (Ginhoux and Guilliams, 2016; Lavin et al., 2014), TF likely also govern monocyte differentiation. In fact, it has been recently shown that the TF Mafb is critical for local monocyte proliferation prior to maturation into lung-resident macrophages (Vanneste et al., 2023). To investigate gut TRM differentiation, we therefore decided to focus on TF differentially expressed among ileal and colonic TRM (Gross-Vered et al., 2020).

The advent of the CRISPR/Cas9 approach has revolutionized biology and was righly awarded with a Nobel Prize for its discoverers (ref). CRISPR/Cas9 allowed the decryption of complex molecular pathway through genome-wide screens (Adamson et al., 2016; Chan et al., 2019; Quinn et al., 2021; Raj et al., 2018; Spanjaard et al., 2018), the study of developmental pathways of entire cell lineages (Jaitin et al., 2016; Weinreb et al., 2020), and the efficient and acurate generation of transgenic animals (Wefers et al., 2017). In recent years, immunological research has embraced the use of CRISPR/Cas9 screens to address multifactorial problems in a relatively affordable manner avoiding the generation of hundreds of transgenic mouse strains. CRISPR/Cas9 screens have primarily focussed on T cells as these cells can be easily grown in culture, transfected with sgRNA libraries, and transferred back into live mice for in vivo studies (Chen et al., 2021; Dong et al., 2019; Huang et al., 2021; LaFleur et al., 2019; Manguso et al., 2017; Shifrut et al., 2018). In contrast, as strictly tissue-resident cells with specific gene signatures related to their tissue-specific niches, however, macrophages cannot be cultured in vitro without a near-total loss of their tissue-specific gene signature (Bohlen et al., 2017; Gosselin et al., 2014).

Here, we studied the effect of the mutagenesis of multiple TF in monocytes on their differentiation into gut macrophages in a pooled *in vivo* CRISPR screen. Specifically, we adopted a chimeric approach (LaFleur et al., 2019), and isolated mutant graft-derived

macrophages from the intestines 4 weeks after HSC transfer. These cells were subjected to scRNAseq to study the effect of sgRNA-induced TF deficiency at the single cell level.

Results

Establishing the CHimeric IMmune Editing (CHIME) workflow

CHimeric IMmune Editing (CHIME) is a workflow developed in the Sharpe laboratory that introduces gene mutations specifically into HSC using the CRISPR/Cas9 technology (LaFleur et al., 2019) (**Fig 1A**). HSC were purified by sorting from the BM of mice expressing the Cas9 gene in the ubiquitously active H11 locus (Chiou et al., 2015). The sorted HSC fraction was defined by the absence of lineage markers (CD11b, CD19, TCRb, NK1.1, Ly6C/G, Ter119), high expression of CD117 (c-Kit) and Sca-1 (termed the LSK fraction, **Fig 1B**). Strictly speaking, this fraction includes short- and long-term HSC, as well as multipotent progenitors.

Sorted LSK were infected overnight with high-titer lentivirus bearing sgRNA (**Fig 1A**). Specifically, we used a five-plasmid lentiviral system established by our collaborator G. Mostoslavsky (Brown University, Boston). This system, entitled 'pHAGE', was previously shown to ensure high infection efficiency in murine HSC (Thomas and Mostoslavsky, 2014). and relies on the non-conventional inclusion of the HIV nef and rev virulence factors (**Fig 1C**). The resulting high lentiviral titers of 10^9 TU/ml were necessary to manipulate the notoriously hard-to-infect murine HSC (Mostoslavsky et al., 2005) (**Fig 1D**). Reassuringly, infection of LSK with high viral titers, ranging from 200 to 500 MOI, resulted in infection efficiencies of up to 30% of labelled peripheral blood cells 2 weeks after transfer, as determined by the expression of a GFP reporter (**Fig 1E**).

To use the pHAGE system in CRISPR screens, we cloned a *S. pyogenes*-derived hU6-sgRNA cassette into the 3'LTR of a ZsGreen-expressing transfer vector by transfer PCR (**Fig 1F**). This non-conventional transfer plasmid design was inspired by the CROPseq plasmid (Datlinger et al., 2017). The integration of the sgRNA cassette into the lentiviral 3'LTR results in the copy of the scaffold to the 5'LTR during lentiviral integration into the host genome. This leads to two functional copies of the sgRNA cassette being expressed (**Fig 1G**). Further, the orientation of the sgRNA cassette downstream of an EF1a promoter allows detection of the sgRNA sequence in scRNAseq as part of a polyadenylated Pol II transcript (Datlinger et al., 2017) (**Fig 1H**). We termed our modified transfer vector CR2pH (short for CROP2pHAGE).

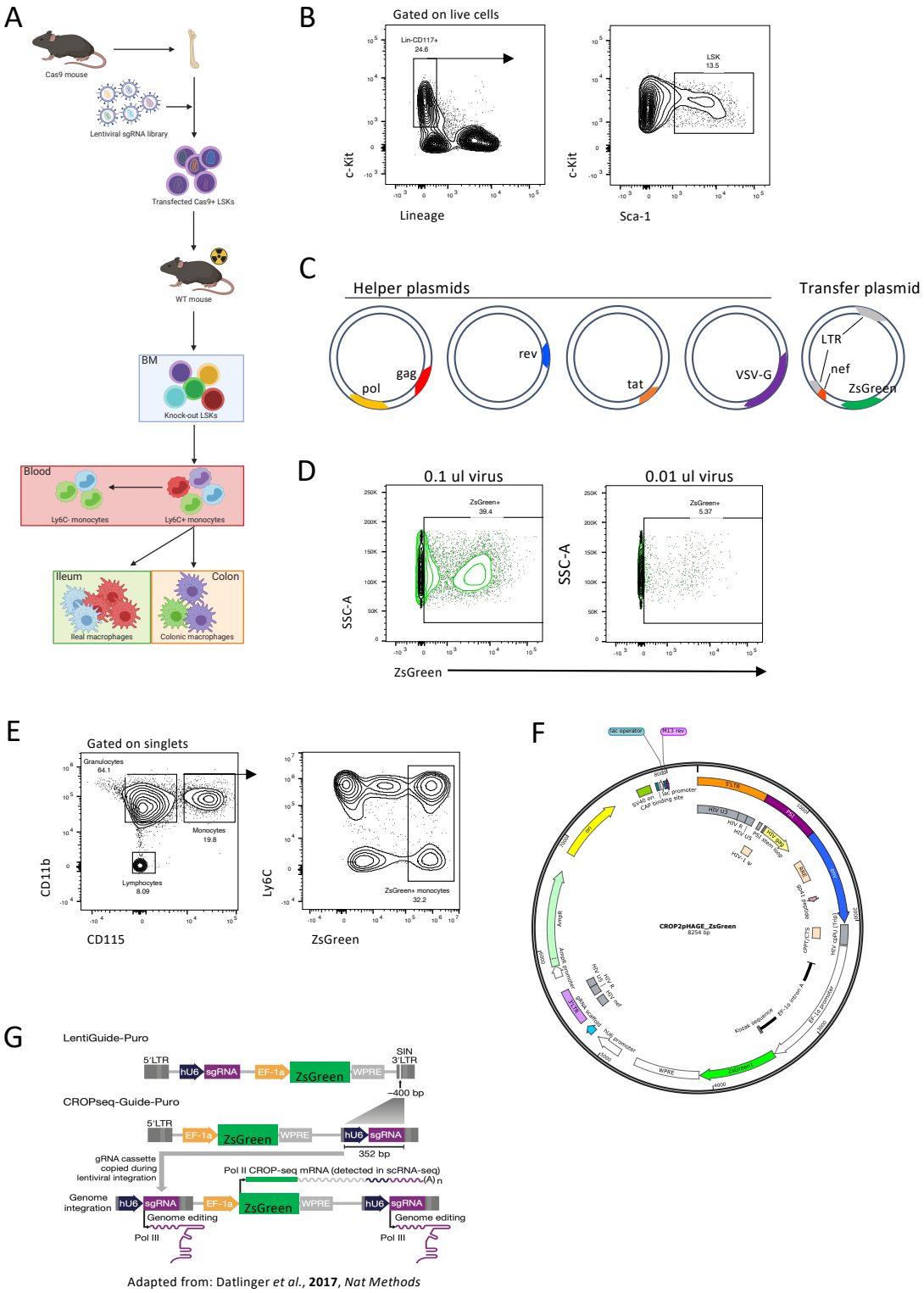

Figure 1: (A) Workflow for CHimeric IMmune Editing (CHIME). Briefly, Cas9-expressing HSC are purified and transfected with a sgRNA library prior to transfer into an irradiated host. Here, transfected HSC give rise to all immune cell lineages. (B) Representative plot for sorting of the LSK (Lineage-, cKit+, Sca1+) fraction in the BM. (C) Graphic depiction of the pHAGE lentiviral system from the Mostoslavsky lab. Addition of the HIV rev and nef elements, unlike in conventional lentivirus systems, increases viral titer. (D) Representative FACS plot of the titration of a lentiviral prep on HEK 293T cells. HEK cells were infected with 1, 0.1, or 0.01 ul of purified lentivirus. The titer in this case was 6.24e9TU/ml. (E) Representative FACS plot for assessing the transfection efficiency of blood cells 2 weeks after chimerism. (F) Vector map of the CR2pH plasmid. The sgRNA cassette

was cloned into the 3'LTR of the pHAGE2 vector. (G) Graphic depiction of the CROPseq method, adapted from Datlinger et al. (2017). The integration of the sgRNA cassette into the 3'LTR leads to its duplication at the 5' end of the lentiviral transcript during integration into the genome, resulting in two functional copies of the sgRNA being expressed. Additionally, the sgRNA sequence can be identified in the gene expression library of single-cell technologies due to its orientation downstream of the EF1a promoter.

Validation of the CHIME approach on blood monocytes

Murine CM are defined by expression of Ly6C, among other surface proteins (Geissmann et al., 2003; Guilliams et al., 2018). Ly6C is encoded by two adjacent loci, *Ly6c1* and *Ly6c2* that are >95% similar. Moreover, commercially available antibodies cannot distinguish the resulting surface receptors (Lee et al., 2013). Surface staining of Ly6C with the HK1.4 clone is highly reliable. Thus, it makes for an ideal target for validating CHIME on blood CM.

The sgRNA used in this study relied on the mouse CRISPR 'Brie' library (Doench et al., 2016). Importantly, all 4 sgRNA of the Brie library against *Ly6c2* target gene sequences shared by the *Ly6c1/2* loci. The 4 a*Ly6c2* sgRNA were cloned into the CR2pH vector bearing a ZsGreen tag. In parallel, 4 scrambled, non-targeting sgRNA were cloned into a tdTomato-encoding CR2pH plasmid. Finally, LSK were co-infected with both viruses.

Two weeks following transfer, 7% of $CD115^{+}CD43^{-}$ CM were labelled in the recipient animals. The resulting cellular compartment consisted of 3 cell fractions: 1) ZsGreen-labelled cells with a presumable *Ly6c2* KO, 2) tdTomato-labelled cells equipped with a non-targeting sgRNA, and 3) non-infected WT cells serving as an internal control (**Fig 2A**). Analysis of Ly6C surface expression on these three fractions validated impaired surface Ly6C expression solely on $ZsGreen^{+}$ cells. (**Fig 2B**). This result was observed in 2 out of 5 recipients. Blood neutrophils of the same animals displayed slightly higher KO efficiency (**Fig 2C,D**).While the underlying reason for this discrepancy remains speculative, it might hint at a more sensitive DNA damage response in monocyte precursors. Altogether, however, we demonstrated the efficient deletion of cell surface molecules on short-lived CM and neutrophils by the CHIME approach.

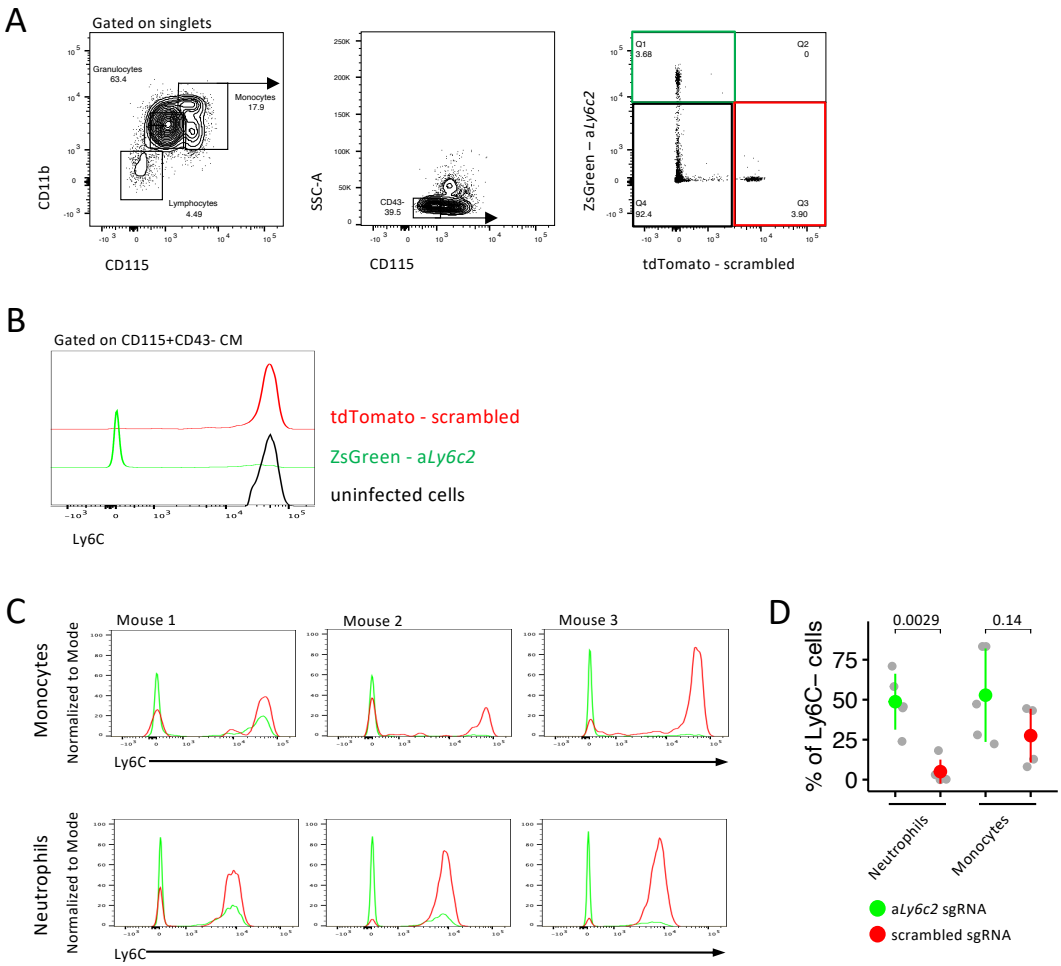

Figure 2: (A) LSK were co-infected with a ZsGreen+ lentivirus targeting *Ly6c2*, and a tdTomato+ lentivirus bearing scrambled sgRNA. Blood analysis 2 weeks after revealed 3 fractions of CD43- CM: green labelled, red labelled, and unlabelled cells. (B) Histogram for Ly6C surface expression on CM of different cell fractions. ZsGreen-labelled cells were devoid of Ly6C expression while tdTomato+ and uninfected cells displayed high Ly6C signal. (C) Biological repeats of *Ly6c2*-targeted and scrambled untargeted cells. Neutrophils displayed higher KO efficiency compared to CM. (D) Statistical analysis of *Ly6c2* KO efficiency on blood neutrophils and CM.

Validation of CHIME on gut macrophages

Next, we intended to manipulate monocyte-derived gut macrophages by targeting the well-studied TF Nr4a1 which is a macrophage survival factor (Hanna et al., 2011; Thomas et al., 2016). Hence, LSK were co-transfected with 2 viruses, a ZsGreen^{+} virus bearing scrambled, non-targeting sgRNA, and a tdTomato^{+} virus targeting *Nr4a1* (4 sgRNA each). Five weeks after HSC transplantation, 10% of CD45^{+} hematopoietic cells in the small intestine were found labelled (**Fig 3A**).

Importantly, the tdTomato^{+} cell fraction was devoid of mature MHC-II^{+} macrophages (located in the 'water fall' P3 gate). Conversely, the ZsGreen^{+} fraction showed an

uncompromised macrophage population (**Fig 3B**). Altogether, we demonstrated the use of CHIME for targeting TF in monocyte-derived gut macrophages.

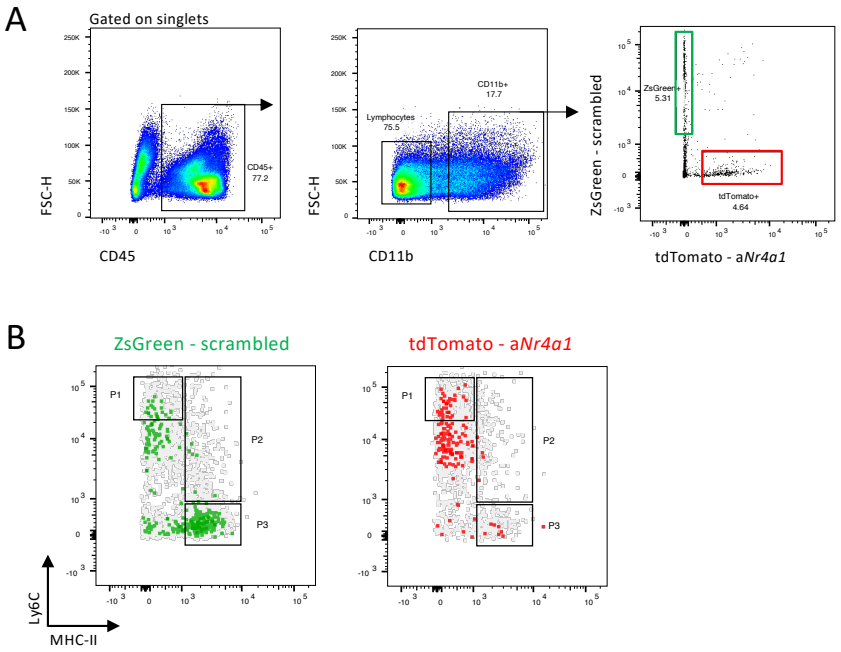

Figure 3: (A) LSK were co-transfected with ZsGreen+ and tdTomato+ viruses bearing scrambled, non-targeting and *Nr4a1*-targeting sgRNA, respectively. 10% of myeloid cells were labelled in the small intestine 5 weeks after chimerism. (B) Density plots of ZsGreen- and tdTomato-labelled myeloid cell populations plotted for Ly6C against MHC-II. P1 and P2 gates represent differentiating monocytes whereas the P3 gate contains mature macrophages.

Inclusion of the 10X capture sequence in the CR2pH vector

Prior to designing the pooled CRISPR screen, we decided to clone the 10X capture sequence 1 (CS1) into the CR2pH vector. This was meant to allow the implementation of a newly 10X Genomics CRISPR workflow. Here, the CS1 in the sgRNA scaffold binds to a complementary sequence on the gel beads of the Chromium platform, allowing for a direct library construction of sgRNA (Replogle et al., 2020) (**Fig 4A**).

First, the CS1 was cloned into the hairpin 1 of the sgRNA scaffold (CR2pH_10Xh) (**Fig 4B**). The KO efficiency with this new construct was evaluated by co-infecting LSK with green a*Ly6c2* CR2pH_10Xh and a red scrambled CR2pH_10Xh. However, no KO of Ly6C could be observed on either CM or neutrophils 2 weeks after chimerism compared to scrambled (**Fig 4C**). Thus, the integration of CS1 into the hairpin 1 likely prevented efficient binding of the sgRNA to the enzyme, thereby reducing editing efficiency. We therefore proceeded to clone the CS1 into the 3' end of the sgRNA scaffold (CR2pH_10Xe) (**Fig 4D**). This time, LSK were co-transfected with ZsGreen+ CR2pH_10Xe and tdTomato+ CR2pH vectors, both bearing

Ly6c2-targeting sgRNA. Two weeks after generation of the chimeras, KO efficiencies were compared on ZsGreen^{+} and tdTomato^{+} CM and neutrophils. Despite low cutting efficiencies, the CR2pH_10Xe vector had a tendency toward higher efficiency in CM (**Fig 4E**). Altogether, we hence deemed the CR2pH_10Xe vector not to be signifantly inferior to the original CR2pH vector and decided to adopt it for the pooled CRISPR screen.

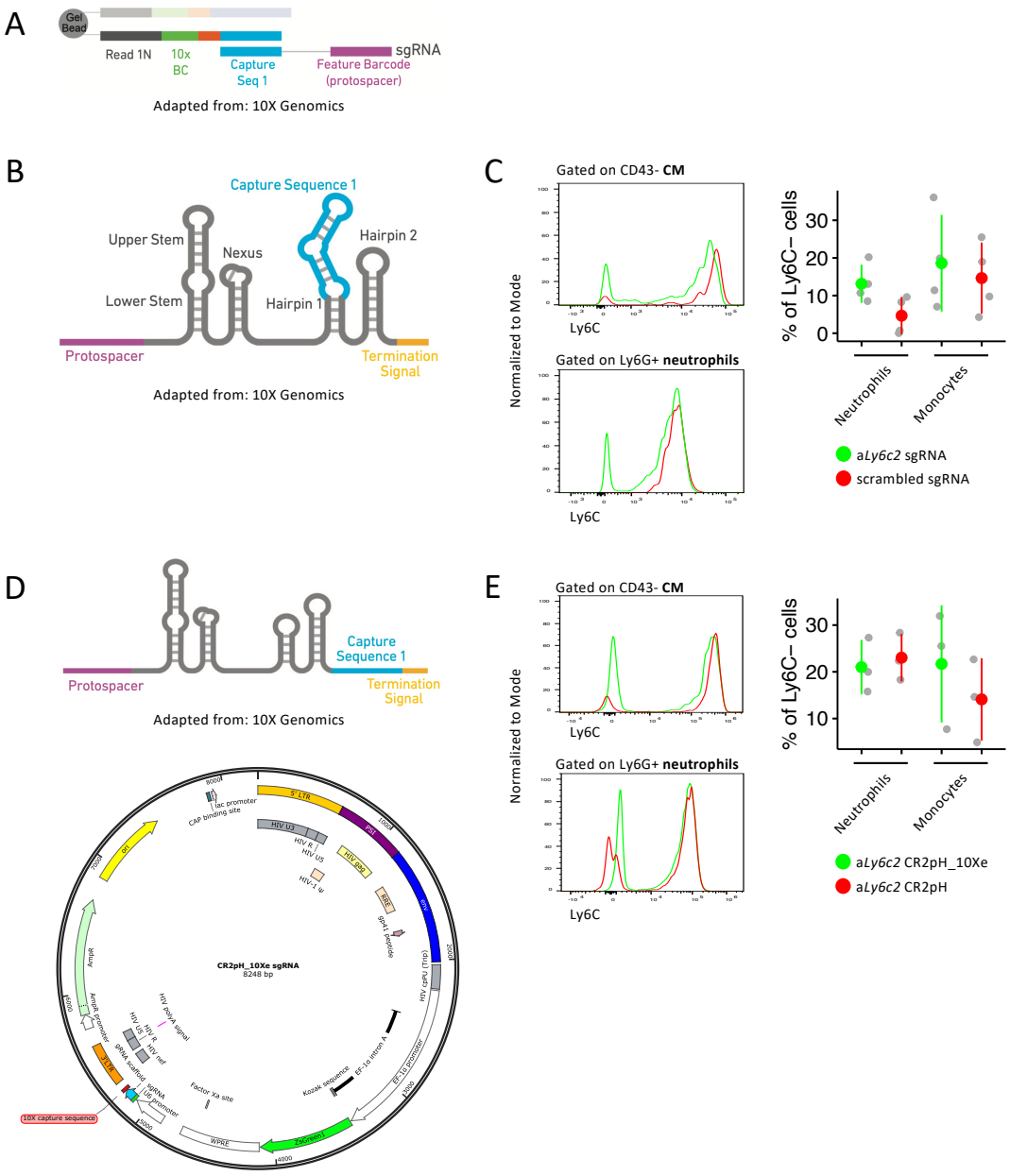

Figure 4: (A) The capture sequence 1 (CS1) expressed as part of the sgRNA scaffold binds to a complementary sequence on the gel beads of the Chromium platform. This allows for direct pull down of the sgRNA which can prepared as a separate library. (B) Integration of the CS1 into the Hairpin 1 of the sgRNA scaffold (CR2pH_10Xh). (C) Assessing KO efficiency using the CR2pH_10Xh sgRNA scaffold by KO of Ly6C. No difference was observed compared to scrambled. (D) Integration of the CS1 into the 3' end of the sgRNA scaffold (CR2pH_10Xe). (E) Assessing KO efficiency using the CR2pH_10Xe sgRNA scaffold in comparison to the unmodified CR2pH plasmid. Equal KO efficiencies were observed.

Targeting ileum- and colon-specific TF in gut macrophages by a pooled CRISPR screen

We have recently published transcriptional differences between ileal and colonic macrophages (Gross-Vered et al., 2020). Hence, the question arose how these differences manifest themselves. TRM in both gut compartments share the same precursor, blood-borne CM. Since TF can be predicted to imprint tissue-specific macrophage gene signatures (Lavin et al., 2014), 5 TF unique to ileal and colonic macrophages, respectively, were selected for mutagenesis. TF were chosen according to three criteria: 1) high and increasing expression in the differentiation process, 2) differential expression in colonic and ileal TRM in normal mice, and 3) absence of expression in blood CM. The chosen TF matching these criteria are shown in **Fig. 5A**. The sgRNA library consisted of 4 sgRNA/gene as well as 4 scrambled, non-targeting sgRNA. All sgRNA sequences were adapted from the Brie library (Doench et al., 2016). In total, 44 sgRNA were cloned into the CR2pH_10Xe vector. Thus, a coverage of 200 was expected, assuming that all sgRNA would be equally represented for each 10'000 cells collected for scRNAseq.

Cas9-expressing LSK were infected with the sgRNA library at 500 MOI. 2 weeks following transfer, a high infection efficiency of up to 30% was observed in peripheral blood cells (**Fig 1E**). Mice were sacrificed 4 weeks after transfer, and ZsGreen^{+} sgRNA-transduced monocyte-derived gut macrophages were sorted to purity according to the reporter gene expression as well as CD64 and Cx3cr1 surface expression. Two samples from each organ were loaded onto the Chromium chip. The 10X workflow using v3.1 chemistry and the Feature Barcode technology for CRISPR screening was followed according to the manufacturer's instruction.

A total of 8'428 cells from the colon and 2'445 cells from the ileum were analyzed after QC (**Fig 5B**). Expectedly, the majority of cells were annotated as macrophages and monocytes (**Fig 5C**). Further, ileal macrophages were found enriched in expression of *Mmp9*, akin to our previously published bulk RNAseq dataset (Gross-Vered et al., 2020) (**Fig 5D**). In summary, the retrieved gene expression data from ileal and colonic macrophages were of high quality and in line with previous published data.

Surprisingly, the pull-down of the sgRNA to the gel beads was unsuccessful. Rather, the Chromium CRISPR library construction resulted in a Tapestation peak of approx. 250 bp across all samples, 50 bp short of the expected result (**Fig 5E**). Nonetheless, the sgRNA libraries were sequenced. However, solely polyA sequences were retrieved. Following consultation with the 10X team, we assume that the presence of the CROPseq feature interfered with efficient binding of the CS1 to the gel beads.

Lastly, only few sgRNA sequences originating from the CROPseq feature could be identified in the gene expression library. Instead, the sequence comprised only the LTR of the lentiviral transcript, due to an additional 150 bp in the 3'LTR of the pHAGE vector system compared to conventional lentivirus systems such as the original CROPseq vector (**Fig 5F**). Thus, ironically, the inclusion of the HIV nef factor, enabling high titers, impeded the sequencing process to reach the sgRNA sequences on the NovaSeq system. Concluding, barely any sgRNA could be assigned to cells. This forced us to pursue other ways of retrieving the sgRNA sequences from our samples.

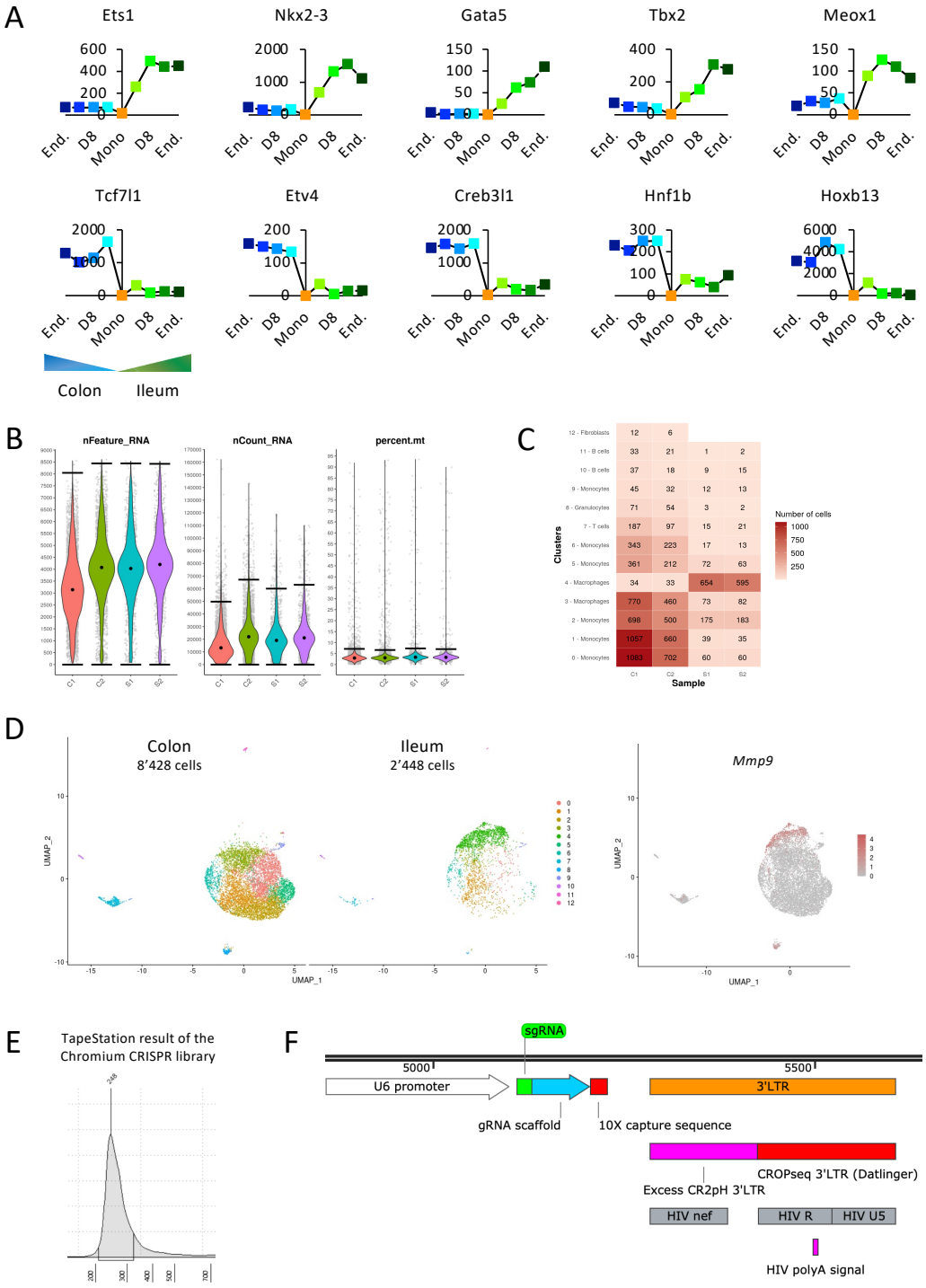

Figure 5: (A) 5 TF specifically expressed in either ileal or colonic macrophages, respectively, were chosen for a pooled CRISPR screen. (B) Quality Control parameters from the 10X experiment on sorted ileal (samples S1, S2) and colonic macrophages (samples C1, C2). Sorted cells were of high quality as reflected in high RNA counts and low percentage of mitochondrial genes. (C) CellRanger classification identified most of the cells as macrophages or monocytes. (D) UMAP of sorted cells from colon and ileum. The ileal cluster displayed high *Mmp9* expression, in line with previously published bulk RNAseq data (Gross-Vered *et al.*, 2020). (E) Representative TapeStation results of the Chromium CRISPR library from our experiment. The product was 50 bp short of the expected result. (F) Scheme showing the 3'LTR of the CR2pH_10Xe vector. The 3' LTR of this specific vector (orange) is longer than the 3'LTR of conventional vectors used for CROPseq (red). This prevented the sequencing to reach the sgRNA (green). Instead, excess LTR (pink) was sequenced.

Retrieving sgRNA sequences from the unfragmented 10X cDNA

Up to 65% of cells could be assigned a sgRNA in the original CROPseq method (Datlinger et al., 2017). To increase the retrieval rate, targeted PCR strategies have been developed that amplify sgRNA sequences from the unfragmented cDNA of scRNAseq technologies (Hill et al., 2018). Recently, a similar protocol has been reported for the 10X v3.1 chemistry (Alda-Catalinas et al., 2021). Specifically, in this three-round semi-nested PCR strategy a primer anneals to the U6 promoter and the Read 1 introduced by the first step of the 10X workflow in a first reaction. Following SPRI clean-up, a second PCR primes right upstream of the sgRNA cassette, introducing the Readd 2 as well as annealing the P5 to the Read 1. Finally, the P7 index is introduced by a third PCR (**Fig 6A**).

At first, we were unable to implement this protocol successfully. Of note, we used the Q5 polymerase from NEB. Our protocol consistently failed at the third PCR. We suspected that the LTR might pose a challenge to polymerase activity due to its high GC content and palindromic repeats. To circumvent this issue, we circularized the second PCR product by phosphorylation and ligation (**Fig 6B**). This would allow to anneal primers to the outer edges of the LTR region and exclude the LTR in the amplification process. New Read 1 and Read 2, and P5 and P7 sequences were annealed to the resulting amplicon in one more PCR step (**Fig 6C**). However, sequencing of the final PCR product revealed a bias in amplification. Further, the presence of two Read 1 sequences lowered the coverage. Altogether, this unusual approach didn't pay off.

Next, we decided to give the Alda-Catalinas protocol another go. This time, we used the KAPA HiFi polymerase as advocated for in the protocol (Alda-Catalinas et al., 2021). Importantly, this small modification proved crucial and we ended up with a peak of the right size (**Fig 6D**). Sequencing of the PCR product proved successful albeit a bias towards certain sgRNA was still present (**Fig 6E**). In total, roughly one third of cells had a sgRNA assigned to them (**Fig 6F**). Further rounds of amplification should even out any amplification bias.

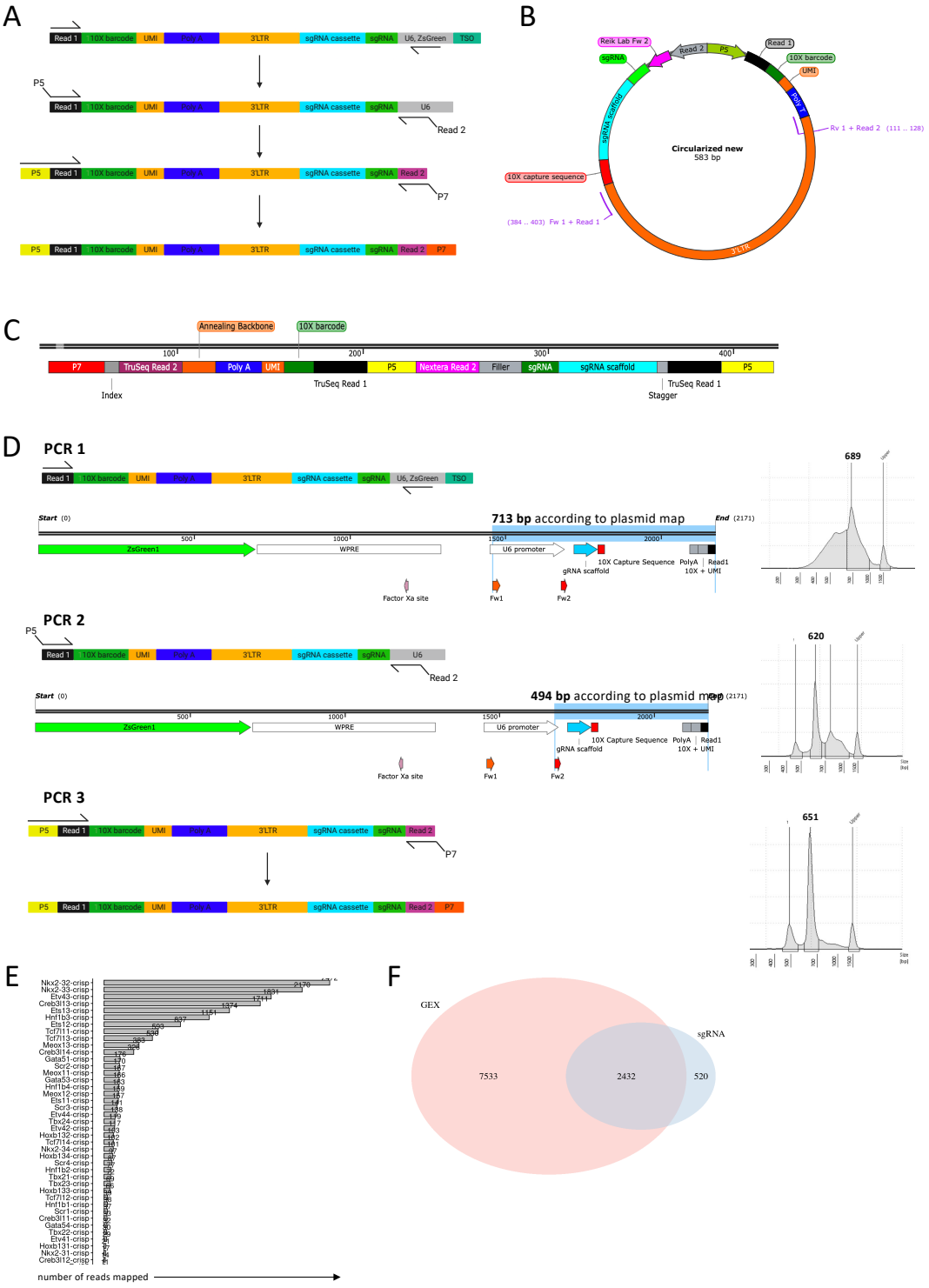

Figure 6: (A) Hemi-nested PCR strategy to specifically amplify sgRNA sequences from the non-fragmented cDNA of the 10X workflow. In a first step, the cDNA is amplified from the U6 onwards. A second PCR primes upstream of the sgRNA cassette, adding a TruSeq Read 2 and the P5 to the Read 1. In a last amplification, the P7 index is added to the Read 2. (B) Circularization off the second PCR product from the sgRNA amplification. Primers annealing the outer edges of the LTR are depicted in magenta. (C) PCR product of the amplification of the non-LTR region of the circularized product. (D) PCR products of each of the 3 steps of the hemi-nested PCR to amplify sgRNA sequences after successful amplification. Tapestation results are included. Deviations from the plasmid map are due to the primer sequences, not included in the plasmid map. (E) All sgRNA detected in sequencing of the final PCR product. Overrepresentation of some guides can be explained by an amplification bias. (F) Mapping of sequenced sgRNA to cells from the GEX showing cells with sgRNA assigned.

Shared features among macrophages that harbor TF deficiencies in ileum and colon

Roughly one third of cells from the gene expression matrix (GEX) could be assigned a sgRNA (**Fig 6F**), most of which were of colonic origin (**Fig 7A**), regardless of whether the sgRNA targeted colon- or ileum-specific TF. This was to be expected as more colonic than ileal macrophages were subjected to scRNAseq (**Fig 5D**). Further, *Nkx2-3* targeting sgRNA were overrepresented whereas others were only sparsely represented, such as Gata5, Tbx2, or Meox1 targeting sgRNA. Ileum-specific TF-targeting sgRNA were comparatively well represented in individual cells except for Hoxb13-targeting sgRNA. The low number of sgRNA mapped to ileal cells is most likely due to the lower number of cells retrieved from that compartment (**Fig 5D**). Of note, scrambled sgRNA (Scr) were barely identified (**Fig 7A**).

After comparison of cells from the same compartment for discrepancies among targeting and non-targeting sgRNA, very few DEG were detected (**Fig 7B**). Of note, very few DEG were detected in ileal cells, regardless of targeted TF. Similarly, colon macrophages also showed very little effect upon mutagenesis of most TF. Curiously, the ileum-specific TF Nkx2-3 showed the most profound knock-out effect in colonic cells (**Fig 7B**). The comparatively high number of DEG was most likely due to the high number of cells targeted by said sgRNA from the large intestine (**Fig 7A**).

To understand which genes might be specific to knock-out effects of each sgRNA family, we first had a look at shared genes. A gene was considered to be shared or unspecific if present in at least two comparisons. Gathering all differentially expressed genes from each compartment between TF-targeting and non-targeting sgRNA revealed 5 commonly expressed genes upon KO in ileal cells, compared to 7 shared features in colonic cells, excluding the effect of Nkx2-3 in colonic cells (**Fig 7C**). Of note, most of these genes were exclusive to either compartment (**Fig 7D**). To understand the nature of these genes, we looked for their expression in our previously published dataset on long-term resident colonic and ileal macrophages (Gross-Vered et al., 2020) (**Fig 7E**). Indeed, the vast majority of these genes were highly expressed in resident colon and ileum MF. Thus, targeting these 10 TF resulted in a loss of intestinal macrophage identity. Alternatively, this set of commonly altered genes might be a result of lentiviral transduction of HSC.

Concluding, very few DEG could be identified between TF-targeted and non-targeted individual cells from the same compartment. An analysis of TF-targeted cells with few DEG revealed that, indeed, intestinal macrophage genes were down-regulated for the most part.

A

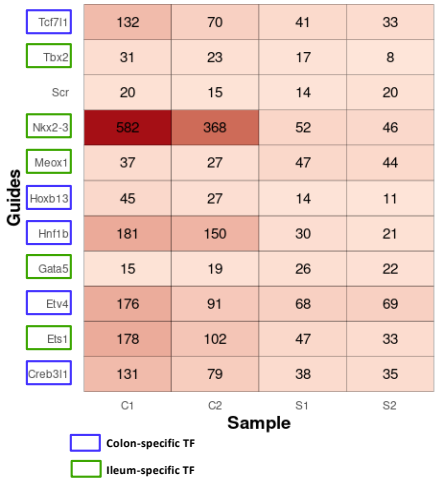

B

Number of DEG per sgRNA family in each sample (C, colon; S, ileum)

	up	down		up	down
Nkx2-3_S	0	2	Etv4_S	0	11
Nkx2-3_C	37	36	Etv4_C	0	2
Ets1_S	3	7	Hnf1b_S	0	2
Ets1_C	0	5	Hnf1b_C	1	7
Gata5_S	0	0	Creb3l1_S	0	0
Gata5_C	0	0	Creb3l1_C	4	8
Meox1_S	0	0	Tcf7l1_S	0	0
Meox1_C	0	0	Tcf7l1_C	0	0
Tbx2_S	0	0	Hoxb13_S	0	0
Tbx2_C	0	0	Hoxb13_C	0	0

C

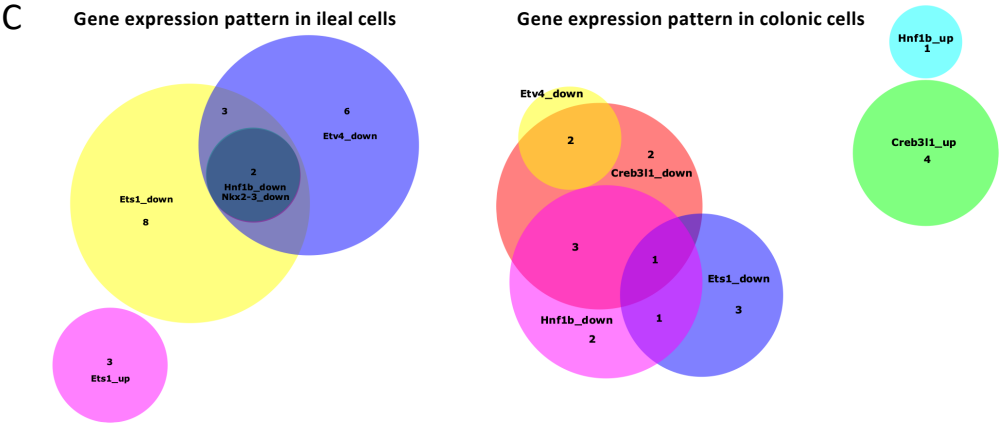

D

Genes shared among at least 2 samples at once

Ileum-expressed DEG	Colon-expressed DEG	Shared
Cd63	Apoe	Adam19
Mmp9	C1qc	C1qa
Npl	Lrrc4c	Pmepa1
Pla2g2d	Ms4a7	Ptgs1
	Pianp	Slco2b1
	Pkm	
	Reps2	
	Rhobtb1	
	S100a11	
	Tanc2	
	Tmem37	
	Tspo	

E

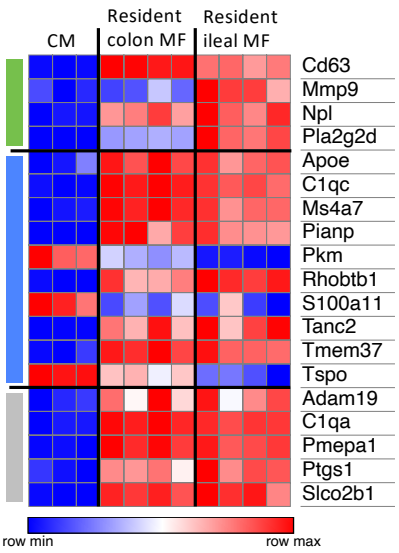

Figure 7: (A) Number of cells mapped to each sgRNA family. Cells with more than 1 sgRNA mapped to were excluded from the analysis. (B) Number of DEG for each targeted TF compared to scrambled in cells from each compartment. (C) Venn Diagrams of all DEG in each compartment except for Nkx2-3 targeted colon macrophages (D) List of DEG shared among at least 2 samples at once. (E) Heatmap of shared DEG in the CRISPR screen in the Gross-Vered *et al.* dataset on colonic and ileal macrophages.

Investigating the biological effect of TF ablation in ileal and colonic macrophages

Having identified commonly regulated genes, we asked ourselves which genes were specific to the knock-outs mediated by each sgRNA family.

Etv4 (ETS translocation variant 4) is a transcriptional activator belonging to the Ets family of TF (first ref uniprot). It was specifically expressed in colonic MF (Gross-Vered et al., 2020). The TRRUST database lists *Mmp9*, *Tgfbr2*, and *Ptgs2* as target genes, a.o. Of note, *Mmp9* was identified as ileal MF-specific gene (Gross-Vered). Curiously, Tgfbr2 mediates TGF-b signalling which is indispensable for tissue-specific differentiation of monocytes into colonic macrophages (Schridde et al., 2017). Lastly, prostaglandin synthases (encoded by *Ptgs2* a.o.) were shown to be upregulated in Il10ra-deficient macrophages which mediate colitis in mice (Zigmond et al., 2014). Interestingly, the effect of Etv4-targeting sgRNA manifested itself solely in ileal macrophages (**Fig 8A**). However, Etv4 was also shown to be upregulated early in tissue-specific differentiation into ileal macrophages (**Fig 8A**). Two genes (*Rhobtb1* and *C1qa*) were downregulated in colon MF. Conversely, ileal MF showed downregulation of the Etv4 target *Mmp9*. Further, *Pla2g2d*, belonging to the phospholipase A family was downregulated. Importantly, members of this enzyme family mediate the first steps of *Ptgs2*-mediated prostaglandin synthesis (Zigmond et al., 2014). However, *Pla2g2d* was prominently downregulated in ileal MF among many sgRNA families (**Fig 7D**). Moreover, *Prxl2a* was downregulated, which was described as a negative regulator of MF-mediated inflammation *in vitro* (Guo et al., 2015).

Creb3l1 (cyclic AMP-responsive element-binding protein 3-like protein 1) is a TF involved in DNA damage and unfolded protein response (Saito et al., 2023). Its precursor form is reported to be located in the endoplasmic reticulum (ER) membrane. It was specifically expressed in colonic MF in our dataset (Gross-Vered et al., 2020) (**Fig 8B**). A total of 11 genes were differentially expressed in colonic MF compared to sgRNA. Notably, only *Tspo* and *Sh3bgrl3* were uniquely upregulated in this knock-out. *Tspo* encodes a translocator protein in mitochondrial membranes, presumably involved in cholesterol transport (Li and Papadopoulos, 1998). Sh3bgrl3 is a cytosolic protein predicted to modulate glutaredoxin activity and cytoskeleton organization. No apparent relation to Creb3l1 could be inferred. Further, no effect was observed in ileal cells.

Hnf1b (hepatocyte nuclear factor 1-beta) is a colon MF-specific TF. 10 genes were differentially expressed in both compartments compared to sgRNA, the vast majority in Hnf1b-targeted colonic MF (**Fig 8C**). 8 of these genes were shared with other samples, such as *Apoe*

in the colon and *Pla2g2d* in the ileum. *Rnf227* and *Rpl36a* were unique to Hnf1b-targeted cells in the colon. The former is a sparsely studied RINF finger protein associated with protein ubiquitination in the UniProt database. The latter is a component of the large ribosomal subunit (Li et al., 2022).

Ets1 (protein C-ets-1) is a TF exclusive to ileal macrophages and and supposedly controlling the expression of cytokine and chemokine genes such as *Il10* and *Ccl2* as predicted by similarity (TRRUST, UniProt databases). Further, it is associated with transcriptional control of *Mmp9* and *Csf1r* a.o., downregulated in Ets1-targeted ileal macrophages (**Fig 8D**). Other downregulated genes in the ileum included *Ptgs1* and the classical macrophage scavenger receptor *Msr1*. *Stab1*, encoding the scavenger receptor stabilin-1, was also downregulated. Of note, upregulated genes were all associated with ribosome biology (*Rpsa, Rpl15, Rplp0*). Interestingly, all colon genes were shared with other knock-outs. Thus, Ets1-mediated effect seemed to be restricted to ileal macrophages.

Finally, Nkx2-3 (homeobox protein Nkx-2.3) is a TF associated with Crohn's disease (Kellermayer et al., 2019; Yu et al., 2012, 2010). Further, it was specifically expressed in ileal macrophages in our dataset (Gross-Vered et al., 2020) (**Fig 8E**). However, and most interestingly, the effect of its knock-out was restricted to colonic cells. This might hint at a crucial role of this gene in the generation of colonic macrophages. Of note, most cells from all samples were mapped to Nkx2-3 sgRNA (**Fig 7A**). A total of 73 genes were differentially expressed in colonic cells. Metascape analysis revealed downregulation of pathways involved in the 'negative regulation of leukocyte differentiation' and 'antigen processing and presentation' as evidenced by lower expression if *Cd74* and *H2-Eb1*. Upregulated pathways included 'positive regulation of cytokine production' such as *Mif* and 'regulation of apoptotic cell clearance'.

Concluding, a true biological effect could only be demonstrated for knock-out of Nkx2-3 due to the low number of differentially expressed genes in other sgRNA families. However, Etv4 and Ets1 could also be shown to have an effect on macrophages given the downregulation of target genes such as *Mmp9* and *Csf1r*. Lastly, Etv4 and Nkx2-3 seemed to have their effect in the compartment in which they were lowest expressed in endogenous gut macrophages.

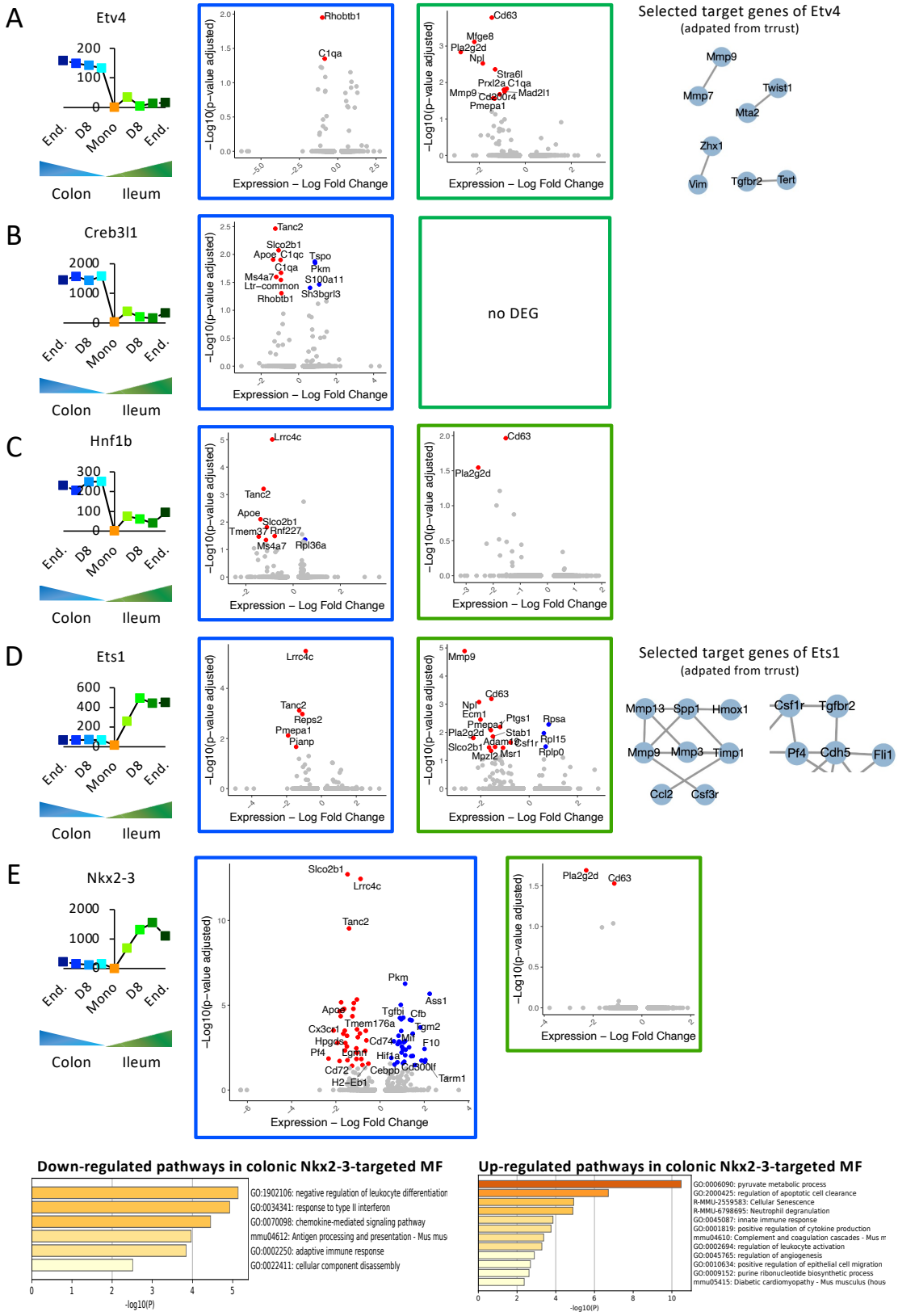

Figure 8: (A) Volcano plots of Etv4-targeted ileal and colonic MF. (B) Volcano plots of Creb3l1-targeted ileal and colonic MF. (C) Volcano plots of Hnf1b-targeted ileal and colonic MF (D) Volcano plots of Ets1-targeted ileal and colonic MF. (E) Volcano plots of Nkx2-3-targeted ileal and colonic MF.

Discussion

One of the main known function of CM is the differentiation into TRM to replenish the short-lived fraction of the gut macrophage compartment (Guilliams et al., 2018). add Bain et al, Varol et al). Given that gut macrophages are major players in gut homeostasis (Mortha et al) and inflammatory bowel disorders (IBD) (Zigmond et al., 2014), in depth understanding of monocyte differentiation in this tissue is of major interest, though remains incompletely understood. This includes extrinsic and intrinsic factors governing the transition from monocytes to gut macrophages. We have previously shown that ileal and colonic monocyte-derived TRM are transcriptionally distinct (Gross-Vered et al., 2020). This included several TF that were differentially upregulated during CM differentiation in either gut compartment (Gross-Vered et al., 2020), which are likely to play a pivotal role for establishing tissue-specific expression signatures of monocytic derivatives.

CM are highly plastic cells and rapidly undergo vast transcriptional changes when entering peripheral tissues (Guilliams et al., 2018). This renders their study notoriously difficult in a tissue-context in both inflammation and homeostasis. To circumvent this issue, and to study multiple TF at once, we decided adopt a model involving BM chimeras combined with *in vivo* CRISPR screening, the CHimeric IMmune Editing approach (LaFleur et al., 2019). We were able to achieve high infection efficiencies of HSC thanks to the pHAGE lentiviral system (Thomas and Mostoslavsky, 2014). Up to 30% of peripheral blood cells were labelled although infection efficiency varied depending on the lentiviral titer.

We validated our approach in blood-borne CM by mutagenesis of the cell surface molecule Ly6C, a canonical CM marker (Geissmann et al., 2003; Guilliams et al., 2018). Mutagenesis efficiency was reasonable in CM compared to a scrambled control, though surprisingly constantly more efficient in neutrophils. We presume that monocytes might have tighter DNA repair control mechanisms that could explain this variation. It might be that monocytes but not neutrophils with a double-strand break in their DNA might undergo apoptosis.

Further, we validated our approach in gut TRM by impairing expression of Nr4a1, a TF that governs macrophage survival (Hanna et al., 2011; Thomas et al., 2016). Indeed, monocytes carrying *Nr4a1*-targeting sgRNA failed, as compared to wt monocytes, to give rise to mature MHC-II^{+} macrophages in the gut of the chimeric animals. This result corroborates the importance of Nr4a1 for the generation of gut TRM.

Once the CHIME approach was established, we proceeded with a pooled CRISPR screen with a total of 44 sgRNAs against 10 ileum- or colon-specific TF that we had previous

identified (Gross-Vered et al., 2020). The gene expression library was of high quality. However, barely any sgRNA could be mapped to gene expression matrices by neither the 10X CRISPR model nor the CROPseq feature. Feedback from the 10X team revealed that the sgRNA sequence in the CROPseq transcript most likely interfered with the binding of canonical sgRNA to the gel beads of the Chromium platform and the inclusion of the HIV nef feature in the 3'LTR of the pHAGE vector system impeded the sequencing platform to reach the sgRNA sequence in the gene expression library after fragmentation.

We then adopted a previously published protocol to amplify the sgRNA sequences from the unfragmented, full-length cDNA library of the 10X workflow. Eventually, sgRNA sequenced could be retrieved and mapped to gene expression matrices. However, only one third of cells could be mapped to a sgRNA. This was most likely due to an amplification bias. However, one cannot exclude that the mapped distribution reflects the *in vivo* distribution as we cannot know which and how many HSC contributed to the repopulation of the recipient's immune system at the time of retrieval of the cells. Future rounds of amplification should elucidate that question.

Another issue that might be solved by further amplification rounds is the low coverage of scrambled sgRNA, which were as non-targeting sgRNA meant to serve as a control to each targeting sgRNA family. Yet, collectively and for reasons unknown, barely 50 cells have been mapped to scrambled sgRNA in our experiment so far. It will be vital to the nature of the experiment to increase this number, since only a conclusive comparison to scrambled sgRNA will help to decipher genes specifically affected by the targeting sgRNAs. This is further evidenced by the high number of shared genes among colonic and ileal samples across all sgRNA families.

Importantly, and corroborating the successful implementation of CHIME on monocyte-derived macrophages, Cas-9 transgenic monocytes that expressed sgRNAs targeting the TF Ets1 and Etv4 and showed a reduction of a predicted targets of these TF, notably *Mmp9* and *Csf1r*. Targeting Nkx2-3 resulted in the most DEG, due to the high number of cells targeted with this sgRNA family. Multiple biological pathways seemed to be directly affected by this gene knock-out, most notably antigen processing and presentation. Further, macrophage marker genes such as *Cx3cr1* and *Pf4* were downregulated upon Nkx2-3 knock-out.

Interestingly, while most TF knock-outs seemed to have the most profound effect, as measured by number of DEG, in the compartment where they were highest expressed, targeting of Nkx2-3 and Etv4 had an opposite effect. Knock-out of Etv4, higher expressed in colon MF, seemed to have a major effect in ileal, but not colonic macrophages. Of note, Etv4 was higher

expressed in ileal macrophages in early phases of tissue adoption compared to later phases (Gross-Vered et al., 2020). Further, the early ileal graft clustered with the colonic one, suggesting that a colonic signature might be the default for infiltrating monocytes regardless of gut compartment (Gross-Vered et al., 2020). Of note, Creb3l1 and Hnf1b expression follows a similar pattern. However, no effect was recorded in ileal macrophages for targeting of these TF in this screen. Thus, Etv4 might play a pivotal role in the adoption of an ileal MF signature in the early phases of differentiation.

Conversely, targeting of Nkx2-3 had a major effect on colonic macrophages but not ileal ones where it is higher expressed (Gross-Vered et al., 2020). This might suggest that ileal macrophages vitally depend on Nkx2-3 to adopt their tissue-specific identity. Of note, however, almost 100 ileal MF could be mapped to Nkx2-3 targeting sgRNA. Thus, it is likely that gene regulatory networks associated with Nkx2-3 might have exerted a compensatory effect in the ileum but not in the colon.

Importantly, given the comparatively low coverage of single-cell technologies, only few genes were differentially expressed after all bioinformatic filtering and correction steps. This prevented the ultimate validation of the screen, i.e. the downregulation of the targeted TF. Further, low number of DEG prevented validation at the level of the target genes in all but two cases. This issue might have been avoided by sequencing at a greater depth than advocated for by the 10X guidelines.

Another explanation for the low number of DEG might be compensatory activity by related TF. For example, Ets2 belongs to the same family as Ets1, thus sharing target genes such as *Csf1r* (TRRUST database). Further, especially in the case of Creb3l1, whose inactive form is part of the ER membrane, protein-protein interactions might have a much larger biological effect than could be identified by scRNAseq. An indel by sgRNA might lead to an altered transcript that, upon successful translation, could have an aberrant conformation preventing its integration into the ER membrane. Similarly, TF might still be translated but the presence of specific indels might impede it from binding their cognate DNA sequence.

Finally, no DEG could be identified for a number of TF (Gata5, Meox1, Tbx2, Tcf7l1, Hoxb13), specific to either gut MF compartment. While this might be a bioinformatic bottleneck simply due to low number of cells containing these sgRNA, it could well be a biological consequence. These TF are poorly characterized in the hematopoietic system and one cannot exclude their expression in early precursors of monocytes. Thus, their effect might have been mediated long before the generation of monocytes, an effect that is masked by the design of the experiment. This could have been prevented by isolation of barcodes (sgRNA

sequences) from mature monocytes in the blood. Here, no effect of Cas9 mutagenesis was to be expected as none of the chosen TF were expressed in monocytes (Gross-Vered et al., 2020). Thus, absence of barcodes in mature monocytes would likely hint at an effect restricted to the BM.

In summary, we have established that the CHIME approach can be used to study monocyte differentiation into gut macrophages and demonstrated that TRM can be manipulated by CRISPR/Cas9 mutagenesis *in vivo* if they have a monocytic intermediate. In turn, this requirement can only be fulfilled in BM chimeras where all macrophage niches are repopulated by HSC-derived monocytes as opposed to WT mice where most macrophages are of embryonic origin. Nonetheless, this system can prove to be a useful tool for future studies on monocyte-derived macrophages in specific settings.

Part II – Studying monocyte heterogeneity

Introduction

Monocytes are short-lived myeloid immune cells with roles in inflammation and as precursors for tissue-resident macrophages, generated in the BM from committed progenitors (Hettinger et al., 2013; Yáñez et al., 2015). Upon maturation, monocytes are released into the bloodstream. In the healthy organism and under homeostasis, monocytes contribute to varying degrees to the replenishment of selected tissue macrophage populations. The latter includes organs like the gut, skin, and those exposed to mechanical stress, such as the heart (Ginhoux and Jung, 2014).

Two primary subsets of monocytes have been identified in humans, mice, and other mammals (Geissmann et al., 2003; Palframan et al., 2001; Passlick et al., 1989; Trzebanski and Jung, 2020). In mice, monocytes are categorized into Ly6C^{hi} CCR2^{+} 'inflammatory' or classical monocytes (CM) and Ly6C^{lo} CCR2^{-} 'patrolling' or non-classical monocytes (NCM) (Auffray et al., 2007; Geissmann et al., 2003; R. T. Palframan et al., 2001). These monocyte subsets not only display distinct surface markers and transcriptomic profiles (Mildner et al., 2017) but also exhibit, as indicated by their names, different functions. CM are primarily produced in the BM and have relatively short circulatory lifespans, lasting about a day in both mice and humans (Patel et al., 2017; Yona et al., 2013). They are significant contributors to tissue-resident macrophage populations, both during normal physiological conditions and in response to inflammation (Guilliams et al., 2018; Liu et al., 2019; Yona et al., 2013). Within tissues, CM give rise to monocyte-derived macrophages (MoMF) and potentially, CD209a+ monocyte-derived DC (MoDC) (Auffray et al., 2009; Briseño et al., 2016; Cheong et al., 2010; Menezes et al., 2016). On the other hand, NCM originate from CM in the circulation through a Notch-dependent mechanism (Gamrekelashvili et al., 2020, 2016; Varol et al., 2007). NCM patrol the blood vessel walls (Auffray et al., 2007; Carlin et al., 2013), rely on Cx3cr1 for their survival (Landsman et al., 2009), have longer lifespans compared to CM (Patel et al., 2017; Yona et al., 2013), and can be considered macrophages residing within the vasculature. While NCM have been reported to give rise to tissue-resident cells (Evren et al., 2020; Hoffman et al., 2021; Schyns et al., 2019), this activity is not established beyond doubt and has also been challenged (Vanneste et al., 2023).

Recent studies reveiled additional complexity in BM monopoiesis (Weinreb et al., 2020; Yáñez et al., 2017). Thus, adoptive cell transfer and lineage tracing studies have suggested the existence of two alternative pathways that generate distinct CM subtypes: GMP-derived neutrophil-like monocytes (NeuMo) and MDP-derived DC-like monocytes (DCMo). (Weinreb et al., 2020; Yáñez et al., 2017). Intriguingly, different challenges seem to result in the selective expansion of GMP-Mo and MDP-Mo populations, hinting at distinct functional roles for these CM subsets (Yáñez et al., 2017). However, CM heterogeneity was predominantly defined by transcriptomics, and the functional contributions and fates of GMP-Mo and MDP-Mo upon their migration into tissues remain unkown.

In this study, we identified surface markers that allow for the discrimination of murine GMP-Mo and MDP-Mo as CD177+ and CD319+ CM, respectively. This distinction enabled us to perform a comprehensive analysis of the *in vitro* and *in vivo* characteristics of these cell populations. In accordance with previous research, mice exposed to various microbial stimuli exhibited distinct GMP-Mo and MDP-Mo dynamics. Furthermore, classical in vitro assays for neutrophil-related activities confirmed the unique activities of GMP-Mo as compared to MDP-Mo. Finally, competitive adoptive transfers of the two CM subsets into macrophage-depleted animals revealed overlapping and distinct contributions of GMP-Mo and MDP-Mo to peripheral TRM, including those in the gut, lung, and meninges.

Results

Identification of surface markers discriminating murine classical monocyte subsets

Recent research suggested the presence of discrete subpopulations within classical monocytes (CM), categorized as GMP-derived Mo and MDP-derived Mo, with neutrophil-like and DC-like features (Trzebanski and Jung, 2020; Weinreb et al., 2020; Yáñez et al., 2017). To identify surface markers that would detect this CM dichotomy, we conducted in collaboration with the laboratory of Kia Movahedi, VUB, Brussels, Belgium, an extensive CITE-seq screen of C57BL/6 BM (**Fig 1A**). Our dataset included representation of all myeloid immune subsets and their precursors (**Fig 1B, Suppl Fig 1A, B, C**).

Through the use of anti-Ly6C and -CD115 TotalSeq antibodies, we effectively identified Csf1r+ and Fcgr3+ monocytes and their precursors (**Fig 1C**). Focusing on mature

monocytes and closely related classical DC (cDC), we pinpointed a small cluster of Ly6C+ CD115+ Fcgr3+ monocytes that lacked the CM marker CD62L (encoded by Sell) (Geissmann et al., 2003; Palframan et al., 2001) (**Fig 1D**). Differential expression analysis between the CD62L+ and CD62L- CM clusters revealed an enrichment of genes related to neutrophils, such as *Chil3*, *Mmp8*, and *Slpi*, in CD62L+ CM, while MHC-II transcripts were upregulated in the CD62L- subset (**Fig 1D, E**). Intriguingly, despite their elevated expression of MHC-II transcripts, these cells exhibited distinctive transcriptional and phenotypic features compared to cDC, suggesting that they might be DC-like monocytes (**Fig 1F**).

Further examination of the list of differentially expressed genes (DEG) between the CD62L+ and CD62L- monocyte clusters revealed *Slamf7* (encoding CD319) to be specific to CD62L- cells (**Fig 1D, E**). Additionally, *Cd177* appeared to be broadly expressed in CD62L+ cells. Remarkably, Cd177 was among the top 10 DEG previously associated with NeuMo (Weinreb et al., 2020) (**Fig 1D, Suppl Fig 1G**). Subsequently, a combined staining for CD319 (using clone 4G2) and CD177 (using clone Y127) allowed for clear separation of two Ly6Chigh CM subsets via flow cytometry (**Fig 1G**). Importantly, the proportions of CD177+ and CD319+ CM corresponded to previous estimates of the steady-state ratio between NeuMo and DCMo (Wolf et al., 2019). Furthermore, an independent LEGENDscreen approach on total blood cells confirmed that CD319 could effectively distinguish CM when plotted against CD177 (**Suppl Fig 1D**). Interestingly, while CD177 expression was restricted to neutrophils, CD319 was expressed on cDC and lymphocytes but not on neutrophils among other blood immune cell subsets (**Suppl Fig 1E, F**).

Phenotypic analysis of CD177+ and CD319+ blood CM through flow cytometry confirmed that both cells had comparable levels of Ccr2 on their surface. However, CD319+ CM exhibited lower CD62L expression compared to CD177+ CM (**Fig 1H**). CD177+ CM displayed increased expression of CD88a and Ly6C, while CD319+ CM showed higher levels of MHC-II, the chemokine receptor Cx3cr1, and the Fc receptor CD64 (Suppl Fig 1G). Crucially, this finding was independently verified in a different animal facility, reinforcing the robustness of our discovery (**Suppl Fig 1I**). Lastly, CD177+ CM expressed higher levels of CD157 (Bst1), consistent with a recent report identifying CD157 and CD88a as markers for neutrophil-like CM (Ikeda et al., 2023) (**Suppl Fig 1J**).

To address concerns of potential contamination in the CD319+ CD11c- CM gate by CD11c+MHC-II- pre-cDCs, we analyzed Flt3 expression and performed intracellular staining for the cDC lineage-determining transcription factor Zbtb46 (Meredith et al., 2012; Satpathy et al., 2012) (**Suppl Fig 1K**). However, neither Zbtb46 nor Flt3 were found to be expressed in CD319+ CM (**Suppl Fig 1L**).

In summary, our investigation has identified CD177 and CD319 as surface markers that differentiate distinct CM subsets, providing a valuable tool for future studies in this area.

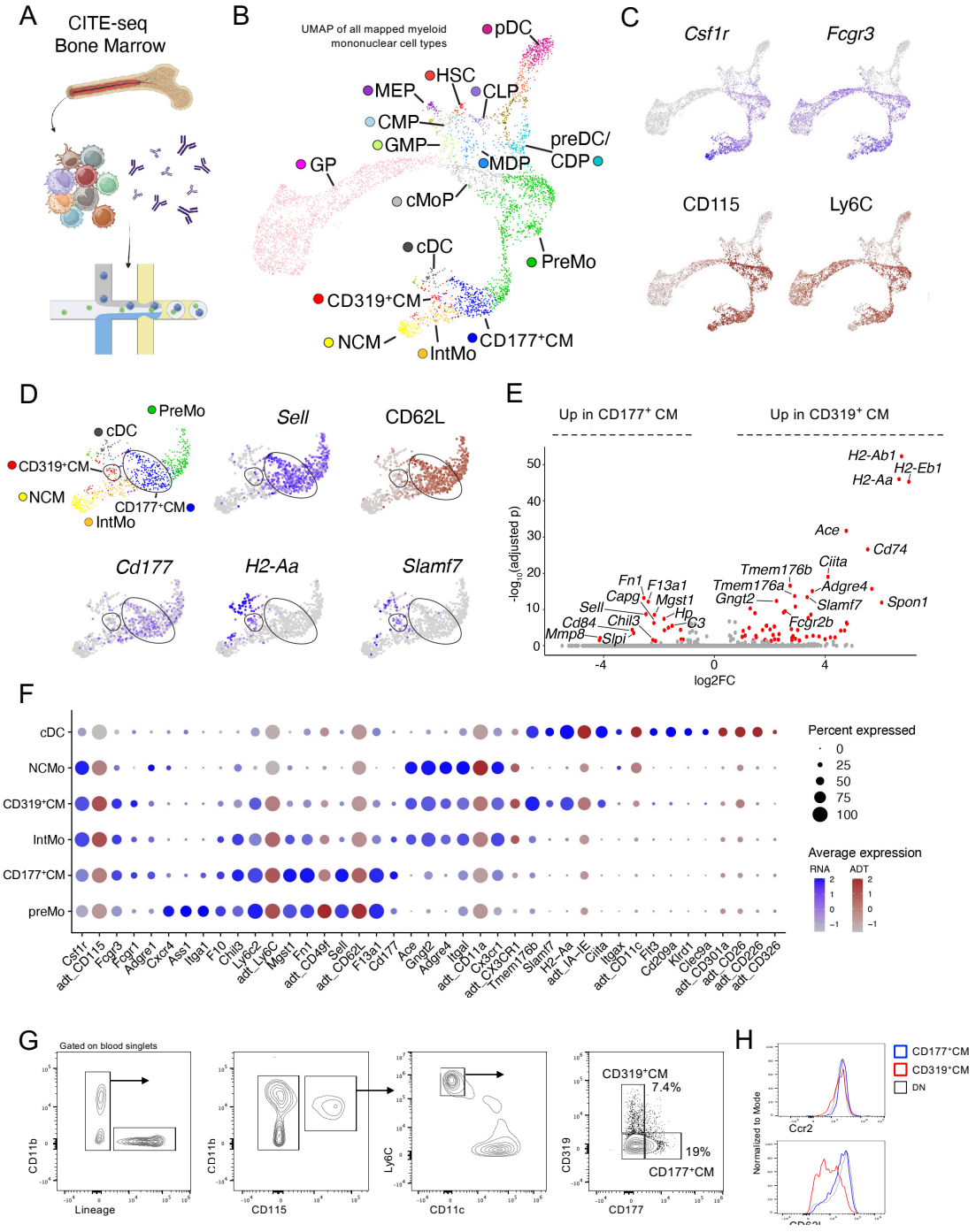

Figure 1: (A) Experimental scheme for the CITE-seq experiment. (B) Curated UMAP plot of the BM monocytes, DC, and their precursors identified by CITE-seq. (C) UMAP plots showing the protein expression of Ly6C and CD115 as identified by CITE-seq antibodies, and *Csf1r* and *Fcgr3* gene expression in the dataset from B. (D) UMAP plot, visualizing the mature monocyte and cDC subsets, and the gene or protein expression of selected markers. (E) DEG between the CD177^{+} CM and CD319^{+} CM clusters identified by CITE-seq. (F) Dot plot showing specific upregulated genes (blue) and proteins (red) for the individual monocyte and cDC subsets as identified by CITE-seq. Dot size represents the percentage of cells expressing the gene and color represents its average expression. (G) Gating on blood monocytes identifying CD177 and CD319 as markers for monocyte subsets. (H) Surface expression of canonical monocyte markers on CD177^{+} Ly6C^{high} CM (blue), CD319^{+} Ly6C^{high} CM (red), and CD177^{-}CD319^{-} Ly6C^{high} CM (black).

CD177^{+} and CD319^{+} CM are NeuMo and DCMo, respectively

To explore the relationship between our newly identified phenotypic subsets of classical monocytes (CM) and the previously described signatures of neutrophil-like (NeuMo) and dendritic cell-like (DCMo) CM (Weinreb et al., 2020; Yáñez et al., 2017), we conducted a comprehensive global RNAseq analysis. We isolated CD177+ and CD319+ Ly6Chigh CM, as well as CD177- CD319- double negative (DN) Ly6Chigh CM, from the peripheral blood of Cx3cr1Gfp/+ animals (Jung et al., 2000) with high purity (**Suppl Fig 2A**).

Our analysis revealed 41 genes that were specifically expressed in CD177+ CM and 67 genes enriched in CD319+ CM (**Fig 2A**). This differential gene signature showed similarities to the putative NeuMo and DCMo clusters observed in the bone marrow using CITE-seq (**Fig 1E**), with many top genes being shared. On a global scale, we identified 141 genes that were differentially expressed in CD319+ CM and 108 genes highly expressed in CD177+ CM and DN cells (**Fig 2B**), suggesting a close relationship between the latter two populations (**Fig 2C**). Importantly, we did not detect the presence of Zbtb46 in either CM subset, confirming the absence of dendritic cell contamination. When we compared our data to a previously published NeuMo / DCMo dataset based on bioinformatic predictions (Weinreb et al., 2020), we found a substantial overlap (**Suppl Fig 2B**). This strongly supports the identification of CD177+ and CD319+ CM as NeuMo and DCMo, respectively. Furthermore, in line with the bulk RNAseq data, we observed higher expression of Clec10a and CD209a on the surface of DCMo compared to CD319- cells (**Suppl Fig 2C**). Notably, NeuMo and DCMo CM gene clusters were also identified in a previously published single-cell dataset of total blood monocytes (Mildner et al., 2017) (**Suppl Fig 2D**).

Confirming their status as bona fide monocytes, all CM subsets exhibited high levels of *Spi1*, encoding the pioneering transcription factor PU.1, as well as *Klf4*, *Cx3cr1*, and *Csf1r* (encoding CD115) as lineage markers (**Fig 2D**). NeuMo, characterized by CD319-, displayed

elevated expression of genes encoding neutrophil-related markers like *Chil3* and *Mmp8* (granule proteins), as well as *Pglyrp1*, a peptidoglycan recognition protein. NeuMo also expressed high levels of *Cebpb* transcripts, encoding a transcription factor known to be important for the conversion of CM into non-classical monocytes (NCM) (Fig 2D). In contrast, DCMo were enriched in transcripts encoding immune-modulatory DC-related molecules such as *H2-Ab1*, *Btla*, *Cd40*, and the transcription factor *Batf3*, akin to previously described Cd209a+ Ly6Cint monocytes (Mildner et al., 2017) (**Fig 2D**).

Moreover, Metascape analysis (Zhou et al., 2019) revealed the enrichment of neutrophil and DC-related modules, such as 'neutrophil degranulation' and 'negative regulation of immune system process' in NeuMo and DCMo, respectively (**Fig 2E**).

In summary, CD177+ NeuMo and CD319+ DCMo exhibited distinct transcriptional profiles, aligning with previously reported signatures. Additionally, our data indicate that the majority of Ly6Chigh CM in the blood of healthy C57BL/6 mice under hyper-hygienic conditions predominantly comprises cells displaying a NeuMo signature.

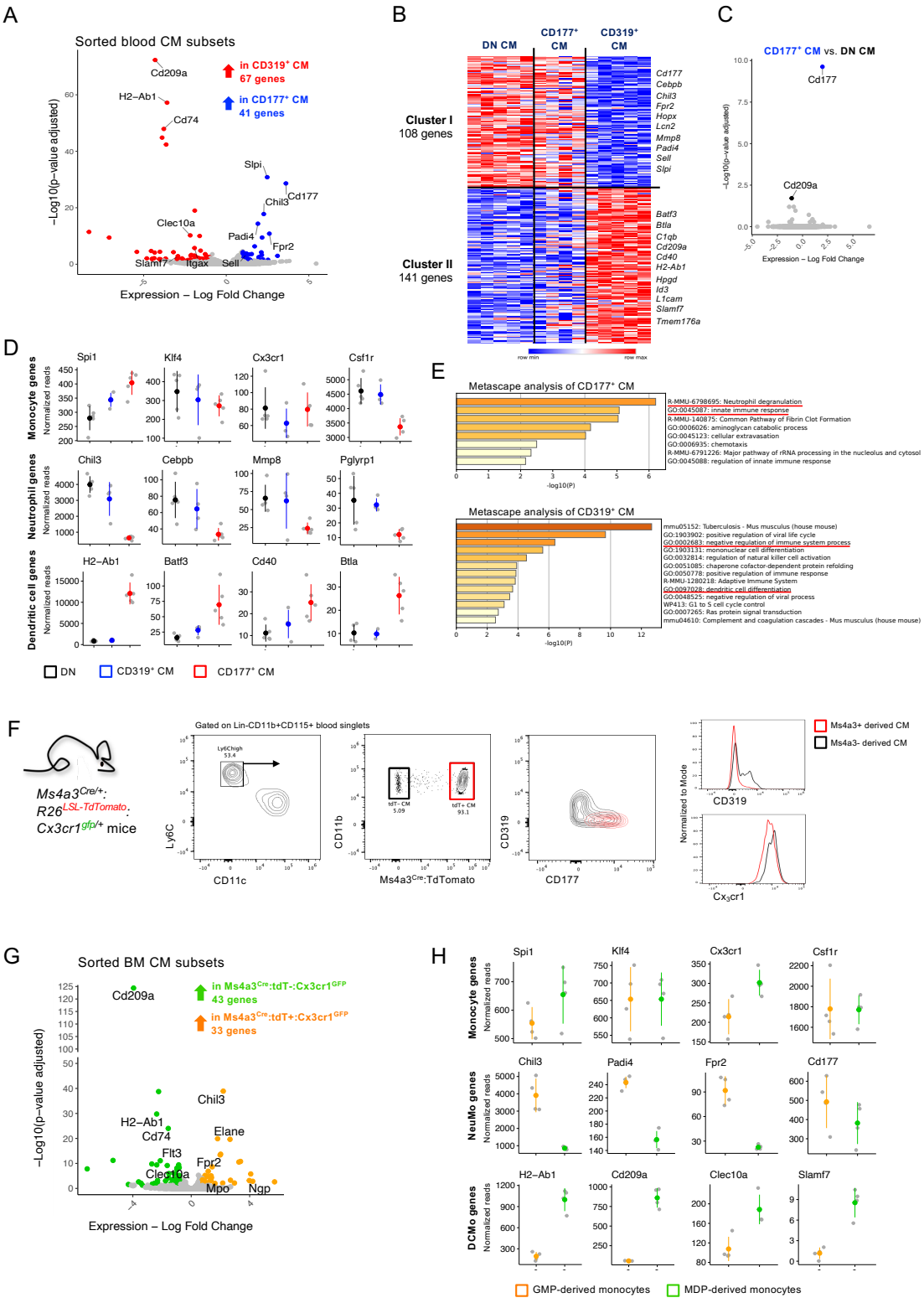

Figure 2: (A) Volcano plot showing differentially expressed genes between CD177^{+} CM (blue dots) and CD319^{+} CM (red dots) from sorted blood cells subjected to bulk RNAseq. CM were defined as Lin^{-} CD11b^{+}CD115^{+}Cx3cr1^{GFP+}Ly6C^{high}CD11c^{-} cells. (B) Heatmap showing DEG between DN (CD177^{-}CD319^{-} CM), CD177^{+} CM, and CD319^{+} CM from sorted blood cells. (C) Volcano plot of DEG among CD177^{+}CD319^{-} CM and CD177^{-}CD319^{-} DN CM. (D) Scatter plots of selected genes among CD177^{+} CM, CD319^{+} CM, and DN CM. Selected 'monocyte genes' were not differentially expressed among subsets. (E) Metascape analysis of DEG in CD177^{+} CM and CD319^{+} CM. (F) Flow cytometry analysis of blood monocytes from *Ms4a3^{Cre}:R26$^{LSL-TdTomato}$:Cx3cr1^{GFP}* mice. (G) Volcano plot of differentially expressed genes among *Ms3a4^{Cre}:R26$^{LSL-TdTomato}$*-

:Cx3cr1^{GFP}+ (MDP-derived) monocytes and *Ms4a3*^{Cre}*:R26*$^{LSL\text{-}TdTomato}$+*:Cx3cr1*^{GFP}+ (GMP-derived) monocytes sorted from BM. CM were defined as CD11b^{+}CD115^{+}CD11c^{-}MHC-II^{-}Ly6C^{high} cells. (H) Scatter plots of selected genes among BM GMP- and MDP-derived CM. Chil3, Fpr2, H2-Ab1, Cd209a, and Clec10a were differentially expressed.

CD177^{+} NeuMo and CD319^{+} DCMo arise in the BM as GMP and MDP progeny, respectively

Goodridge and colleagues have proposed that neutrophil-like monocytes (NeuMo) and dendritic cell-like monocytes (DCMo) derive from granulocyte and macrophage progenitors (GMP) and monocyte and dendritic cell precursors (MDP), respectively (Yáñez et al., 2017). Consequently, it would be expected that CD177+ NeuMo primarily originate from GMP, while CD319+ DCMo should be the progeny of MDP. As previously reported (Liu et al., 2019), a small proportion of unlabeled blood classical monocytes (CM) exists in Ms4a3Cre:R26LSL-TdTomato mice, which enable the tracing of GMP fate (**Fig 2F**). Interestingly, these unlabeled cells exhibited robust, although not exclusive, expression of CD319, as well as higher levels of Cx3cr1, resembling blood DCMo (**Fig 1F,I, Suppl Fig 1F**).

To further investigate the relationship between ontogeny and NeuMo and DCMo, we utilized double reporter mice (Ms4a3Cre:R26LSL-TdTomato:Cx3cr1gfp) in which GMP- and MDP-derived cells can be distinguished based on reporter gene expression. We isolated TdTomato+ GFP+ and TdTomato- GFP+ BM monocytes from these mice, further enriching them for the absence of CD11c and MHC-II expression to exclude conventional dendritic cells (cDC) and their precursors (**Suppl Fig 2E**), and performed bulk RNAseq analysis. Consistent with the proposed developmental scheme (Liu et al., 2019; Yáñez et al., 2017), GFP+ BM monocytes expressed higher levels of DC-related transcripts, such as *H2-Ab1* and *Cd209a*, whereas TdTomato+ GFP+ BM monocytes exhibited a gene expression signature resembling that of neutrophil-like cells, including *Chil3* and *Elane* (**Fig 2G, H, Suppl Fig 2F**). Furthermore, MDP- and GMP-derived cells exclusively overlapped with the transcriptomes of DCMo and NeuMo, respectively (**Suppl Fig 2G**). Notably, the expression of *Cd177* and *Slamf7* was relatively low in BM monocytes (**Fig 2H**). This may be attributed to the broad CD11b sorting gate (**Suppl Fig 2E**), which likely includes immature CD11bint transitional pre-monocytes (Chong et al., 2016). Additionally, this explains the presence of *Flt3* and neutrophil granule proteins like *Mpo* and *Ngp*, which were absent in blood monocytes (**Fig 2G**).

In conclusion, our findings support the previous notion that bone marrow monopoiesis is bifurcated and comprises a GMP - NeuMo and a MDP - DCMo axis.

NeuMo and DCMo prevalence following exposure to microbial stimuli and IFNg

The classical monocyte (CM) population responds dynamically to various challenges, including exercise, metabolic changes, and encounters with pathogens (Janssen et al., 2023; Steppich et al., 2000). When exposed to parasitic and bacterial inflammation along with IFN-gamma exposure, CM have been observed to upregulate the expression of the stem cell marker Sca1 (Ly6a) while simultaneously downregulating the monocyte/macrophage lineage marker Cx3cr1 (Askenase et al., 2015; Biram et al., 2022).

It has been reported that NeuMo derived from GMP and DCMo derived MDP exhibit differential expansion in animals challenged with LPS and CpG (Yáñez et al., 2017). Consistent with these findings, when wild-type C57BL/6 animals were exposed to LPS (2.5 ug/g, i.p. or i.v.), an increase in CD177+ cells was observed by day 1, while DCMo remained proportionally unaffected (**Fig 3A, B, Suppl Fig 3B**). Interestingly, Cx3cr1 surface expression was selectively reduced on NeuMo, while DCMo maintained normal Cx3cr1 levels (Fig 3C). Conversely, DCMo and DN CM (CD177- CD319-) upregulated Sca1 (Fig 3C). Additionally, DCMo and DN CM exhibited an induction of DCMo markers, including CD64, CD11c, and CD209a (**Suppl Fig 3C**). Notably, changes in Cx3cr1 and Sca1 expression were also found to be correlated in Ly6C+ GMP and MDP within the bone marrow (BM) (**Suppl Fig 3D, E, F**).

The Toll-like receptor 9 (TLR9) agonist CpG was reported to expand DC-like monocytes (Yáñez et al., 2017). Accordingly, administration of CpG + DOTAP (5 ug/mouse and 25 ug/mouse, respectively) increased the representation of DCMo within the blood Ly6C+ CM population at the expense of NeuMo (**Fig 3D, E, Suppl Fig 3G**). In contrast to the LPS regimen, both CM subsets were equally affected following this challenge. Specifically, Sca1 was strongly upregulated on all CM subsets while Cx3cr1 expression remained unaltered (**Fig 3F**). Unlike LPS-treated mice, and indicating monocyte plasticity, NeuMo upregulated DCMo markers CD64, CD11c, and CD209a following CpG exposure (**Suppl Fig 3H**). Once again, BM precursors exhibited distinct surface phenotypes after CpG activation (**Suppl Fig 3I, J, K**).

Infection-associated IFN-gamma leads to the emergence of Sca1+ monocytes (Askenase et al., 2015; Biram et al., 2022). Indeed, similar to the CpG challenge, DCMo significantly expanded within the CM population in mice that received a single injection of 5 ug recombinant IFN-gamma (rIFN-gamma), at the expense of CD177+ NeuMo (**Fig 3G, H, Suppl Fig 3L**). Cx3cr1 expression did not significantly change on any of the subsets, while Sca-1 was significantly higher expressed on DCMo (**Fig 3I**). CD319- CM modestly upregulated MHC-II, whereas DCMo expressed high levels of both MHC-II and CD11c (**Suppl Fig 3M**). Transcriptome analysis of sorted Sca1+ and Sca1- CM isolated from the blood of animals subjected to repetitive rIFN-gamma challenges (**Suppl Fig 3N**) revealed that Sca-1+ CM expressed *Slamf7* (encoding CD319), whereas Sca-1- CM displayed higher expression of *Cd177* and *Fpr2* (**Suppl Fig 3O, P, Q**). This suggests that distinct NeuMo and DCMo signatures are retained, at least at the transcriptional level, following challenges.

In summary, similar to GMP- and MDP-derived BM monocytes, CD177+ NeuMo and CD319+ DCMo differentially expand following exposure to microbial stimuli, indicating alterations in monopoiesis.

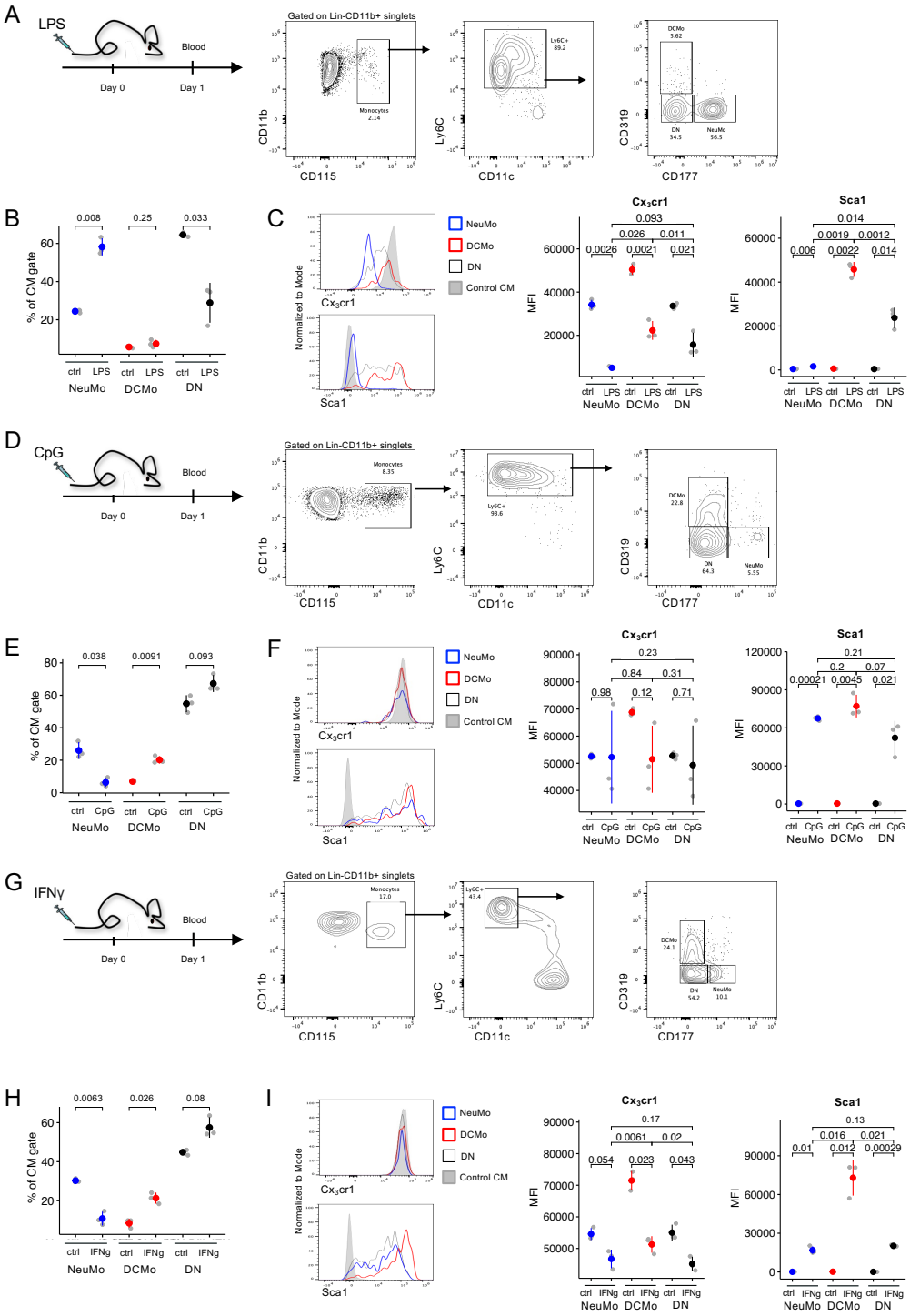

Figure 3: (A) Experimental scheme and blood analysis of LPS-treated mice one day after treatment. (B) Quantification of changes in the CM compartment after LPS treatment. (C) Histograms and quantification of changes in Cx3cr1 and Sca1 surface expression among CM subsets following LPS treatment. (D) Experimental scheme and blood analysis of CpG-treated mice one day after treatment. (E) Quantification of changes in the CM compartment after CpG treatment. (F) Histograms and quantification of changes in Cx3cr1 and Sca1 surface expression among CM subsets following CpG treatment. (G) Experimental scheme and blood analysis of IFNg-treated mice one day after treatment. (H) Quantification of changes in the CM compartment after IFNg treatment. (I) Histograms and quantification of changes in Cx3cr1 and Sca1 surface expression among CM subsets following IFNg treatment.

NeuMo but not DCMo display distinct neutrophil-like functions in vitro

Neutrophils are the initial responders at both sterile and non-sterile injury sites, where they act as phagocytes and counteract extracellular pathogens (Castanheira and Kubes, 2019; Kolaczkowska and Kubes, 2013; Papayannopoulos, 2018). To explore whether NeuMo, in addition to their shared transcriptomic characteristics, exhibit functional neutrophil features, we conducted a series of *in vitro* experiments (**Fig 4A**).

N-formylpeptides are products resulting from the breakdown of bacterial and mitochondrial proteins, serving as potent chemoattractants for neutrophils (Hartt et al., 1999). We observed robust and distinct expression of the N-formylpeptide receptor 2 (Fpr2) in NeuMo (**Fig 4B**). To assess its functionality, we selectively isolated CD115+ BM monocytes and subjected them to a migration assay using 100 nM fMLP or a carrier control (**Fig 4C, Suppl. Fig 4A, B**). Analysis of their migration towards fMLP-supplemented medium revealed a tenfold increase in CD177+ NeuMo compared to the control condition, whereas CD319+ DCMo did not exhibit any migration in this assay (**Fig 4C**).

A defining feature of neutrophil activation is the generation of extracellular traps (ET), which are associated with the expression of granule proteins like MPO, as well as histone citrullination and deamination (Papayannopoulos, 2018). NeuMo, but not DCMo, expressed one of the critical factors necessary for chromatin de-condensation, namely protein-arginine deiminase type-4 (Padi4), along with high levels of intracellular MPO (Li et al., 2010) (**Fig 4D**). To assess whether Padi4 conferred NeuMo with the potential to form ET, CD177+ NeuMo, CD319+ DCMo, and neutrophils were purified and activated with PMA for six hours. Staining for DNA, MPO, and citrullinated H3 revealed a significantly greater propensity for triple-positive events in NeuMo compared to DCMo (**Fig 4E**). This aligns with previous reports of ET formation by human monocytes (Granger et al., 2017).

To evaluate the phagocytic capacity of NeuMo and DCMo, CD177+ and CD319+ BM monocytes were isolated to purity and exposed to GFP-expressing *Salmonella typhimurii* for two hours. Flow-cytometric analysis demonstrated that NeuMo exhibited a superior ability to internalize bacteria (**Fig. 4F, Suppl Fig 4C**). However, DCMo also displayed strong phagocytic activity in this assay, consistent with their monocyte characteristics.

In summary, these in vitro experiments suggest that, in addition to their transcriptomic differences, NeuMo exhibit functional attributes that set them apart from DCMo. These include typical neutrophil functions such as attraction to bacterial peptides, ET formation, and phagocytosis.

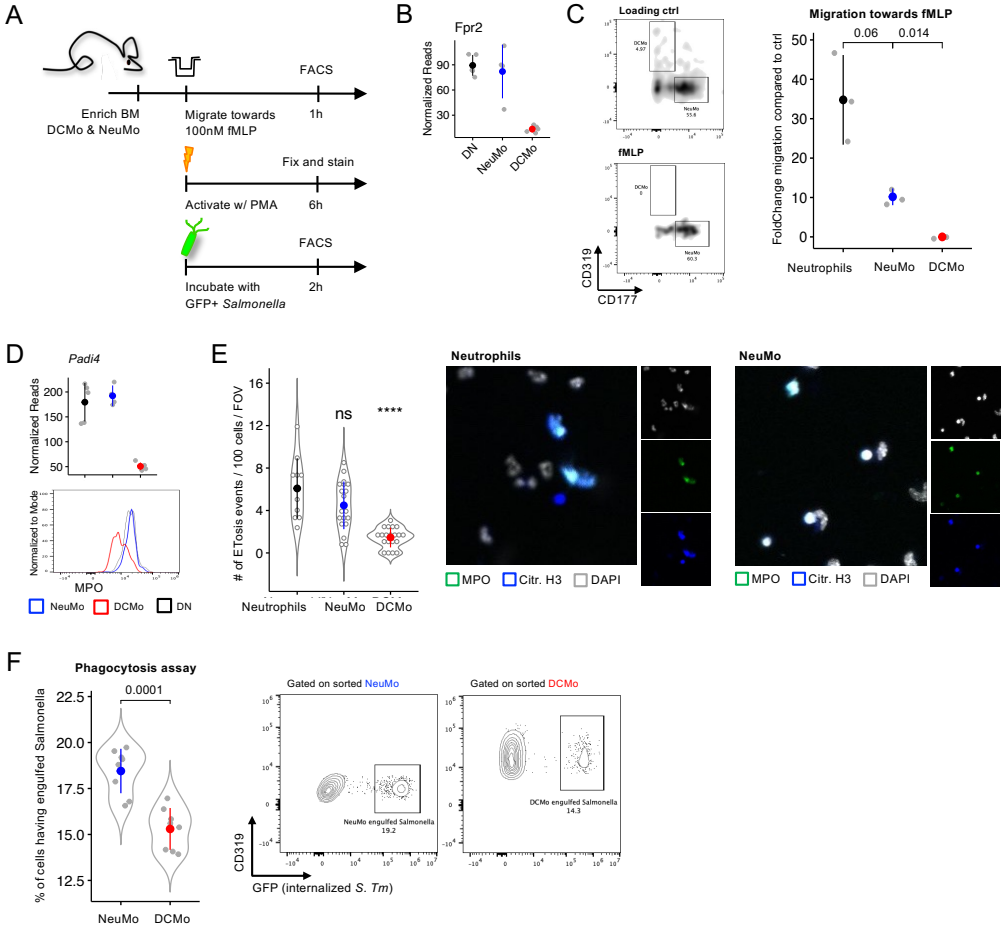

Figure 4: (A) Schematic of performed *in vitro* assays. (B) Transcriptional expression of the formyl-methionine peptide receptor 2 (Fpr2) among CM subsets. (C) Quantification of migration of BM monocytes and neutrophils towards fMLP (100 nM) compared to control (DMSO), as assessed by flow cytometry. (D) Transcriptional expression of the protein amine deiminase 4 (Padi4) protein among CM subsets and intracellular staining for myeloperoxidase (MPO) among CM subsets by flow cytometry. (E) Quantification and microscopy images of the initiation of ETosis events as evidenced by co-staining for DNA, MPO, and citrullinated histone 3 (H3) as assessed by microscopy. (F) Quantification and representative flow cytometry plots off phagocytosis of GFP-expressing *Salmonella Tyhpimurium* by NeuMo and DCMo.

NeuMo and DCMo give rise to NCM and intestinal macrophages

One of the primary roles of monocytes in maintaining homeostasis is to preserve specific, long-lasting tissue-resident macrophage populations, particularly in mucosal tissues (Ginhoux and Guilliams, 2016; Guilliams et al., 2018; Mildner et al., 2013). To investigate the potential future paths of CD177+ NeuMo and CD319+ DCMo, we isolated these two monocyte subsets from genetically marked animals, such as Cx3cr1gfp, Cx3cr1Cre:R26LSL-TdTomato,

and Ms4a3Cre:R26LSL-TdTomato mice (Jung et al., 2000; Liu et al., 2019; Yona et al., 2013), and conducted adoptive transfer experiments. To create a niche for engraftment in recipient animals, we utilized irradiation chimeras that were generated using Cx3cr1DTR bone marrow (BM) as recipients. Specifically, by treating these animals with diphtheria toxin (DTx), we could deplete both monocytes and Cx3cr1+ macrophage populations (Aychek et al., 2015; Diehl et al., 2013).

Equal quantities of NeuMo and DCMo (2e5) were co-transferred into DTx-treated Cx3cr1DTR>WT chimeras approximately 8-10 weeks after irradiation and BM transfer (BMT) (**Fig 5A**). The depletion of blood monocytes, encompassing both CM and NCM subsets, by DTx was verified through flow cytometry (**Fig 5B**). On the first day following transfer, blood analysis of some recipient animals revealed the presence of circulating engrafted TdTom+ NeuMo and GFP+ DCMo at approximately equal numbers (**Fig 5C**). In line with previous reports and indicating a shift towards NCM (Varol et al., 2007), both cell types had begun to downregulate Ly6C (**Fig 5C**). When blood was collected on the third day after transfer, flow cytometric analysis showed that both NeuMo and DCMo cells had transformed into Ly6Clow NCM while maintaining the ratios (**Fig 5D**). Surface marker profiling revealed similar levels of the integrin CD11c among NCM derived from NeuMo and DCMo (**Fig 5E**). However, DCMo-derived NCM exhibited significantly higher expression of PDL1, a marker recently associated with NCM (Bianchini et al., 2019) (**Fig 5E**). Conversely, classical monocyte markers CD115 and CD11b were more highly expressed on NCM derived from NeuMo, although not reaching statistical significance (**Fig 5E**).

On the twelfth day after transfer, various organs of recipient mice were harvested to assess the potential of NeuMo and DCMo to give rise to long-lived tissue-resident macrophages (Gross-Vered et al., 2020; Varol et al., 2009, 2007). In both the ileum and colon, clones of macrophages derived from NeuMo and DCMo were found to have undergone clonal expansion (Varol et al., 2009) (**Fig 5F**). Quantitative analysis of graft-derived macrophages through microscopy and flow cytometry showed equal contributions to both the ileal and colonic macrophage populations (**Fig 5F, G, H**).

In summary, our findings demonstrate that following engraftment, both NeuMo and DCMo give rise to NCM and gut macrophages with comparable efficiency in a competitive setting (Varol et al., 2009, 2007). Notably, NCM derived from NeuMo and DCMo exhibit

distinct phenotypes, including differential PDL1 expression. This differential ontogeny may have an impact on the functions of NCM.

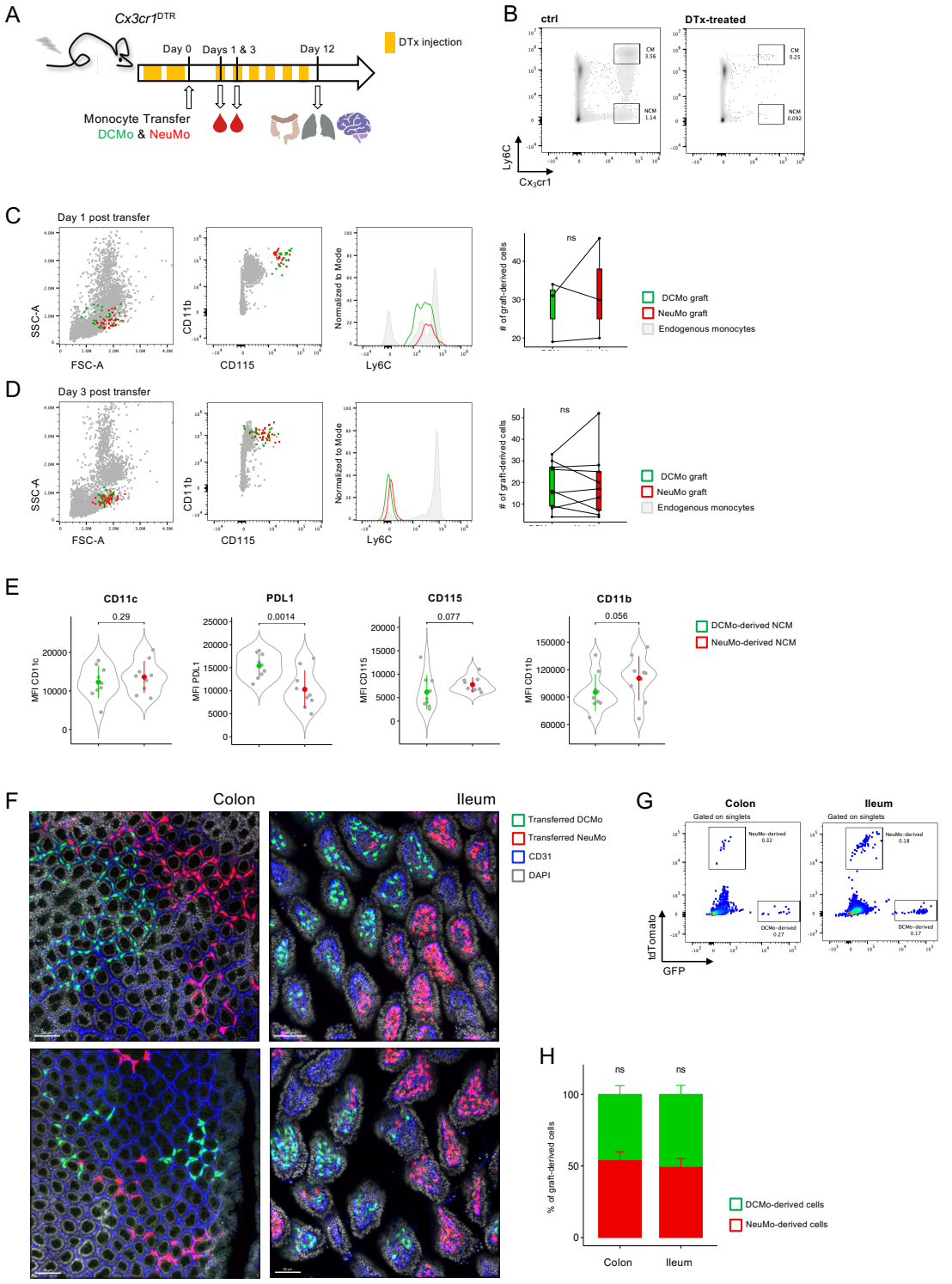

Figure 5: (A) Experimental scheme of adoptive transfer of 2e5 NeuMo and DCMo, each. Cx3cr1DTR chimerase were depleted of Cx3cr1-expressing cells by repeated injection of 18 ng/g DTx / g bodyweight 8-10 weeks after chimerism. On day 0, CM subsets were adoptively co-transferred. Hereafter, mice were administered 12 ng DTx / g bodyweight every other day until sacrifice. (B) Blood analysis of DTx- and PBS-treated Cx3cr1DTR chimeras. (C) Blood analysis of circulating graft cells one day after adoptive transfer. (D) Blood analysis of circulating graft cells three days after adoptive transfer. (E) Quantification of surface marker expression on graft cells in the blood

three days after transfer. (F) Microscopy images of graft-derived TRM in the colon and ileum of recipient animals. Scale bar = 80-100 um. (G) Flow cytometry analysis of graft-derived TRM in the colon and ileum of recipient animals. (H) Quantification of the distribution of graft-derived TRM in colon and ileum of recipient animals.

NeuMo and DCMo fates in the lung

Pulmonary interstitial macrophages (IM) are diverse, consisting of both CD206- and CD206+ IM (Gibbings et al., 2017), as well as lung-resident CD16.2+ cells (Schyns et al., 2019). The latter have been considered IM precursors (Schyns et al., 2019), supported by observations in humanized animals (Evren et al., 2020). However, recent data indicate that IM may develop from classical monocytes (CM) through an intermediate stage involving proliferation (Vanneste et al., 2023).

On day 12, TdTom+ NeuMo- and GFP+ DCMo-derived cells successfully engrafted in the recipient lungs, as confirmed through histological and flow cytometric analysis (**Fig 6A, B, Suppl Fig 5A**). Importantly, only a minimal number of these grafted cells were detected in the blood on day 12 (**Suppl Fig 5B**). Interestingly, TdTom+ and GFP+ cells showed significant differences in their distribution within specific subpopulations in the pulmonary myeloid compartment. Notably, the majority of grafted cells in the lung originated from DCMo (**Fig 6C**). While both NeuMo- and DCMo-derived cells were present in roughly similar numbers among CD16.2+ precursors, mature IM derived from DCMo far outnumbered those derived from NeuMo (**Fig 6C**). In fact, DCMo-derived IM were approximately four times more abundant than DCMo-derived CD16.2+ precursors, while the ratio among NeuMo-derived cells was around 1 (**Fig 6D**). This delayed or absent differentiation into mature IM by NeuMo was further supported by higher CD16.2 expression and lower MHC-II surface expression on NeuMo-derived IM compared to DCMo-derived IM (**Fig 6E, Suppl Fig 5C**).

To gain further insights into the pulmonary progeny of NeuMo and DCMo, we conducted bulk RNA sequencing on engrafted TdTom+ and GFP+ cells retrieved from the recipient lungs (**Suppl Fig 5D**). Out of a total of 220 differentially expressed genes (DEGs), 48 genes were preferentially expressed in DCMo-derived cells, while 172 genes displayed higher transcription levels in NeuMo-derived cells (**Fig 6F, Suppl Fig 5E**). Metascape analysis (Zhou et al., 2019) revealed an enrichment of angiogenesis and wound healing pathways in the transcriptome of NeuMo-derived IM (**Suppl Fig 5F**). Conversely, DCMo-derived IM were associated with gene modules that regulate the immune response and leukocyte differentiation (**Suppl Fig 5F**). Intriguingly, the transcriptome of NeuMo progeny exhibited a significant

overlap with an expression signature previously reported for Lyve1+MHC-IIlow lung IM, while DCMo progeny resembled Lyve1-MHC-IIhi lung IM (Chakarov et al., 2019) (**Fig 6G, Suppl Fig 5G, H**). Moreover, compared to NeuMo-derived IM, cells derived from DCMo showed approximately twice the expression of *Mafb*, a transcription factor recently suggested to be crucial for CM differentiation into lung IM (Vanneste et al., 2023) (**Fig 6H**). In contrast, the expression of *Maf*, which encodes c-MAf and is proposed to determine CD206+ IM identity (Vanneste et al., 2023), did not significantly differ between NeuMo- and DCMo-derived IM (**Fig 6H**).

To directly link this divergence to ontogeny, we performed a competitive adoptive transfer of monocytes derived from granulocyte-macrophage progenitors (GMP) and monocyte-dendritic cell progenitors (MDP) isolated from the bone marrow of Ms4a3Cre:R26LSL-TdTomato:Cx3cr1gfp mice (**Fig 6I**). Indeed, GFP+ monocytes derived from MDP also preferentially gave rise to IM over TdTom+GFP+ CM derived from GMP (**Fig 6J, K**). Furthermore, CD16.2 expression was higher on GMP-derived CD206+ IM, consistent with the phenotype of NeuMo-derived IM (**Fig 6L**). Interestingly, and in accordance with the transcriptome data, GMP-derived IM expressed higher surface levels of Lyve1. However, we did not observe differential MHC-II expression in either of the graft-derived IM populations.

In conclusion, through a competitive adoptive transfer approach, we demonstrate that NeuMo and DCMo follow distinct differentiation pathways upon their entry into the lung, and these outcomes are determined by their ontogeny.

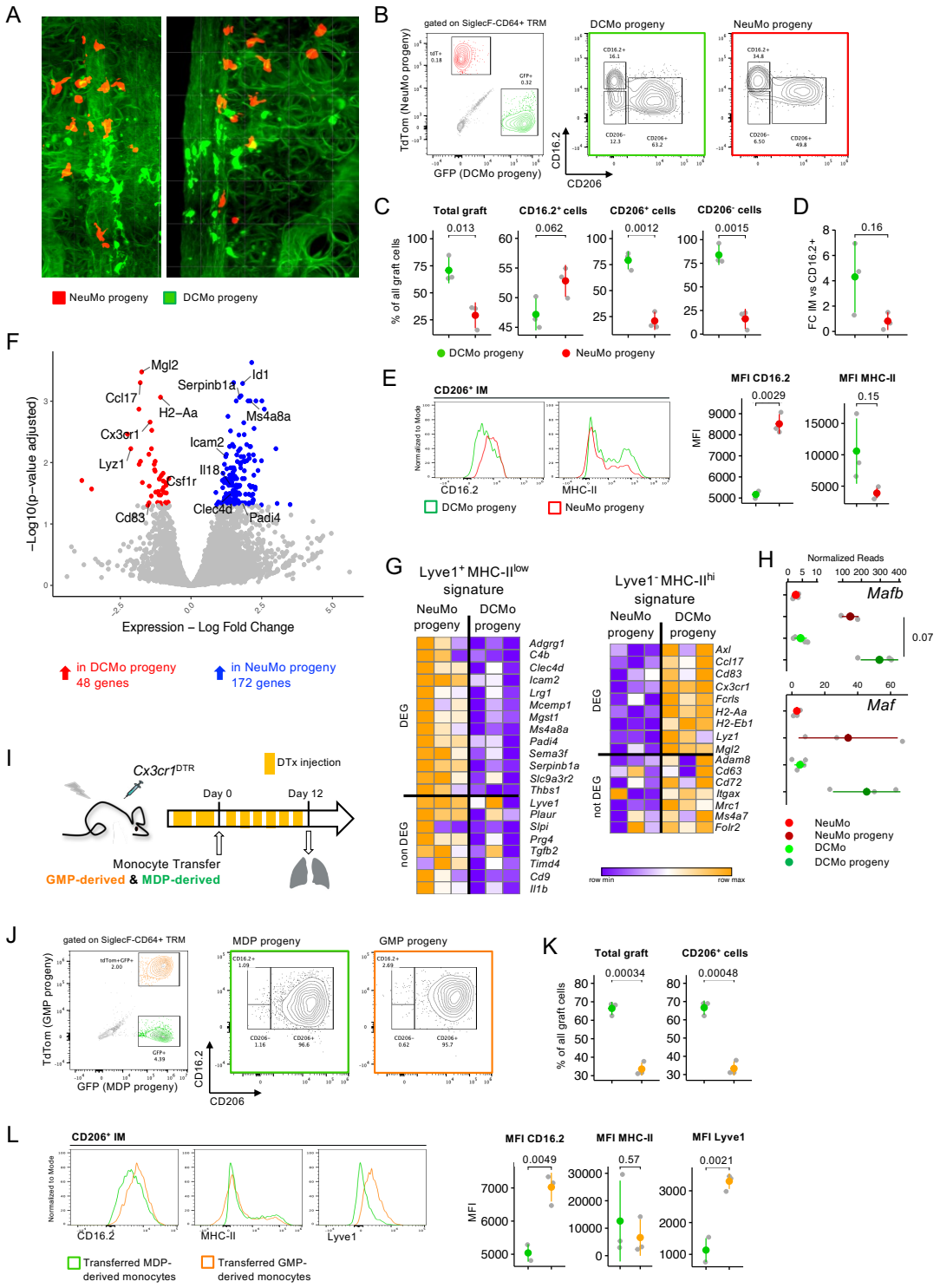

Figure 6: (A) Representative microscopy image of CUBIC-cleared lungs showing graft-derived cells in the parenchyma. (B) Flow cytometry plots of graft-derived cells in the lungs of recipient animals, and CD16.2 vs CD206 plots for each graft-derived population. (C) Quantification of the contribution of DCMo- and NeuMo-derived populations to selected lung phagocyte populations, normalized to total number of graft-derived cells in the respective gates. (D) Foldchange in the ratio of mature IM to CD16.2+ precursors for DCMo- and NeuMo-derived graft cells. (E) Histogram plots and quantification of the surface expression of CD16.2 and MHC-II on CD206+ DCMo- and NeuMo-derived IM. (F) Volcano plot of DEG among total DCMo- and NeuMo-derived phagocyte populations from the lungs of recipient animals. (G) Heatmap of selected differentially and non-differentially expressed genes attributed to Lyve1^{+}MHC-II^{low} and Lyve1^{-}MHC-II^{hi} IM as defined by Chakarov *et al.* (H) Experimental scheme for adoptive transfer of GMP- and MDP-derived monocytes from *Ms4a3*^{Cre}:*R26*$^{LSL-}$

^{TdTomato}:*Cx3cr1*^{GFP} mice. *Cx3cr1*^{DTR} chimeras were depleted off Cx$_3$cr1-expressing cells by twice injection of 18 ng/g DTx / g bodyweight 8-10 weeks after chimerism. On day 0, CM subsets were adoptively co-transferred. Hereafter, mice were administered 12 ng/g DTx / g bodyweight every other day until sacrifice. (I) Flow cytometry plots of graft-derived cells in the lungs of recipient animals, and CD16.2 vs CD206 plots for each graft-derived population. (J) Quantification of the contribution of MDP- and GMP-derived populations to selected lung phagocyte populations, normalized to total number of graft-derived cells in the respective gates. (K) Histogram plots and quantification of the surface expression of CD16.2, MHC-II, and Lyve1 on CD206+ MDP- and GMP-derived IM.

NeuMo but not DCMo give rise to meningeal dura mater macrophages

The macrophage population within the central nervous system (CNS) includes microglia in the brain parenchyma, meningeal macrophages found in the dura mater and leptomeninges, as well as macrophages located in the perivascular space and choroid plexus (Goldmann et al., 2016; Hove et al., 2019).

To assess the capacity of NeuMo and DCMo to replenish CNS macrophage niches, we examined the brains of DTx-treated Cx3cr1DTR chimeras on days 12 and 21 after engraftment (**Fig 5A**). Notably, the brain parenchyma of these recipient mice did not contain any labeled graft-derived cells. This is consistent with the brain parenchyma being insensitive to DTx treatment due to limited replacement of microglia by DTR transgenic cells in the BM chimeras (Shemer et al., 2018) (**Suppl Fig 6A**). In contrast, the DTx regimen partially depleted meningeal macrophages in the Cx3cr1DTR chimeras (**Suppl Fig 6B**). However, we did not detect labeled cells in the leptomeninges of the recipient mice (**Suppl Fig 6B**). Surprisingly, we observed efficient repopulation of macrophages in the dura mater, but exclusively by TdTom+ NeuMo (**Fig 7A, B**). These cells were concentrated along the sagittal sinus but could also be found in more distant regions (**Fig 7A, Suppl Fig 6C**). This engraftment was sustained, as TdTom+ cells were still abundant 3 weeks after transfer, suggesting in situ proliferation of the graft (**Fig 7B**). We confirmed these results in independent transfer experiments where we used switched labels, engrafting TdTom+ DCMo and GFP+ NeuMo (**Suppl Fig 6D**). By day 12, NeuMo-derived cells had acquired low levels of CD206 expression, a characteristic feature of dura mater macrophages (Hove et al., 2019) (**Fig 7C**). However, surface expression of MHC II and higher levels of CD206 were only detected at day 21, indicating in situ maturation of the cells (**Fig 7D**).

To investigate the underlying mechanism behind the selective recruitment of NeuMo but not DCMo to the dura mater, we examined the list of differentially expressed trafficking molecules. In particular, we noticed a high level of expression of Sell, which encodes for

CD62L, by NeuMo (and DN CM), as compared to DCMo, both at the transcriptional and protein level (**Fig 7E**). This observation was also supported by CITE-seq analysis of BM subsets (**Fig 1D**). To explore the functional significance of CD62L in the dura mater seeding by CM, we transferred labeled NeuMo into recipient mice that were treated intravenously with αCD62L antibody (100 µg per mouse) or an isotype control on two consecutive days (**Fig 7F**). The unimpaired seeding of the colon by grafted cells at day 12 ruled out any cytotoxicity of the treatment (**Fig 7F, Suppl Fig 6E**). Analysis of the dura mater in the recipient mice after transfer revealed that αCD62L blockade led to a reduction in TdTom+ dura mater macrophages compared to control mice (**Fig 7F**).

In conclusion, our findings establish differential homing potential between the two CM subpopulations, where NeuMo but not DCMo are capable of repopulating an experimentally depleted dura mater macrophage niche. This suggests that the differential seeding is associated with the expression of CD62L on NeuMo.

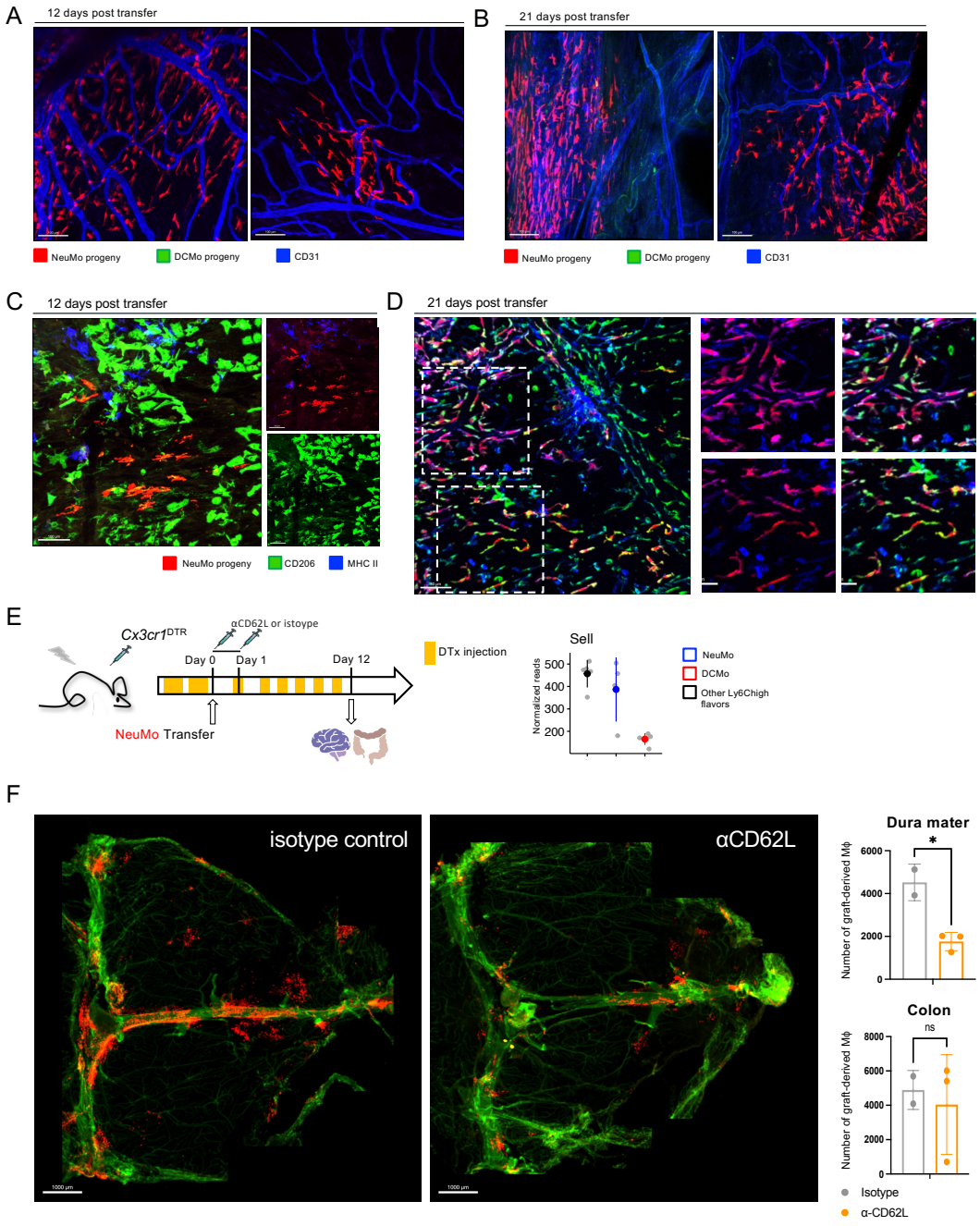

Figure 7: (A) Microscopy image of the dura mater of recipient mice 12 days after transfer. Both images depict the peripheral dura. Scale bars = 100 um. (B) Microscopy image of the dura mater of recipient mice 21 days after transfer. Left: sagittal sinus, right: periphery. Scale bars = 100 um. (C) Microscopy image of the dura mater. NeuMo-derived BAM were stained for CD206 (green) and MHC-II (blue), 12 days after transfer. Scale bar = 100 um. (D) Microscopy image of dura mater. NeuMo-derived BAM were stained for CD206 (green) and MHC-II (blue), 21 days after transfer. Scale bar = 80 um. (E) Left: Schematic of the adoptive transfer experiment probing for the effect of CD62L on NeuMo recruitment to the dura mater. 2e5 NeuMo were injected to each mouse. Mice were administered aCD62L or isotype antibody (100 ug i.v., each) 1 hour before and 24 hours after cell transfer. Right: Noramlized reads for *Sell*, encoding CD62L among blood CM subsets, as assessed by bulk RNAseq. (F) Tile scans of the dura mater of aCD62L- and isotype-treated mice (left and middle) as well as quantification of total cell numbers detected in dura amter and colon in each treatment group (right). Scale bars = 1000 um.

Discussion

In this study, we have uncovered two surface markers, CD177 and CD319, that help distinguish phenotypically and functionally distinct classical monocyte subsets in mice under both steady-state and challenge conditions. This discovery significantly expands upon recent groundbreaking findings regarding the heterogeneity of bone marrow monocytes (BM monocytes) and classical monocytes (CM) (Weinreb et al., 2020; Yáñez et al., 2017). Additionally, we have elucidated the shared and differential *in vivo* destinies of these monocyte subsets in specific tissues using adoptive transfer experiments into macrophage-depleted animals.

The concept of monocyte subsets was initially identified in human blood (Passlick et al., 1989), and subsequent efforts led to the identification of their murine counterparts in Cx3cr1Gfp reporter mice (Geissmann et al., 2003; Jung et al., 2000; Palframan et al., 2001). This paved the way for functional studies of these cells in an organismal context. Notably, Ly6Clow CCR2- murine monocytes were found to patrol blood vessel walls, while Ly6Chigh CCR2+ "inflammatory" monocytes performed classical monocyte functions, including recruitment to sites of acute inflammation for both promoting and resolving inflammation, as well as giving rise to long-lived macrophages at injury sites (Ginhoux and Jung, 2014; Auffray et al., 2007). Unlike transient neutrophils, CM also have the capacity to replace embryo-derived macrophages with their progeny in selected tissue macrophage compartments, potentially affecting tissue physiology during aging (Bain et al., 2014; Varol et al., 2009). Importantly, CM, being HSC progeny, are susceptible to somatic mutations associated with age-related clonal hematopoiesis (CH), and emerging evidence suggests that CH-affected monocyte-derived macrophages (MoMF) may contribute to cardiovascular and CNS pathologies (Cobo et al., 2022) (Kim et al., submitted).

Recent research has provided transcriptomic evidence of CM heterogeneity, revealing signatures resembling those of neutrophils and dendritic cells (DCs) (Weinreb et al., 2020; Yáñez et al., 2017). In our study, we have identified surface markers that discriminate between these proposed NeuMo and DCMo subsets among murine Ly6C+ BM and blood CM. In a steady-state, the majority of murine CM exhibit a NeuMo signature, including CD177+ NeuMo and CD177- CD319- (DN) CM. It's worth noting that our analysis was conducted in mice kept under hyper-hygienic special pathogen-free (SPF) conditions, and the ratio of NeuMo to DCMo

may differ in outbred animals in a natural environment, as these subsets can be influenced by environmental factors.

We have identified CD177 as a marker for NeuMo, consistent with a recent study that identified NeuMo based on their Ym1 (Chil3) expression, as well as surface expression of CD157 (Bst11) and CD88a (Ikeda et al., 2023). These findings align with our results, as CD177+ NeuMo but not CD319+ DCMo expressed these proteins on their surface. Additionally, Ym1 reporter-negative CM in the Ikeda et al. study had higher surface expression of Cx3cr1 compared to Ym1+ CM (Ikeda et al., 2023), supporting the definition of NeuMo and DCMo as proposed in our study.

We have identified CD319 (SLAM family member 7) as a marker for DCMo. Notably, distinguishing between DCMo and DCs, including their precursors, can be challenging, as these cell types share many surface markers due to their common MDP ancestry (Anderson et al., 2020; Hettinger et al., 2013; Yáñez et al., 2017). A recent discovery of a Flt3+ BM monocyte subset with antigen-presenting properties highlights the complexity of this classification (Kamio et al., 2021), although this study did not use CD11c as a discriminator between bona fide CM and DC. We propose that Flt3 may be uniquely expressed in the DC lineage among mature immune cells, as it was not detected in the deep sequencing of Ly6Chigh CD319+ CD11c- DCMo. This suggests that DCMo, as defined in our study, are genuine monocytes rather than DCs. Furthermore, we observed that Clec10a and CD209a can serve as additional markers for DCMo among CM.

We have confirmed differential expression of neutrophil and DC gene modules in blood NeuMo and DCMo, respectively. Classical markers for neutrophils and DCs, such as *Padi4*, *Fpr2*, *Chil3*, *H2-Ab1*, *Cd74*, and *Cd209a*, were robustly expressed in these respective subsets. Additionally, *Cebpb* and *Batf3* were differentially expressed in NeuMo and DCMo, suggesting the regulatory roles of these transcription factors in the repression of DC-like features in CM. Importantly, Cebpb-/- CM were found to express higher levels of *Batf3*, *H2-Ab1*, and *Cd209a* (Mildner et al., 2017), indicating the involvement of CEBPb in this regulatory process. These findings suggest that CEBPb plays a pivotal role in repressing DC-like features in most CM, with DCMo displaying a distinct transcriptional profile compared to NeuMo.

It's crucial to note that while DCMo share transcriptional similarities with previously described CD209a+ Ly6Cint monocytes (Mildner et al., 2017), the cells analyzed in our study were defined and sorted as Ly6Chigh cells under steady-state conditions. Furthermore, CD319- CM, rather than CD319+ DCMo, displayed higher levels of C/EBPb, which is critical for the conversion of CM to non-classical monocytes (NCM) via the Ly6Cint monocyte (Mildner et al., 2017). The relationship between CD319+ Ly6Chigh CM and CD209a+ Ly6Cint cells warrants further investigation.

Our study also supports the notion that NeuMo and DCMo originate from GMP and MDP, respectively (Yáñez et al. 2017). We corroborated this by using Ms4a3Cre:R26LSL-tdTomato mice, a well-established GMP fate mapping model. This aligns with the transcriptomes of NeuMo and CD177-CD319- CM, as the majority of blood CM in these reporter mice were labeled. However, a small fraction of unlabeled CM in the reporter animals expressed higher levels of CD319 and Cx3cr1, suggesting that most DCMo originate from a Ms4a3-independent progenitor, likely MDP. Importantly, sequencing of Ms4a3Cre tagged and non-tagged BM CM confirmed differential expression of neutrophil and DC genes, consistent with our findings in blood NeuMo and DCMo. The precise ontogeny of these CM subsets requires further investigation.

Our data reveal that, in adult C57BL/6 mice under hyper-hygienic conditions, NeuMo dominate the CM population in steady-state conditions. However, following challenges such as CpG and IFN-γ treatment, DCMo become the predominant subset. IFN-γ, in particular, plays a crucial role in differentiating CM into inflammatory CNS-resident MoMF (Amorim et al., 2022), consistent with previous reports of pathogenic Cxcl10+ CM emerging during autoimmune neuroinflammation (Giladi et al., 2020). Additionally, recent findings have highlighted an accumulation of DCMo in aged mice, as evidenced by transcriptional profiling and MHC-II surface expression (Barman et al., 2022; Goodridge, 2023). Together, these data, along with our findings, suggest that DCMo may represent "inflammatory" monocytes that emerge specifically in response to certain inflammatory stimuli and with aging. Further research is needed to thoroughly characterize DCMo, distinguish them from cDCs, and explore their functions.

One of the main functions of monocytes is the differentiation into monocyte-derived tissue resident macrophages. Competitive adoptive cell transfer experiments conducted in our

study demonstrated equal contributions of NeuMo and DCMo to NCM and gut macrophages, although it remains to be determined whether NeuMo and DCMo progeny are identical. In contrast, DCMo preferentially gave rise to lung interstitial macrophages (IM). Furthermore, DCMo-derived IM exhibited higher surface expression of MHC-II, indicative of CM heterogeneity translating to tissue resident macrophage compartments. Interestingly, we observed the persistence of CD16.2+ precursors 12 days after transfer in the lung, which were previously hypothesized to be closely related to NCM (Schyns et al., 2019). However, graft-derived NCM were barely present in the blood on day 12 after transfer, suggesting that lung resident CD16.2+ precursors differ from NCM and warrant further investigation.

Deep sequencing revealed significant differences between DCMo- and NeuMo-derived IM, including the expression of *H2-Aa*. Conversely, NeuMo-derived IM expressed gene modules associated with vasculature development and wound healing, consistent with previous associations of Chil3+ monocytes with inflammation resolution (Ikeda et al., 2018). Additionally, the stratification of differentially expressed genes (DEGs) based on the proposed dichotomy of Lyve1highMHC-IIlow and Lyve1-MHC-IIhigh macrophages across tissues revealed that NeuMo-IM and DCMo-IM fell into the former and latter categories, respectively. This finding contributes to the understanding of tissue resident macrophage heterogeneity.

Lastly, our study demonstrated that NeuMo, but not DCMo, give rise to dura mater macrophages in adoptive transfer experiments. The exact mechanism for this selective recruitment remains to be defined. However, NeuMo differentially express CD62L, and we have shown that the administration of αCD62L antibody prior to NeuMo transfer significantly prevents engraftment. While the specific ligand for CD62L in the dura mater requires further investigation, differential adhesion molecule expression by NeuMo may also contribute to selective extravasation to other peripheral tissues.

It is important to acknowledge that this study involves an adoptive cell transfer model, which may have some limitations in terms of replicating natural physiological processes. However, under steady-state conditions, blood NeuMo are overwhelmingly more abundant than DCMo, necessitating the use of equal numbers of both subsets for the engraftment approach in order to compare their potential fates.

In conclusion, our study identifies surface markers that distinguish murine CM subsets with distinct neutrophil- and DC-like features, consistent with previous reports. We establish that NeuMo and DCMo are genuine monocytes that recirculate in the blood and have the capacity to give rise to tissue resident macrophages. Importantly, NeuMo and DCMo exhibit distinct homing and differentiation patterns in peripheral tissues such as the lung and meninges. Our findings suggest the existence of specialized niches for ontogenically distinct monocytes and propose that NeuMo and DCMo, whose proportions change under various challenges, give rise to transcriptionally and functionally distinct subsets of tissue resident macrophages.

Supplementary Materials

Supplementary Figures

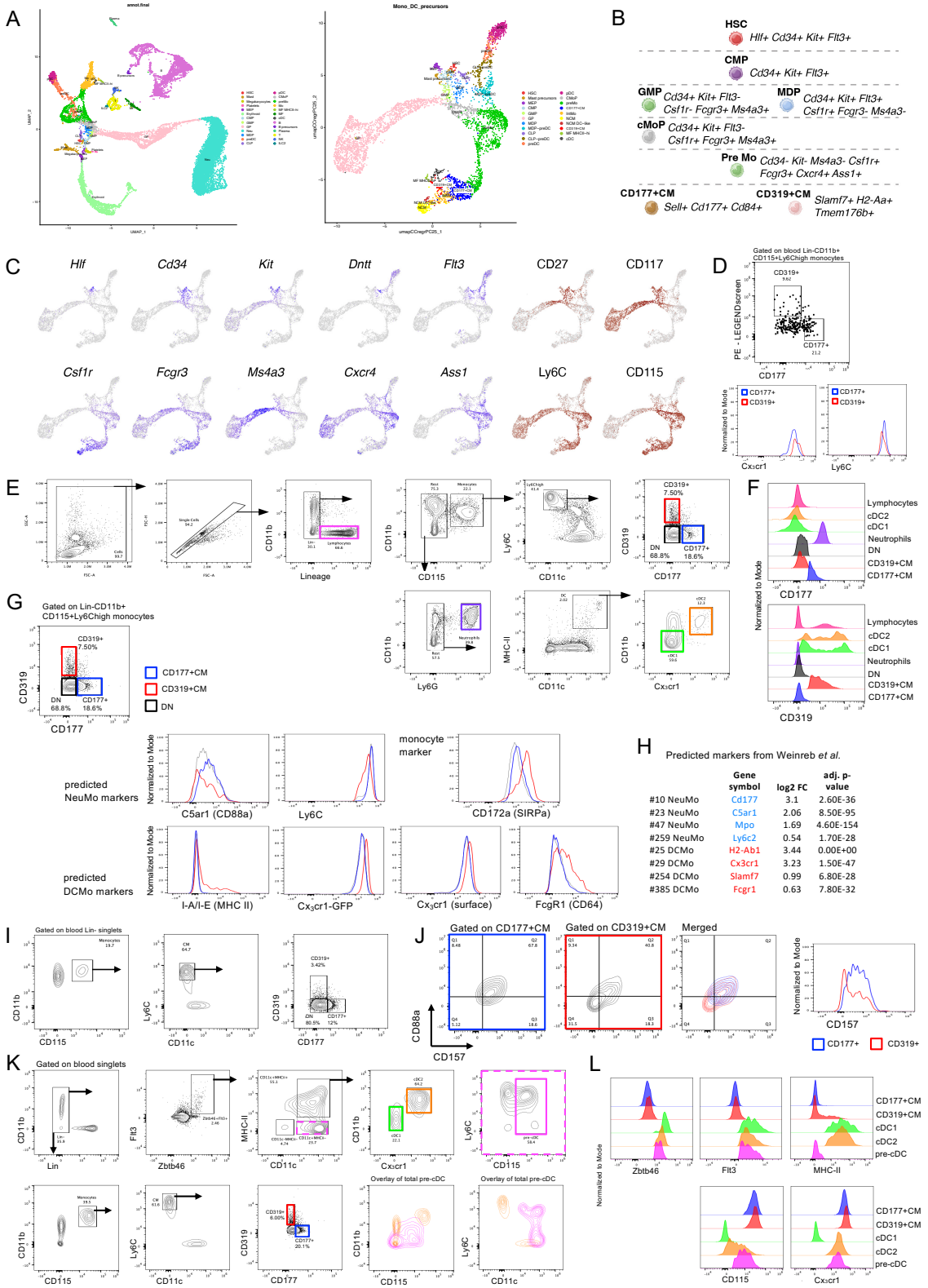

Suppl Figure 1

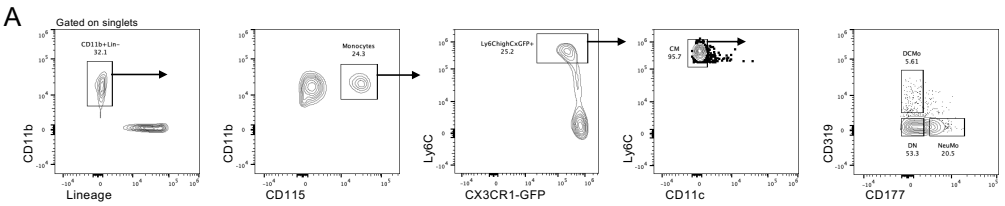

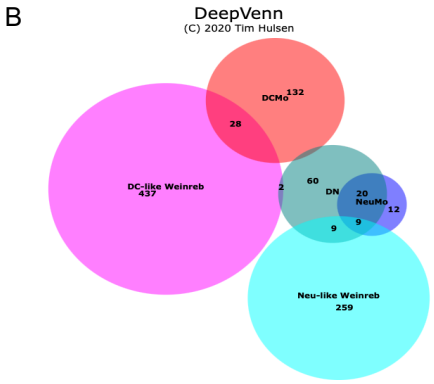

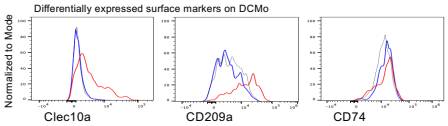

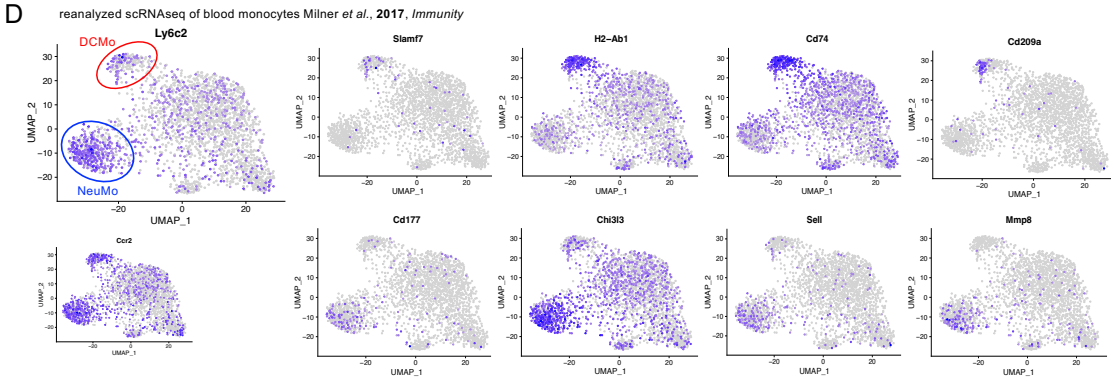

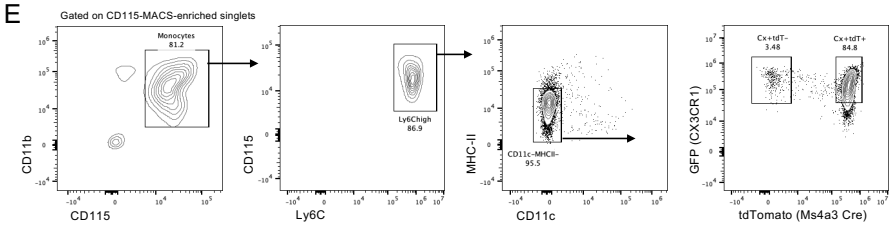

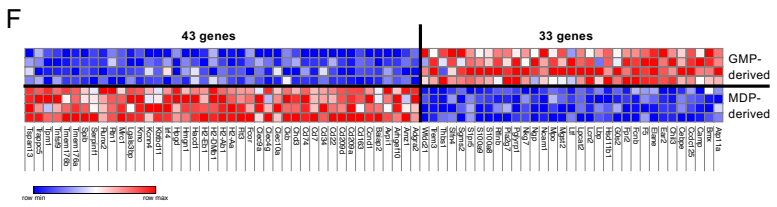

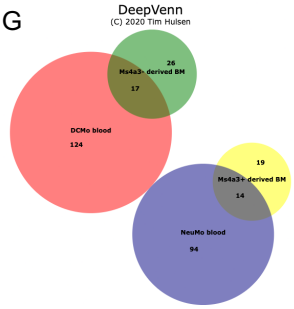

Suppl Figure 2

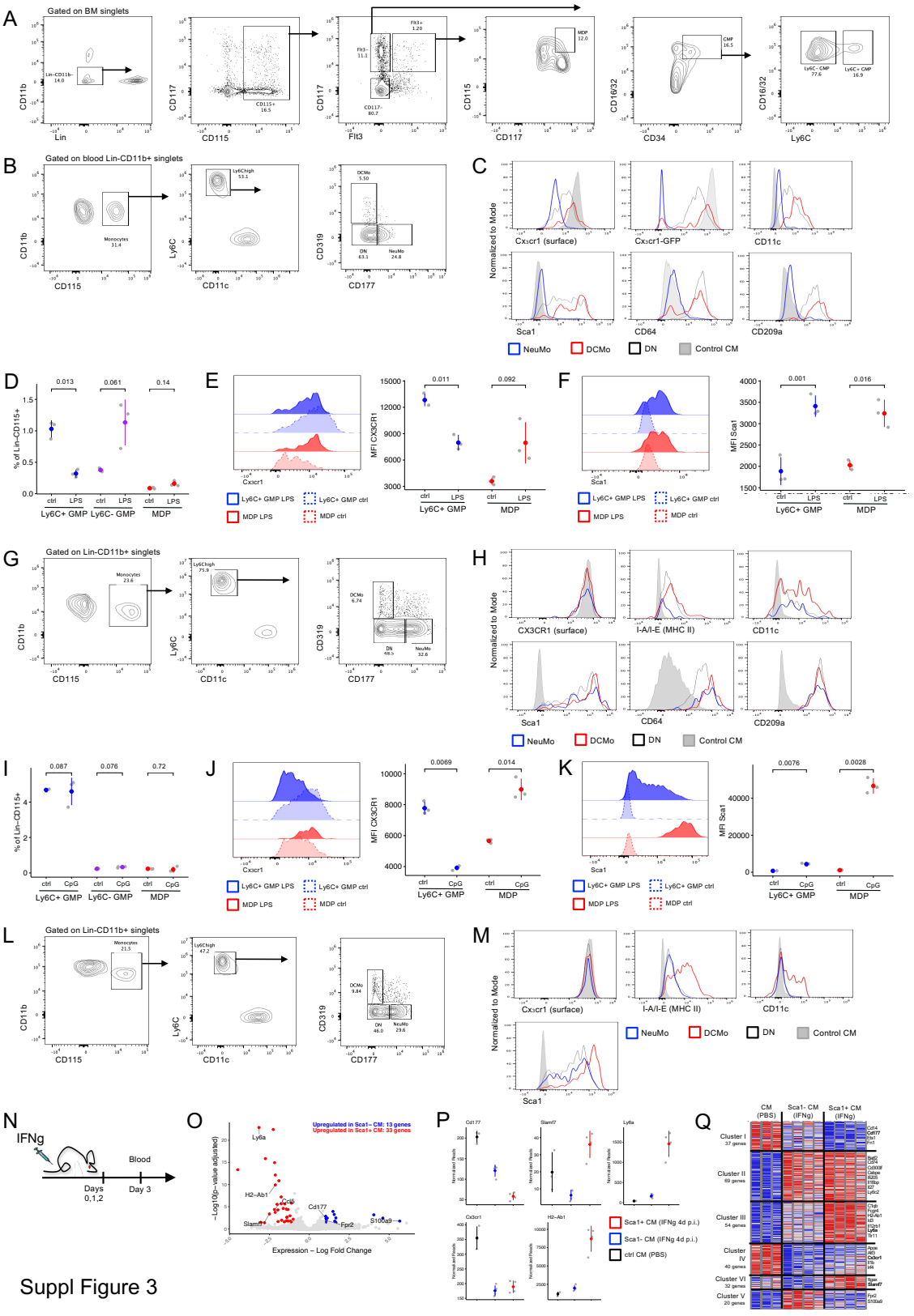

Suppl Figure 3

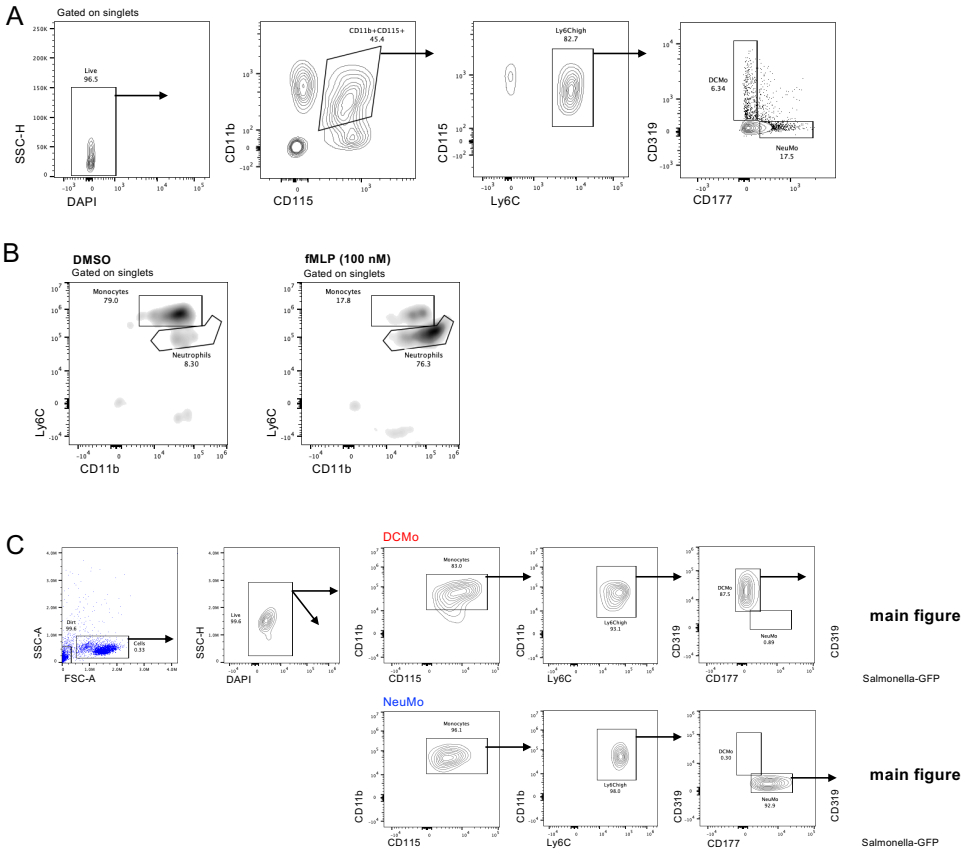

Suppl Figure 4

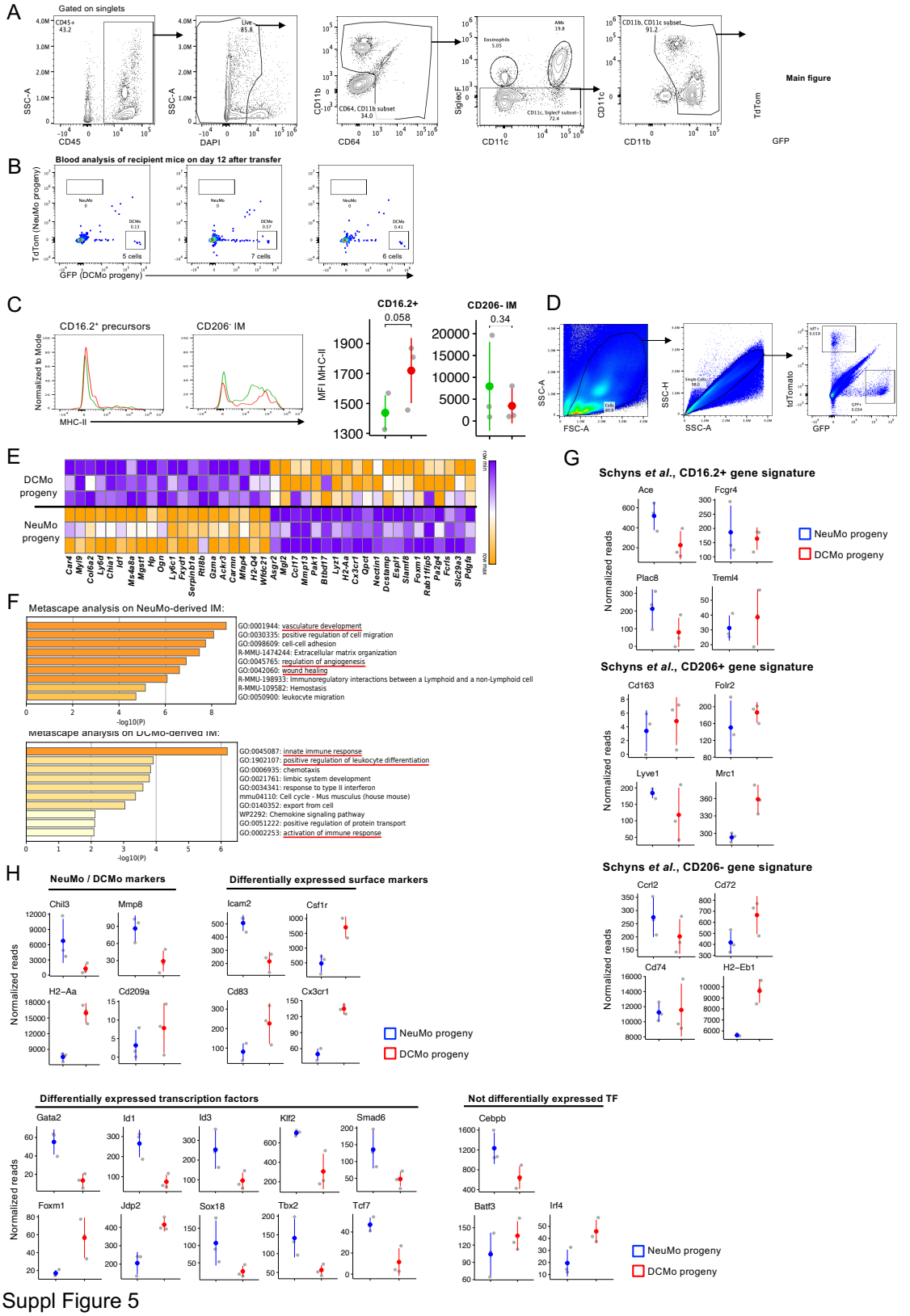

Suppl Figure 5

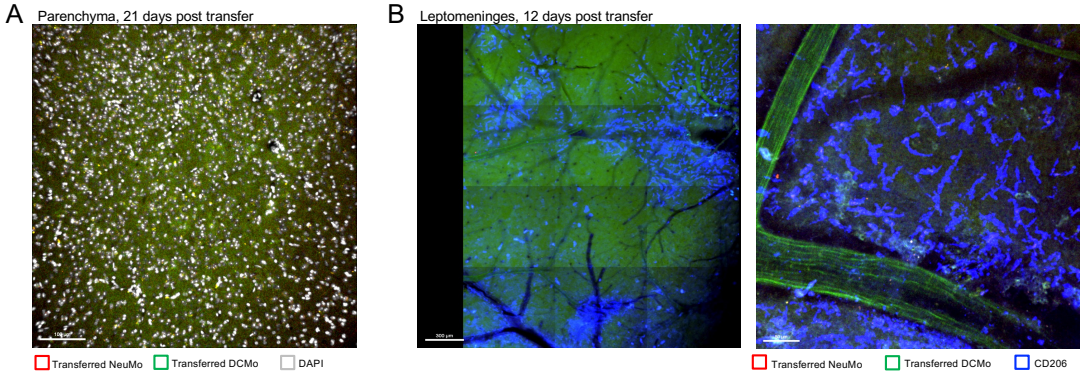

Suppl Figure 6

Supplementary figure legends

Supplemental Figure 1:

(A) UMAP plots of all identified BM cells. Monocytes, DCs and their precursors were selected and analyzed separately, as shown on the right.
(B) Marker genes of BM cell types.
(C) Expression of selected marker genes and proteins (the latter based on CITEseq antibodies) in tha dataset from A.
(D) Dot plot from the LEGENDscreen identifying CD319 as blood CM marker. Histograms for Cx3cr1 and Ly6C shown as a validation for differences to CD177+ cells.
(E) Gating strategy for identification of blood immune subsets.
(F) Histograms showing the expression of CD177 and CD319 among blood immune subsets. (n=4)
(G) Distribution of selected markers for NeuMo and DCMo on CM subsets as predicted by Weinreb et al. (n=3-5)
(H) Table of NeuMo / DCMo markers showing log2 FC and adjusted p-value as adapted from Weinreb *et al*.
(I) Gating strategy for $CD177^+$ and $CD319^+$ from the VIB mouse facility in Brussels, Belgium. (n=3)
(J) Expression of CD88a and CD157 on NeuMo and DCMo in the blood. (n=3)
(K) Gating strategy for identification of a possible contamination of $Zbtb46^+Flt3^+$ cells in the blood CM gate used in this study. (n=3)
(L) Histograms showing the distribution of DC and monocyte markers on monocyte and DC subsets in the blood. (n=3)

Supplemental Figure 2

(A) Gating strategy for sorting CM subsets from the blood of *Cx3cr1*$^{GFP/+}$ mice for bulk RNAseq. (n=4-5)
(B) Venn diagram of DEG genes among CM subsets from this study and DEG from Weinreb et al.
(C) Histograms for differentially expressed surface markers in our bulk RNAseq dataset. (n=3)
(D) Reanalysis of a scRNAseq dataset on total blood monocytes.
(E) Gating strategy for sorting GMP- and MDP-derived CM from the BM of *Ms4a3*^{Cre}*:R26*$^{LSL\text{-}TdTomato}$*:Cx3cr1*^{GFP} mice. (n=4)
(F) Heatmap of all DEG among GMP- and MDP-derived BM CM.
(G) Venn diagram of DEG among GMP- and MDP-derived BM CM and blood NeuMo and DCMo.

Supplementary Figure 3

(A) Gating strategy for BM monocyte precursors.
(B) Gating strategy for PBS-treated mice in the LPS experiment. (n=9 from 3 independent experiments)
(C) Histograms for various markers on CM subsets in LPS-treated mice. (n=9 from 3 independent experiments)
(D) Quantification of BM monocyte precursors in PBS- (ctrl) and LPS-treated mice. (n=3)
(E) Histogram and quantification of Sca1 surface expression on BM monocyte precursors in ctrl and LPS-treated mice. (n=3)
(F) Histogram and quantification of Cx3cr1 surface expression on BM monocyte precursors in ctrl and LPS-treated mice. (N=3)
(G) Gating strategy for PBS-treated mice in the CpG experiment. (n=6 from 2 independent experiments)
(H) Histograms for various markers on CM subsets in CpG-treated mice. (n=6 from 2 independent experiments)
(I) Quantification of BM monocyte precursors in PBS- (ctrl) and CpG-treated mice. (n=3)
(J) Histogram and quantification of Sca1 surface expression on monocyte precursors in ctrl and CpG-treated mice. (n=3)
(K) Histogram and quantification of Cx3cr1 surface expression on monocyte precursors in ctrl and CpG-treated mice. (N=3)
(L) Gating strategy for PBS-treated mice in the IFNg experiment. (n=6 from 2 independent experiments)
(M) Histograms for various markers on CM subsets in IFNg-treated mice. (n=6 from 2 independent experiments)
(N) Experimental scheme for the sorting of $Sca1^+$ and $Sca1^-$ CM after IFNg treatment on 3 consecutive days.
(O) Volcano plot of DEG genes among $Sca1^+$ and $Sca1^-$ CM from IFNg-treated mice.
(P) Gene expression plots of selected genes from $Sca1^+$ and $Sca1^-$ CM from IFNg-treated mice.
(Q) Heat map of DEG among CM from control and IFNg-treated mice.

Supplementary Figure 4

(A) Gating strategy for sorting NeuMo and DCMo from the BM for functional assays.
(B) Density plots of migrated cells from DMSO (ctrl) and fMLP wells. (n=6 from 2 independent experiments)
(C) Gating strategy for measuring engulfment of *S. Tm* in sorted NeuMo and DCMo. (n=13 from 2 independent experiments)

Supplementary Figure 5

(A) Gating strategy for lung IM.
(B) Blood of recipient mice on day 12 after transfer. Each plot represent a biological replicate.
(C) Expression of MHC-II on the surface of CD16.2^{+} precursors and CD206^{-} IM, including MFI quantification. (n=6 from 2 independent experiments)
(D) Gating strategy for sorting NeuMo- and DCMo-derived IM for bulk RNAseq analysis.
(E) Heatmap of the 30 top DEG from NeuMo- and DCMo-derived IM.
(F) Metascape analysis of DEG in NeuMo- and DCMo-derived IM.
(G) Gene plots for gene signatures of lung IM and precursors from Schyns *et al.*
(H) Gene plots for selected genes of interest among NeuMo- and DCMo-derived IM. Among 'NeuMo / DCMo markers', *Mmp8* and *H2-Aa* were differentially expressed.

Supplementary Figure 6

(A) Microscopy picture of the brain parenchyma of DTx-treated recipient mice. Scale bar = 100 µm. (n=3)
(B) Microscopy picture of the leptomeninges of DTx-treated recipient mice. Scale bar = 300 µm. (n=3)
(C) Tile scan of the dura mater of DTx-treated recipient mice. Scale bar = 500 µm. (n=1)
(D) Microscopy pictures of the dura mater of DTx-treated mice transferred with *Cx3cr1*^{GFP} NeuMo and *Cx3cr1*^{Cre}*:R26*$^{LSL\text{-}TdTomato}$ DCMo (2x10^{5} each). Scale bars = 80-100 µm. (n=3)
(E) Tile scans of the colons of isotype- and aCD62L-treated mice. Scale bars = 500-700 µm. (n=2-3)

References

Adamson, B., Norman, T.M., Jost, M., Cho, M.Y., Nuñez, J.K., Chen, Y., Villalta, J.E., Gilbert, L.A., Horlbeck, M.A., Hein, M.Y., Pak, R.A., Gray, A.N., Gross, C.A., Dixit, A., Parnas, O., Regev, A., Weissman, J.S., 2016. A Multiplexed Single-Cell CRISPR Screening Platform Enables Systematic Dissection of the Unfolded Protein Response. Cell 167, 1867-1882.e21. https://doi.org/10.1016/j.cell.2016.11.048

Ahuja, V., Miller, S., Howell, D., 1995. Identification of Two Subpopulations of Rat Monocytes Expressing Disparate Molecular Forms and Quantities of CD43. Cell Immunol 163, 59–69. https://doi.org/10.1006/cimm.1995.1099

Alda-Catalinas, C., Eckersley-Maslin, M.A., Reik, W., 2021. Pooled CRISPR-activation screening coupled with single-cell RNA-seq in mouse embryonic stem cells. Star Protoc 2, 100426. https://doi.org/10.1016/j.xpro.2021.100426

Amit, I., Winter, D., Jung, S., 2016. The role of the local environment and epigenetics in shaping macrophage identity and their effect on tissue homeostasis. Nat Immunol 17, 18–25. https://doi.org/10.1038/ni.3325

Anderson, D.A., Dutertre, C.-A., Ginhoux, F., Murphy, K.M., 2020. Genetic models of human and mouse dendritic cell development and function. Nat Rev Immunol 1–15. https://doi.org/10.1038/s41577-020-00413-x

Askenase, M.H., Han, S.-J., Byrd, A.L., Morais da Fonseca, D., Bouladoux, N., Wilhelm, C., Konkel, J.E., Hand, T.W., Lacerda-Queiroz, N., Su, X., Trinchieri, G., Grainger, J.R., Belkaid, Y., 2015. Bone-Marrow-Resident NK Cells Prime Monocytes for Regulatory Function during Infection. Immunity 42, 1130–1142. https://doi.org/10.1016/j.immuni.2015.05.011

Auffray, C., Fogg, D., Garfa, M., Elain, G., Join-Lambert, O., Kayal, S., Sarnacki, S., Cumano, A., Lauvau, G., Geissmann, F., 2007. Monitoring of Blood Vessels and Tissues by a Population of Monocytes with Patrolling Behavior. Science 317, 666–670. https://doi.org/10.1126/science.1142883

Auffray, C., Fogg, D.K., Narni-Mancinelli, E., Senechal, B., Trouillet, C., Saederup, N., Leemput, J., Bigot, K., Campisi, L., Abitbol, M., Molina, T., Charo, I., Hume, D.A., Cumano, A., Lauvau, G., Geissmann, F., 2009. CX3CR1+ CD115+ CD135+ common macrophage/DC precursors and the role of CX3CR1 in their response to inflammation. J. Exp. Med. 206, 595–606. https://doi.org/10.1084/jem.20081385

Bain, C.C., Bravo-Blas, A., Scott, C.L., Perdiguero, E.G., Geissmann, F., Henri, S., Malissen, B., Osborne, L.C., Artis, D., Mowat, A.M., 2014. Constant replenishment from circulating

monocytes maintains the macrophage pool in the intestine of adult mice. Nat Immunol 15, 929–937. https://doi.org/10.1038/ni.2967

Bianchini, M., Duchêne, J., Santovito, D., Schloss, M.J., Evrard, M., Winkels, H., Aslani, M., Mohanta, S.K., Horckmans, M., Blanchet, X., Lacy, M., Hundelshausen, P. von, Atzler, D., Habenicht, A., Gerdes, N., Pelisek, J., Ng, L.G., Steffens, S., Weber, C., Megens, R.T.A., 2019. PD-L1 expression on nonclassical monocytes reveals their origin and immunoregulatory function. Sci Immunol 4, eaar3054. https://doi.org/10.1126/sciimmunol.aar3054

Biram, A., Liu, J., Hezroni, H., Davidzohn, N., Schmiedel, D., Khatib-Massalha, E., Haddad, M., Grenov, A., Lebon, S., Salame, T.M., Dezorella, N., Hoffman, D., Karam, P.A., Biton, M., Lapidot, T., Bemark, M., Avraham, R., Jung, S., Shulman, Z., 2022. Bacterial infection disrupts established germinal center reactions through monocyte recruitment and impaired metabolic adaptation. Immunity 55, 442-458.e8. https://doi.org/10.1016/j.immuni.2022.01.013

Bohlen, C.J., Bennett, F.C., Tucker, A.F., Collins, H.Y., Mulinyawe, S.B., Barres, B.A., 2017. Diverse Requirements for Microglial Survival, Specification, and Function Revealed by Defined-Medium Cultures. Neuron 94, 759-773.e8. https://doi.org/10.1016/j.neuron.2017.04.043

Bonnardel, J., T'Jonck, W., Gaublomme, D., Browaeys, R., Scott, C.L., Martens, L., Vanneste, B., Prijck, S.D., Nedospasov, S.A., Kremer, A., Hamme, E.V., Borghgraef, P., Toussaint, W., Bleser, P.D., Mannaerts, I., Beschin, A., Grunsven, L.A. van, Lambrecht, B.N., Taghon, T., Lippens, S., Elewaut, D., Saeys, Y., Guilliams, M., 2019. Stellate Cells, Hepatocytes, and Endothelial Cells Imprint the Kupffer Cell Identity on Monocytes Colonizing the Liver Macrophage Niche. Immunity. https://doi.org/10.1016/j.immuni.2019.08.017

Bosteels, C., Neyt, K., Vanheerswynghels, M., Helden, M.J. van, Sichien, D., Debeuf, N., Prijck, S.D., Bosteels, V., Vandamme, N., Martens, L., Saeys, Y., Louagie, E., Lesage, M., Williams, D.L., Tang, S.-C., Mayer, J.U., Ronchese, F., Scott, C.L., Hammad, H., Guilliams, M., Lambrecht, B.N., 2020. Inflammatory Type 2 cDCs Acquire Features of cDC1s and Macrophages to Orchestrate Immunity to Respiratory Virus Infection. Immunity. https://doi.org/10.1016/j.immuni.2020.04.005

Briseño, C.G., Haldar, M., Kretzer, N.M., Wu, X., Theisen, D.J., KC, W., Durai, V., Grajales-Reyes, G.E., Iwata, A., Bagadia, P., Murphy, T.L., Murphy, K.M., 2016. Distinct Transcriptional Programs Control Cross-Priming in Classical and Monocyte-Derived Dendritic Cells. Cell Reports 15, 2462–2474. https://doi.org/10.1016/j.celrep.2016.05.025

Buttgereit, A., Lelios, I., Yu, X., Vrohlings, M., Krakoski, N.R., Gautier, E.L., Nishinakamura, R., Becher, B., Greter, M., 2016. Sall1 is a transcriptional regulator defining microglia identity and function. Nat Immunol 17, 1397–1406. https://doi.org/10.1038/ni.3585

Chakarov, S., Lim, H.Y., Tan, L., Lim, S.Y., See, P., Lum, J., Zhang, X.-M., Foo, S., Nakamizo, S., Duan, K., Kong, W.T., Gentek, R., Balachander, A., Carbajo, D., Bleriot, C., Malleret, B., Tam, J.K.C., Baig, S., Shabeer, M., Toh, S.-A.E.S., Schlitzer, A., Larbi,

A., Marichal, T., Malissen, B., Chen, J., Poidinger, M., Kabashima, K., Bajenoff, M., Ng, L.G., Angeli, V., Ginhoux, F., 2019. Two distinct interstitial macrophage populations coexist across tissues in specific subtissular niches. Science 363, eaau0964. https://doi.org/10.1126/science.aau0964

Chan, M.M., Smith, Z.D., Grosswendt, S., Kretzmer, H., Norman, T.M., Adamson, B., Jost, M., Quinn, J.J., Yang, D., Jones, M.G., Khodaverdian, A., Yosef, N., Meissner, A., Weissman, J.S., 2019. Molecular recording of mammalian embryogenesis. Nature 1–6. https://doi.org/10.1038/s41586-019-1184-5

Chang, P., Hao, L., Offermanns, S., Medzhitov, R., 2014. The microbial metabolite butyrate regulates intestinal macrophage function via histone deacetylase inhibition. Proc National Acad Sci 111, 2247–2252. https://doi.org/10.1073/pnas.1322269111

Chen, Z., Arai, E., Khan, O., Zhang, Z., Ngiow, S.F., He, Y., Huang, H., Manne, S., Cao, Z., Baxter, A.E., Cai, Z., Freilich, E., Ali, M.A., Giles, J.R., Wu, J.E., Greenplate, A.R., Hakeem, M.A., Chen, Q., Kurachi, M., Nzingha, K., Ekshyyan, V., Mathew, D., Wen, Z., Speck, N.A., Battle, A., Berger, S.L., Wherry, E.J., Shi, J., 2021. In vivo CD8+ T cell CRISPR screening reveals control by Fli1 in infection and cancer. Cell 184, 1262-1280.e22. https://doi.org/10.1016/j.cell.2021.02.019

Cheong, C., Matos, I., Choi, J.-H., Dandamudi, D.B., Shrestha, E., Longhi, M.P., Jeffrey, K.L., Anthony, R.M., Kluger, C., Nchinda, G., Koh, H., Rodriguez, A., Idoyaga, J., Pack, M., Velinzon, K., Park, C.G., Steinman, R.M., 2010. Microbial Stimulation Fully Differentiates Monocytes to DC-SIGN/CD209+ Dendritic Cells for Immune T Cell Areas. Cell 143, 416–429. https://doi.org/10.1016/j.cell.2010.09.039

Chiou, S.-H., Winters, I.P., Wang, J., Naranjo, S., Dudgeon, C., Tamburini, F.B., Brady, J.J., Yang, D., Grüner, B.M., Chuang, C.-H., Caswell, D.R., Zeng, H., Chu, P., Kim, G.E., Carpizo, D.R., Kim, S.K., Winslow, M.M., 2015. Pancreatic cancer modeling using retrograde viral vector delivery and in vivo CRISPR/Cas9-mediated somatic genome editing. Gene Dev 29, 1576–1585. https://doi.org/10.1101/gad.264861.115

Chong, S.Z., Evrard, M., Devi, S., Chen, J., Lim, J.Y., See, P., Zhang, Y., Adrover, J.M., Lee, B., Tan, L., Li, J.L.Y., Liong, K.H., Phua, C., Balachander, A., Boey, A., Liebl, D., Tan, S.M., Chan, J.K.Y., Balabanian, K., Harris, J.E., Bianchini, M., Weber, C., Duchene, J., Lum, J., Poidinger, M., Chen, Q., Rénia, L., Wang, C.-I., Larbi, A., Randolph, G.J., Weninger, W., Looney, M.R., Krummel, M.F., Biswas, S.K., Ginhoux, F., Hidalgo, A., Bachelerie, F., Ng, L.G., 2016. CXCR4 identifies transitional bone marrow premonocytes that replenish the mature monocyte pool for peripheral responses. J Exp Med 213, 2293–2314. https://doi.org/10.1084/jem.20160800

Christ, A., Günther, P., Lauterbach, M.A.R., Duewell, P., Biswas, D., Pelka, K., Scholz, C.J., Oosting, M., Haendler, K., Baßler, K., Klee, K., Schulte-Schrepping, J., Ulas, T., Moorlag, S.J.C.F.M., Kumar, V., Park, M.H., Joosten, L.A.B., Groh, L.A., Riksen, N.P., Espevik, T., Schlitzer, A., Li, Y., Fitzgerald, M.L., Netea, M.G., Schultze, J.L., Latz, E., 2018. Western Diet Triggers NLRP3-Dependent Innate Immune Reprogramming. Cell 172, 162-175.e14. https://doi.org/10.1016/j.cell.2017.12.013

Datlinger, P., Rendeiro, A.F., Schmidl, C., Krausgruber, T., Traxler, P., Klughammer, J., Schuster, L.C., Kuchler, A., Alpar, D., Bock, C., 2017. Pooled CRISPR screening with single-cell transcriptome readout. Nat Methods 14, 297–301. https://doi.org/10.1038/nmeth.4177

Doench, J.G., Fusi, N., Sullender, M., Hegde, M., Vaimberg, E.W., Donovan, K.F., Smith, I., Tothova, Z., Wilen, C., Orchard, R., Virgin, H.W., Listgarten, J., Root, D.E., 2016. Optimized sgRNA design to maximize activity and minimize off-target effects of CRISPR-Cas9. Nat Biotechnol 34, 184–191. https://doi.org/10.1038/nbt.3437

Dong, M.B., Wang, G., Chow, R.D., Ye, L., Zhu, L., Dai, X., Park, J.J., Kim, H.R., Errami, Y., Guzman, C.D., Zhou, X., Chen, K.Y., Renauer, P.A., Du, Y., Shen, J., Lam, S.Z., Zhou, J.J., Lannin, D.R., Herbst, R.S., Chen, S., 2019. Systematic Immunotherapy Target Discovery Using Genome-Scale In Vivo CRISPR Screens in CD8 T Cells. Cell 178, 1189-1204.e23. https://doi.org/10.1016/j.cell.2019.07.044

Fogg, D.K., Sibon, C., Miled, C., Jung, S., Aucouturier, P., Littman, D.R., Cumano, A., Geissmann, F., 2006. A Clonogenic Bone Marrow Progenitor Specific for Macrophages and Dendritic Cells. Science 311, 83–87. https://doi.org/10.1126/science.1117729

Furth, R. van, Cohn, Z.A., 1968. THE ORIGIN AND KINETICS OF MONONUCLEAR PHAGOCYTES. J Exp Medicine 128, 415–435. https://doi.org/10.1084/jem.128.3.415

Gamrekelashvili, J., Giagnorio, R., Jussofie, J., Soehnlein, O., Duchene, J., Briseño, C.G., Ramasamy, S.K., Krishnasamy, K., Limbourg, A., Häger, C., Kapanadze, T., Ishifune, C., Hinkel, R., Radtke, F., Strobl, L.J., Zimber-Strobl, U., Napp, L.C., Bauersachs, J., Haller, H., Yasutomo, K., Kupatt, C., Murphy, K.M., Adams, R.H., Weber, C., Limbourg, F.P., 2016. Regulation of monocyte cell fate by blood vessels mediated by Notch signalling. Nat Commun 7, 12597. https://doi.org/10.1038/ncomms12597

Gamrekelashvili, J., Kapanadze, T., Sablotny, S., Ratiu, C., Dastagir, K., Lochner, M., Karbach, S., Wenzel, P., Sitnow, A., Fleig, S., Sparwasser, T., Kalinke, U., Holzmann, B., Haller, H., Limbourg, F.P., 2020. Notch and TLR signaling coordinate monocyte cell fate and inflammation. Elife 9, e57007. https://doi.org/10.7554/elife.57007

Geissmann, F., Jung, S., Littman, D.R., 2003. Blood Monocytes Consist of Two Principal Subsets with Distinct Migratory Properties 19. https://doi.org/10.1016/s1074-7613(03)00174-2

Giladi, A., Paul, F., Herzog, Y., Lubling, Y., Weiner, A., Yofe, I., Jaitin, D., Cabezas-Wallscheid, N., Dress, R., Ginhoux, F., Trumpp, A., Tanay, A., Amit, I., 2018. Single-cell characterization of haematopoietic progenitors and their trajectories in homeostasis and perturbed haematopoiesis. Nat Cell Biol 20, 836–846. https://doi.org/10.1038/s41556-018-0121-4

Giladi, A., Wagner, L.K., Li, H., Dörr, D., Medaglia, C., Paul, F., Shemer, A., Jung, S., Yona, S., Mack, M., Leutz, A., Amit, I., Mildner, A., 2020. Cxcl10+ monocytes define a pathogenic subset in the central nervous system during autoimmune neuroinflammation. Nat Immunol 1–10. https://doi.org/10.1038/s41590-020-0661-1

Ginhoux, F., Guilliams, M., 2016. Tissue-Resident Macrophage Ontogeny and Homeostasis. Immunity 44, 439–449. https://doi.org/10.1016/j.immuni.2016.02.024

Ginhoux, F., Jung, S., 2014. Monocytes and macrophages: developmental pathways and tissue homeostasis. Nat Rev Immunol 14, 392–404. https://doi.org/10.1038/nri3671

Goldmann, T., Wieghofer, P., Jordão, M.J.C., Prutek, F., Hagemeyer, N., Frenzel, K., Amann, L., Staszewski, O., Kierdorf, K., Krueger, M., Locatelli, G., Hochgerner, H., Zeiser, R., Epelman, S., Geissmann, F., Priller, J., Rossi, F.M.V., Bechmann, I., Kerschensteiner, M., Linnarsson, S., Jung, S., Prinz, M., 2016. Origin, fate and dynamics of macrophages at central nervous system interfaces. Nat Immunol 17, 797–805. https://doi.org/10.1038/ni.3423

Gosselin, D., Link, V.M., Romanoski, C.E., Fonseca, G.J., Eichenfield, D.Z., Spann, N.J., Stender, J.D., Chun, H.B., Garner, H., Geissmann, F., Glass, C.K., 2014. Environment Drives Selection and Function of Enhancers Controlling Tissue-Specific Macrophage Identities. Cell 159, 1327–1340. https://doi.org/10.1016/j.cell.2014.11.023

Gross-Vered, M., Trzebanski, S., Shemer, A., Bernshtein, B., Curato, C., Stelzer, G., Salame, T.-M., David, E., Boura-Halfon, S., Chappell-Maor, L., Leshkowitz, D., Jung, S., 2020. Defining murine monocyte differentiation into colonic and ileal macrophages. Elife 9, e49998. https://doi.org/10.7554/elife.49998

Guilliams, M., Mildner, A., Yona, S., 2018. Developmental and Functional Heterogeneity of Monocytes. Immunity 49, 595–613. https://doi.org/10.1016/j.immuni.2018.10.005

Guilliams, M., Scott, C.L., 2017. Does niche competition determine the origin of tissue-resident macrophages? Nat Rev Immunol 17, 451–460. https://doi.org/10.1038/nri.2017.42

Guo, F., He, H., Fu, Z.-C., Huang, S., Chen, T., Papasian, C.J., Morse, L.R., Xu, Y., Battaglino, R.A., Yang, X.-F., Jiang, Z., Xin, H.-B., Fu, M., 2015. Adipocyte-derived PAMM suppresses macrophage inflammation by inhibiting MAPK signalling. Biochem. J. 472, 309–18. https://doi.org/10.1042/bj20150019

Hagemeyer, N., Kierdorf, K., Frenzel, K., Xue, J., Ringelhan, M., Abdullah, Z., Godin, I., Wieghofer, P., Jordão, M.J.C., Ulas, T., Yorgancioglu, G., Rosenbauer, F., Knolle, P.A., Heikenwalder, M., Schultze, J.L., Prinz, M., 2016. Transcriptome-based profiling of yolk sac-derived macrophages reveals a role for Irf8 in macrophage maturation. Embo J 35, 1730–1744. https://doi.org/10.15252/embj.201693801

Hanna, R.N., Carlin, L.M., Hubbeling, H.G., Nackiewicz, D., Green, A.M., Punt, J.A., Geissmann, F., Hedrick, C.C., 2011. The transcription factor NR4A1 (Nur77) controls bone marrow differentiation and the survival of Ly6C− monocytes. Nat Immunol 12, 778. https://doi.org/10.1038/ni.2063

Hettinger, J., Richards, D.M., Hansson, J., Barra, M.M., Joschko, A.-C., Krijgsveld, J., Feuerer, M., 2013. Origin of monocytes and macrophages in a committed progenitor. Nat Immunol 14, ni.2638. https://doi.org/10.1038/ni.2638

Hill, A.J., McFaline-Figueroa, J.L., Starita, L.M., Gasperini, M.J., Matreyek, K.A., Packer, J., Jackson, D., Shendure, J., Trapnell, C., 2018. On the design of CRISPR-based single-cell molecular screens. Nat Methods 15, 271. https://doi.org/10.1038/nmeth.4604

Hoeffel, G., Ginhoux, F., 2018. Fetal Monocytes and the Origins of Tissue-Resident Macrophages. Cell Immunol. https://doi.org/10.1016/j.cellimm.2018.01.001

Hou, X., Chen, G., Bracamonte-Baran, W., Choi, H.S., Diny, N.L., Sung, J., Hughes, D., Won, T., Wood, M.K., Talor, M.V., Hackam, D.J., Klingel, K., Davogustto, G., Taegtmeyer, H., Coppens, I., Barin, J.G., Čiháková, D., 2019. The Cardiac Microenvironment Instructs Divergent Monocyte Fates and Functions in Myocarditis. Cell Reports 28, 172-189.e7. https://doi.org/10.1016/j.celrep.2019.06.007

Hove, H.V., Martens, L., Scheyltjens, I., Vlaminck, K.D., Antunes, A.R.P., Prijck, S.D., Vandamme, N., Schepper, S.D., Isterdael, G.V., Scott, C.L., Aerts, J., Berx, G., Boeckxstaens, G.E., Vandenbroucke, R.E., Vereecke, L., Moechars, D., Guilliams, M., Ginderachter, J.A.V., Saeys, Y., Movahedi, K., 2019. A single-cell atlas of mouse brain macrophages reveals unique transcriptional identities shaped by ontogeny and tissue environment. Nat Neurosci 22, 1021–1035. https://doi.org/10.1038/s41593-019-0393-4

Huang, H., Zhou, P., Wei, J., Long, L., Shi, H., Dhungana, Y., Chapman, N.M., Fu, G., Saravia, J., Raynor, J.L., Liu, S., Palacios, G., Wang, Y.-D., Qian, C., Yu, J., Chi, H., 2021. In vivo CRISPR screening reveals nutrient signaling processes underpinning CD8+ T cell fate decisions. Cell 184, 1245-1261.e21. https://doi.org/10.1016/j.cell.2021.02.021

Ikeda, N., Asano, K., Kikuchi, K., Uchida, Y., Ikegami, H., Takagi, R., Yotsumoto, S., Shibuya, T., Makino-Okamura, C., Fukuyama, H., Watanabe, T., Ohmuraya, M., Araki, K., Nishitai, G., Tanaka, M., 2018. Emergence of immunoregulatory Ym1+Ly6Chi monocytes during recovery phase of tissue injury. Sci Immunol 3, eaat0207. https://doi.org/10.1126/sciimmunol.aat0207

Ikeda, N., Kubota, H., Suzuki, R., Morita, M., Yoshimura, A., Osada, Y., Kishida, K., Kitamura, D., Iwata, A., Yotsumoto, S., Kurotaki, D., Nishimura, K., Nishiyama, A., Tamura, T., Kamatani, T., Tsunoda, T., Murakawa, M., Asahina, Y., Hayashi, Y., Harada, H., Harada, Y., Yokota, A., Hirai, H., Seki, T., Kuwahara, M., Yamashita, M., Shichino, S., Tanaka, M., Asano, K., 2023. The early neutrophil-committed progenitors aberrantly differentiate into immunoregulatory monocytes during emergency myelopoiesis. Cell Reports 42, 112165. https://doi.org/10.1016/j.celrep.2023.112165

Ingersoll, M., Spanbroek, R., Lottaz, C., Gautier, E., Frankenberger, M., Hoffmann, R., Lang, R., Haniffa, M., Collin, M., Tacke, F., Habenicht, A., Ziegler-Heitbrock, L., Randolph, G., 2010. Comparison of gene expression profiles between human and mouse monocyte subsets. Blood 115, e10–e19. https://doi.org/10.1182/blood-2009-07-235028

Jaitin, D.A., Weiner, A., Yofe, I., Lara-Astiaso, D., Keren-Shaul, H., David, E., Salame, T.M., Tanay, A., Oudenaarden, A. van, Amit, I., 2016. Dissecting Immune Circuits by Linking CRISPR-Pooled Screens with Single-Cell RNA-Seq. Cell 167, 1883-1896.e15. https://doi.org/10.1016/j.cell.2016.11.039

Jung, S., Aliberti, J., Graemmel, P., Sunshine, M.J., Kreutzberg, G.W., Sher, A., Littman, D.R., 2000. Analysis of Fractalkine Receptor CX3CR1 Function by Targeted Deletion and Green Fluorescent Protein Reporter Gene Insertion. Mol Cell Biol 20, 4106–4114. https://doi.org/10.1128/mcb.20.11.4106-4114.2000

Kellermayer, Z., Vojkovics, D., Dakah, T.A., Bodó, K., Botz, B., Helyes, Z., Berta, G., Kajtár, B., Schippers, A., Wagner, N., Scotto, L., O'Connor, O.A., Arnold, H.-H., Balogh, P., 2019. IL-22–Independent Protection from Colitis in the Absence of Nkx2.3 Transcription Factor in Mice. J. Immunol. 202, 1833–1844. https://doi.org/10.4049/jimmunol.1801117

Kim, W., Sun, Y., Do, H., Autissier, P., Halpern, E., Piatak, M., Lifson, J., Burdo, T., McGrath, M., Williams, K., 2010. Monocyte heterogeneity underlying phenotypic changes in monocytes according to SIV disease stage. J Leukocyte Biol 87, 557–567. https://doi.org/10.1189/jlb.0209082

Kwissa, M., Nakaya, H., Oluoch, H., Pulendran, B., 2012. Distinct TLR adjuvants differentially stimulate systemic and local innate immune responses in nonhuman primates. Blood 119, 2044–2055. https://doi.org/10.1182/blood-2011-10-388579

LaFleur, M.W., Nguyen, T.H., Coxe, M.A., Miller, B.C., Yates, K.B., Gillis, J.E., Sen, D.R., Gaudiano, E.F., Abosy, R.A., Freeman, G.J., Haining, W.N., Sharpe, A.H., 2019. PTPN2 regulates the generation of exhausted CD8+ T cell subpopulations and restrains tumor immunity. Nat Immunol 20, 1335–1347. https://doi.org/10.1038/s41590-019-0480-4

Lavin, Y., Winter, D., Blecher-Gonen, R., David, E., Keren-Shaul, H., Merad, M., Jung, S., Amit, I., 2014. Tissue-Resident Macrophage Enhancer Landscapes Are Shaped by the Local Microenvironment. Cell 159, 1312–1326. https://doi.org/10.1016/j.cell.2014.11.018

Lee, P.Y., Wang, J., Parisini, E., Dascher, C.C., Nigrovic, P.A., 2013. Ly6 family proteins in neutrophil biology. J Leukocyte Biol 94, 585–594. https://doi.org/10.1189/jlb.0113014

Li, H., Huo, Y., He, X., Yao, L., Zhang, H., Cui, Y., Xiao, H., Xie, W., Zhang, D., Wang, Y., Zhang, S., Tu, H., Cheng, Y., Guo, Y., Cao, X., Zhu, Y., Jiang, T., Guo, X., Qin, Y., Sha, J., 2022. A male germ-cell-specific ribosome controls male fertility. Nature 612, 725–731. https://doi.org/10.1038/s41586-022-05508-0

Li, H., Papadopoulos, V., 1998. Peripheral-type benzodiazepine receptor function in cholesterol transport. Identification of a putative cholesterol recognition/interaction amino acid sequence and consensus pattern. Endocrinology 139, 4991–7. https://doi.org/10.1210/endo.139.12.6390

Liu, Z., Wang, Haiting, Li, Z., Dress, R.J., Zhu, Y., Zhang, S., Feo, D.D., Kong, W.T., Cai, P., Shin, A., Piot, C., Yu, J., Gu, Y., Zhang, M., Gao, C., Chen, L., Wang, Honglin, Vétillard, M., Guermonprez, P., Kwok, I., Ng, L.G., Chakarov, S., Schlitzer, A., Becher, B., Dutertre, C.-A., Su, B., Ginhoux, F., 2023. Dendritic cell type 3 arises from Ly6C+ monocyte-dendritic cell progenitors. Immunity 56, 1761-1777.e6. https://doi.org/10.1016/j.immuni.2023.07.001

Liu, Zhaoyuan, Gu, Y., Chakarov, S., Bleriot, C., Kwok, I., Chen, X., Shin, A., Huang, W., Dress, R.J., Dutertre, C.-A., Schlitzer, A., Chen, J., Ng, L.G., Wang, H., Liu, Zhiduo, Su, B., Ginhoux, F., 2019. Fate Mapping via Ms4a3-Expression History Traces Monocyte-Derived Cells. Cell 178, 1509-1525.e19. https://doi.org/10.1016/j.cell.2019.08.009

Manguso, R.T., Pope, H.W., Zimmer, M.D., Brown, F.D., Yates, K.B., Miller, B.C., Collins, N.B., Bi, K., LaFleur, M.W., Juneja, V.R., Weiss, S.A., Lo, J., Fisher, D.E., Miao, D., Allen, E.V., Root, D.E., Sharpe, A.H., Doench, J.G., Haining, W.N., 2017. In vivo CRISPR screening identifies Ptpn2 as a cancer immunotherapy target. Nature 547, 413. https://doi.org/10.1038/nature23270

Mass, E., Ballesteros, I., Farlik, M., Halbritter, F., Günther, P., Crozet, L., Jacome-Galarza, C.E., Händler, K., Klughammer, J., Kobayashi, Y., Gomez-Perdiguero, E., Schultze, J.L., Beyer, M., Bock, C., Geissmann, F., 2016. Specification of tissue-resident macrophages during organogenesis. Science 353, aaf4238. https://doi.org/10.1126/science.aaf4238

Menezes, S., Melandri, D., Anselmi, G., Perchet, T., Loschko, J., Dubrot, J., Patel, R., Gautier, E.L., Hugues, S., Longhi, M.P., Henry, J.Y., Quezada, S.A., Lauvau, G., Lennon-Duménil, A.-M., Gutiérrez-Martínez, E., Bessis, A., Gomez-Perdiguero, E., Jacome-Galarza, C.E., Garner, H., Geissmann, F., Golub, R., Nussenzweig, M.C., Guermonprez, P., 2016. The Heterogeneity of Ly6Chi Monocytes Controls Their Differentiation into iNOS+ Macrophages or Monocyte-Derived Dendritic Cells. Immunity 45, 1205–1218. https://doi.org/10.1016/j.immuni.2016.12.001

Meredith, M., Liu, K., Darrasse-Jeze, G., Kamphorst, A., Schreiber, H., Guermonprez, P., Idoyaga, J., Cheong, C., Yao, K., Niec, R., Nussenzweig, M., 2012. Expression of the zinc finger transcription factor zDC (Zbtb46, Btbd4) defines the classical dendritic cell lineage. J Exp Medicine 209, 1153–1165. https://doi.org/10.1084/jem.20112675

Mildner, A., Schönheit, J., Giladi, A., David, E., Lara-Astiaso, D., Lorenzo-Vivas, E., Paul, F., Chappell-Maor, L., Priller, J., Leutz, A., Amit, I., Jung, S., 2017. Genomic Characterization of Murine Monocytes Reveals C/EBPβ Transcription Factor Dependence of Ly6C− Cells. Immunity 46, 849-862.e7. https://doi.org/10.1016/j.immuni.2017.04.018

Misharin, A.V., Cuda, C.M., Saber, R., Turner, J.D., Gierut, A.K., Haines, G.K., Berdnikovs, S., Filer, A., Clark, A.R., Buckley, C.D., Mutlu, G.M., Budinger, G.R.S., Perlman, H., 2014. Nonclassical Ly6C− Monocytes Drive the Development of Inflammatory Arthritis in Mice. Cell Reports 9, 591–604. https://doi.org/10.1016/j.celrep.2014.09.032

Mortha, A., Chudnovskiy, A., Hashimoto, D., Bogunovic, M., Spencer, S.P., Belkaid, Y., Merad, M., 2014. Microbiota-Dependent Crosstalk Between Macrophages and ILC3 Promotes Intestinal Homeostasis. Science 343, 1249288. https://doi.org/10.1126/science.1249288

Mostoslavsky, G., Kotton, D.N., Fabian, A.J., Gray, J.T., Lee, J.-S., Mulligan, R.C., 2005. Efficiency of transduction of highly purified murine hematopoietic stem cells by lentiviral and oncoretroviral vectors under conditions of minimal in vitro manipulation. Mol Ther 11, 932–940. https://doi.org/10.1016/j.ymthe.2005.01.005

Nahrendorf, M., Swirski, F.K., Aikawa, E., Stangenberg, L., Wurdinger, T., Figueiredo, J.-L., Libby, P., Weissleder, R., Pittet, M.J., 2007. The healing myocardium sequentially mobilizes two monocyte subsets with divergent and complementary functions. J Exp Medicine 204, 3037–3047. https://doi.org/10.1084/jem.20070885

Naik, S., Perié, L., Swart, E., Gerlach, C., Rooij, N., Boer, Rj., Schumacher, T., 2013. Diverse and heritable lineage imprinting of early haematopoietic progenitors. Nature 496, 229–232. https://doi.org/10.1038/nature12013

Nestorowa, S., Hamey, F., Sala, B., Diamanti, E., Shepherd, M., Laurenti, E., Wilson, N., Kent, D., Göttgens, B., 2016. A single-cell resolution map of mouse hematopoietic stem and progenitor cell differentiation. Blood 128, e20-31. https://doi.org/10.1182/blood-2016-05-716480

Okabe, Y., Medzhitov, R., 2014. Tissue-Specific Signals Control Reversible Program of Localization and Functional Polarization of Macrophages. Cell 157, 832–844. https://doi.org/10.1016/j.cell.2014.04.016

Olsson, A., Venkatasubramanian, M., Chaudhri, V., Aronow, B., Salomonis, N., Singh, H., Grimes, H., 2016. Single-cell analysis of mixed-lineage states leading to a binary cell fate choice. Nature 537, 698–702. https://doi.org/10.1038/nature19348

Palframan, R., Jung, S., Cheng, G., Weninger, W., Luo, Y., Dorf, M., Littman, D., Rollins, B., Zweerink, H., Rot, A., Andrian, Uh., 2001. Inflammatory Chemokine Transport and Presentation in HEV A Remote Control Mechanism for Monocyte Recruitment to Lymph Nodes in Inflamed Tissues. J Exp Medicine 194, 1361–1374. https://doi.org/10.1084/jem.194.9.1361

Passlick, B., Flieger, D., Ziegler-Heitbrock, H., 1989. Identification and characterization of a novel monocyte subpopulation in human peripheral blood. Blood 74, 2527–2534. https://doi.org/10.1182/blood.v74.7.2527.bloodjournal7472527

Patel, A., Zhang, Y., Fullerton, J., Boelen, L., Rongvaux, A., Maini, A., Bigley, V., Flavell, R., Gilroy, D., Asquith, B., Macallan, D., Yona, S., 2017. The fate and lifespan of human monocyte subsets in steady state and systemic inflammationHuman monocyte kinetics. J Exp Medicine 214, 1913–1923. https://doi.org/10.1084/jem.20170355

Paul, F., Arkin, Y., Giladi, A., Jaitin, D., Kenigsberg, E., Keren-Shaul, H., Winter, D., Lara-Astiaso, D., Gury, M., Weiner, A., David, E., Cohen, N., Lauridsen, F., Haas, S., Schlitzer, A., Mildner, A., Ginhoux, F., Jung, S., Trumpp, A., Porse, B., Tanay, A., Amit, I., 2015. Transcriptional Heterogeneity and Lineage Commitment in Myeloid Progenitors. Cell 163, 1663–1677. https://doi.org/10.1016/j.cell.2015.11.013

Prinz, M., Jung, S., Priller, J., 2019. Microglia Biology: One Century of Evolving Concepts. Cell 179, 292–311. https://doi.org/10.1016/j.cell.2019.08.053

Quinn, J.J., Jones, M.G., Okimoto, R.A., Nanjo, S., Chan, M.M., Yosef, N., Bivona, T.G., Weissman, J.S., 2021. Single-cell lineages reveal the rates, routes, and drivers of metastasis in cancer xenografts. Science 371, eabc1944. https://doi.org/10.1126/science.abc1944

Raj, B., Gagnon, J.A., Schier, A.F., 2018. Large-scale reconstruction of cell lineages using single-cell readout of transcriptomes and CRISPR–Cas9 barcodes by scGESTALT. Nat Protoc 13, 2685–2713. https://doi.org/10.1038/s41596-018-0058-x

Replogle, J.M., Norman, T.M., Xu, A., Hussmann, J.A., Chen, J., Cogan, J.Z., Meer, E.J., Terry, J.M., Riordan, D.P., Srinivas, N., Fiddes, I.T., Arthur, J.G., Alvarado, L.J., Pfeiffer, K.A., Mikkelsen, T.S., Weissman, J.S., Adamson, B., 2020. Combinatorial single-cell CRISPR screens by direct guide RNA capture and targeted sequencing. Nat Biotechnol 1–8. https://doi.org/10.1038/s41587-020-0470-y

Rooks, M.G., Garrett, W.S., 2016. Gut microbiota, metabolites and host immunity. Nat Rev Immunol 16, 341–352. https://doi.org/10.1038/nri.2016.42

Saito, A., Kamikawa, Y., Ito, T., Matsuhisa, K., Kaneko, M., Okamoto, T., Yoshimaru, T., Matsushita, Y., Katagiri, T., Imaizumi, K., 2023. p53-independent tumor suppression by cell-cycle arrest via CREB/ATF transcription factor OASIS. Cell Rep. 42, 112479. https://doi.org/10.1016/j.celrep.2023.112479

Satoh, T., Nakagawa, K., Sugihara, F., Kuwahara, R., Ashihara, M., Yamane, F., Minowa, Y., Fukushima, K., Ebina, I., Yoshioka, Y., Kumanogoh, A., Akira, S., 2017. Identification of an atypical monocyte and committed progenitor involved in fibrosis. Nature 541, 96. https://doi.org/10.1038/nature20611

Satpathy, A., KC, W., Albring, J., Edelson, B., Kretzer, N., Bhattacharya, D., Murphy, T., Murphy, K., 2012. Zbtb46 expression distinguishes classical dendritic cells and their committed progenitors from other immune lineages. J Exp Medicine 209, 1135–1152. https://doi.org/10.1084/jem.20120030

Schridde, A., Bain, C.C., Mayer, J.U., Montgomery, J., Pollet, E., Denecke, B., Milling, S.W.F., Jenkins, S.J., Dalod, M., Henri, S., Malissen, B., Pabst, O., Mowat, A.M., 2017. Tissue-specific differentiation of colonic macrophages requires TGFβ receptor-mediated signaling. Mucosal Immunol 10, 1387. https://doi.org/10.1038/mi.2016.142

Schulthess, J., Pandey, S., Capitani, M., Rue-Albrecht, K.C., Arnold, I., Franchini, F., Chomka, A., Ilott, N.E., Johnston, D.G.W., Pires, E., McCullagh, J., Sansom, S.N., Arancibia-Cárcamo, C.V., Uhlig, H.H., Powrie, F., 2019. The Short Chain Fatty Acid Butyrate Imprints an Antimicrobial Program in Macrophages. Immunity 50, 432-445.e7. https://doi.org/10.1016/j.immuni.2018.12.018

Schyns, J., Bai, Q., Ruscitti, C., Radermecker, C., Schepper, S.D., Chakarov, S., Farnir, F., Pirottin, D., Ginhoux, F., Boeckxstaens, G., Bureau, F., Marichal, T., 2019. Non-classical tissue monocytes and two functionally distinct populations of interstitial macrophages populate the mouse lung. Nat Commun 10, 3964. https://doi.org/10.1038/s41467-019-11843-0

Serbina, N.V., Pamer, E.G., 2006. Monocyte emigration from bone marrow during bacterial infection requires signals mediated by chemokine receptor CCR2. Nat Immunol 7, 311–317. https://doi.org/10.1038/ni1309

Shaw, T.N., Houston, S.A., Wemyss, K., Bridgeman, H.M., Barbera, T.A., Zangerle-Murray, T., Strangward, P., Ridley, A.J.L., Wang, P., Tamoutounour, S., Allen, J.E., Konkel, J.E., Grainger, J.R., 2018. Tissue-resident macrophages in the intestine are long lived and defined by Tim-4 and CD4 expression. J Exp Med 215, jem.20180019. https://doi.org/10.1084/jem.20180019

Shemer, A., Grozovski, J., Tay, T.L., Tao, J., Volaski, A., Süß, P., Ardura-Fabregat, A., Gross-Vered, M., Kim, J.-S., David, E., Chappell-Maor, L., Thielecke, L., Glass, C.K., Cornils, K., Prinz, M., Jung, S., 2018. Engrafted parenchymal brain macrophages differ from microglia in transcriptome, chromatin landscape and response to challenge. Nat Commun 9, 5206. https://doi.org/10.1038/s41467-018-07548-5

Shifrut, E., Carnevale, J., Tobin, V., Roth, T.L., Woo, J.M., Bui, C.T., Li, P.J., Diolaiti, M.E., Ashworth, A., Marson, A., 2018. Genome-wide CRISPR Screens in Primary Human T Cells Reveal Key Regulators of Immune Function. Cell. https://doi.org/10.1016/j.cell.2018.10.024

Spanjaard, B., Hu, B., Mitic, N., Olivares-Chauvet, P., Janjuha, S., Ninov, N., Junker, J.P., 2018. Simultaneous lineage tracing and cell-type identification using CRISPR–Cas9-induced genetic scars. Nat Biotechnol 36, 469. https://doi.org/10.1038/nbt.4124

Swirski, F., Nahrendorf, M., Etzrodt, M., Wildgruber, M., Cortez-Retamozo, V., Panizzi, P., Figueiredo, J., Kohler, R., Chudnovskiy, A., Waterman, P., Aikawa, E., Mempel, T., Libby, P., Weissleder, R., Pittet, M., 2009. Identification of Splenic Reservoir Monocytes and Their Deployment to Inflammatory Sites. Science 325, 612–616. https://doi.org/10.1126/science.1175202

Tamoutounour, S., Guilliams, M., Montanana Sanchis, F., Liu, H., Terhorst, D., Malosse, C., Pollet, E., Ardouin, L., Luche, H., Sanchez, C., Dalod, M., Malissen, B., Henri, S., 2013. Origins and Functional Specialization of Macrophages and of Conventional and Monocyte-Derived Dendritic Cells in Mouse Skin. Immunity 39, 925–938. https://doi.org/10.1016/j.immuni.2013.10.004

Tamoutounour, S., Henri, S., Lelouard, H., Bovis, B. de, Haar, C. de, Woude, C.J. van der, Woltman, A.M., Reyal, Y., Bonnet, D., Sichien, D., Bain, C.C., Mowat, A.McI., Sousa, C.R. e, Poulin, L.F., Malissen, B., Guilliams, M., 2012. CD64 distinguishes macrophages from dendritic cells in the gut and reveals the Th1-inducing role of mesenteric lymph node macrophages during colitis. Eur J Immunol 42, 3150–3166. https://doi.org/10.1002/eji.201242847

Thomas, D., Mostoslavsky, G., 2014. Gene Correction, Methods and Protocols 441–450. https://doi.org/10.1007/978-1-62703-761-7_29

Thomas, G.D., Hanna, R.N., Vasudevan, N.T., Hamers, A.A., Romanoski, C.E., McArdle, S., Ross, K.D., Blatchley, A., Yoakum, D., Hamilton, B.A., Mikulski, Z., Jain, M.K., Glass, C.K., Hedrick, C.C., 2016. Deleting an Nr4a1 Super-Enhancer Subdomain Ablates Ly6Clow Monocytes while Preserving Macrophage Gene Function. Immunity 45, 975–987. https://doi.org/10.1016/j.immuni.2016.10.011

Trzebanski, S., Jung, S., 2020. Plasticity of Monocyte Development and Monocyte Fates. Immunol Lett 227, 66–78. https://doi.org/10.1016/j.imlet.2020.07.007

Vanneste, D., Bai, Q., Hasan, S., Peng, W., Pirottin, D., Schyns, J., Maréchal, P., Ruscitti, C., Meunier, M., Liu, Z., Legrand, C., Fievez, L., Ginhoux, F., Radermecker, C., Bureau, F., Marichal, T., 2023. MafB-restricted local monocyte proliferation precedes lung interstitial macrophage differentiation. Nat. Immunol. 24, 827–840. https://doi.org/10.1038/s41590-023-01468-3

Varol, C., Landsman, L., Fogg, D.K., Greenshtein, L., Gildor, B., Margalit, R., Kalchenko, V., Geissmann, F., Jung, S., 2007. Monocytes give rise to mucosal, but not splenic, conventional dendritic cells. J Exp Medicine 204, 171–180. https://doi.org/10.1084/jem.20061011

Varol, C., Vallon-Eberhard, A., Elinav, E., Aychek, T., Shapira, Y., Luche, H., Fehling, H.J., Hardt, W.-D., Shakhar, G., Jung, S., 2009. Intestinal Lamina Propria Dendritic Cell Subsets Have Different Origin and Functions. Immunity 31, 502–512. https://doi.org/10.1016/j.immuni.2009.06.025

Wefers, B., Bashir, S., Rossius, J., Wurst, W., Kühn, R., 2017. Gene editing in mouse zygotes using the CRISPR/Cas9 system. Methods 121, 55–67. https://doi.org/10.1016/j.ymeth.2017.02.008

Weinreb, C., Rodriguez-Fraticelli, A., Camargo, F.D., Klein, A.M., 2020. Lineage tracing on transcriptional landscapes links state to fate during differentiation. Science eaaw3381. https://doi.org/10.1126/science.aaw3381

Werner, Y., Mass, E., Kumar, P.A., Ulas, T., Händler, K., Horne, A., Klee, K., Lupp, A., Schütz, D., Saaber, F., Redecker, C., Schultze, J.L., Geissmann, F., Stumm, R., 2020. Cxcr4 distinguishes HSC-derived monocytes from microglia and reveals monocyte immune responses to experimental stroke. Nat Neurosci 1–12. https://doi.org/10.1038/s41593-020-0585-y

Wolf, A.A., Yáñez, A., Barman, P.K., Goodridge, H.S., 2019. The Ontogeny of Monocyte Subsets. Front Immunol 10, 1642. https://doi.org/10.3389/fimmu.2019.01642

Wolf, Y., Boura-Halfon, S., Cortese, N., Haimon, Z., Shalom, H.S., Kuperman, Y., Kalchenko, V., Brandis, A., David, E., Segal-Hayoun, Y., Chappell-Maor, L., Yaron, A., Jung, S., 2017. Brown-adipose-tissue macrophages control tissue innervation and homeostatic energy expenditure. Nat Immunol 18, ni.3746. https://doi.org/10.1038/ni.3746

Yáñez, A., Coetzee, S.G., Olsson, A., Muench, D.E., Berman, B.P., Hazelett, D.J., Salomonis, N., Grimes, H.L., Goodridge, H.S., 2017. Granulocyte-Monocyte Progenitors and Monocyte-Dendritic Cell Progenitors Independently Produce Functionally Distinct Monocytes. Immunity 47, 890-902.e4. https://doi.org/10.1016/j.immuni.2017.10.021

Yáñez, A., Ng, M.Y., Hassanzadeh-Kiabi, N., Goodridge, H.S., 2015. IRF8 acts in lineage-committed rather than oligopotent progenitors to control neutrophil vs monocyte production. Blood 125, 1452–1459. https://doi.org/10.1182/blood-2014-09-600833

Yona, S., Kim, K.-W., Wolf, Y., Mildner, A., Varol, D., Breker, M., Strauss-Ayali, D., Viukov, S., Guilliams, M., Misharin, A., Hume, D.A., Perlman, H., Malissen, B., Zelzer, E., Jung, S., 2013. Fate Mapping Reveals Origins and Dynamics of Monocytes and Tissue Macrophages under Homeostasis. Immunity 38, 79–91. https://doi.org/10.1016/j.immuni.2012.12.001

Yu, W., Lin, Z., Hegarty, J.P., Chen, X., Kelly, A.A., Wang, Y., Poritz, L.S., Koltun, W.A., 2012. Genes Differentially Regulated by NKX2-3 in B Cells Between Ulcerative Colitis and Crohn's Disease Patients and Possible Involvement of EGR1. Inflammation 35, 889–899. https://doi.org/10.1007/s10753-011-9390-9

Yu, W., Lin, Z., Pastor, D.M., Hegarty, J.P., Chen, X., Kelly, A.A., Wang, Y., Poritz, L.S., Koltun, W.A., 2010. Genes Regulated by Nkx2-3 in Sporadic and Inflammatory Bowel Disease-Associated Colorectal Cancer Cell Lines. Dig. Dis. Sci. 55, 3171–3180. https://doi.org/10.1007/s10620-010-1138-0

Zelante, T., Iannitti, R.G., Cunha, C., De Luca, A., Giovannini, G., Pieraccini, G., Zecchi, R., D'Angelo, C., Massi-Benedetti, C., Fallarino, F., Carvalho, A., Puccetti, P., Romani, L., 2013. Tryptophan Catabolites from Microbiota Engage Aryl Hydrocarbon Receptor and Balance Mucosal Reactivity via Interleukin-22. Immunity 39, 372–385. https://doi.org/10.1016/j.immuni.2013.08.003

Zhu, J., Luo, L., Tian, L., Yin, S., Ma, X., Cheng, S., Tang, W., Yu, J., Ma, W., Zhou, X., Fan, X., Yang, X., Yan, J., Xu, X., Lv, C., Liang, H., 2018. Aryl Hydrocarbon Receptor Promotes IL-10 Expression in Inflammatory Macrophages Through Src-STAT3 Signaling Pathway. Front Immunol 9, 2033. https://doi.org/10.3389/fimmu.2018.02033

ZIEGLER-HEITBROCK, H., APPL, B., KÄFFERLEIN, E., LÖFFLER, T., JAHN-HENNINGER, H., GUTENSOHN, W., NORES, J., MCCULLOUGH, K., PASSLICK, B., LABETA, M., IZBICKI, J., 1994. The Antibody MY4 Recognizes CD14 on Porcine Monocytes and Macrophages. Scand J Immunol 40, 509–514. https://doi.org/10.1111/j.1365-3083.1994.tb03497.x

Zigmond, E., Bernshtein, B., Friedlander, G., Walker, C.R., Yona, S., Kim, K.-W., Brenner, O., Krauthgamer, R., Varol, C., Müller, W., Jung, S., 2014. Macrophage-Restricted Interleukin-10 Receptor Deficiency, but Not IL-10 Deficiency, Causes Severe Spontaneous Colitis. Immunity 40, 720–733. https://doi.org/10.1016/j.immuni.2014.03.012

Zigmond, E., Varol, C., Farache, J., Elmaliah, E., Satpathy, A.T., Friedlander, G., Mack, M., Shpigel, N., Boneca, I.G., Murphy, K.M., Shakhar, G., Halpern, Z., Jung, S., 2012. Ly6Chi Monocytes in the Inflamed Colon Give Rise to Proinflammatory Effector Cells and Migratory Antigen-Presenting Cells. Immunity 37, 1076–1090. https://doi.org/10.1016/j.immuni.2012.08.026